TALEN-mediated site-specific integration of human CFTR gene by a helper-dependent adenoviral vector

by

Yi Qian Zhang

A thesis submitted in conformity with the requirements
for the degree of Master of Science
Department of Laboratory Medicine and Pathobiology
University of Toronto

TALEN-mediated site-specific integration of human CFTR gene by a helper-dependent adenoviral vector

Yi Qian Zhang

Master of Science

Department of Laboratory Medicine and Pathobiology

University of Toronto

2018

Abstract

Approximately 2,000 different mutations in CFTR gene have been identified to cause cystic fibrosis (CF). Gene therapies are being developed to target all types of CFTR mutations and to reduce drug burdens in long term. Major challenges of CFTR gene transfer to the lung are the efficient delivery to relevant cells and the safe integration for long-lasting expression. Exploiting the maximized packing capacity of helper-dependent adenoviral vectors (HD-Ad), we are able to deliver a donor CFTR expression cassette together with site-specific TALEN gene editing system in one single vector for accurate transgene integration. We show an approximately 5-7% integration efficiency at the AAVS1 locus in IB3-1 cells by delivering a LacZ reporter with the HD-Ad-TALEN system. Furthermore, we show expression of CFTR mRNA and functional protein by delivering a CFTR expression cassette. Overall, these results demonstrate great potential of the HD-Ad-TALEN system as a novel strategy for CF lung disease.

Acknowledgments

I would like to express the deepest gratitude to my supervisor Dr. Jim Hu for all the guidance he provided to my research project. His passion as a scientist is contagious and his advice as a mentor has always been inspiring.

I would like especially to thank Dr. Fushan Shi for his contribution to the molecular cloning of HD-Ad plasmid vectors. I am thankful to Jun Li and Rongqi Duan for their assistance in HD-Ad viral production. I thank Emily Xia for her help with the flow cytometry assay, and I would like to thank Dr. Huibi Cao for helping me to set up the FLIPR membrane potential assay. I am also grateful to all other former and current lab members: Leo Yang, Kyle Siegel, Zhichang Zhou, Alexandra Georgiou, Dr. Yang Yang, Dr. Yong Wei, Dr. Miao Li, Cathy Huang, Jailyn Yen, and Randolph Kissoon for the extraordinary support for my work, thought-provoking discussions about the project, and warm friendship in the past two years.

My sincere thanks also go to my committee members Dr. David Hwang, Dr. Neil Sweezey, and Dr. Nades Palaniyar for their insightful comments and suggestions.

Furthermore, I would like to thank the Department of Laboratory Medicine and Pathobiology at the University of Toronto and the Department of Translational Medicine at the Hospital for Sick Children for offering academic courses, training opportunities, and access to the laboratory facilities.

Last but not the least, I would like to thank my mom and dad for the incredible support and unconditioned love during the writing of this thesis and in my life.

This project was funded by Canadian Institute of Health Research (CIHR).

Table of Contents

List of Tables

List of Figures

List of Abbreviations

Ψ:	Adenoviral packaging signal
7-AAD:	7-aminoactinomycin D
AAV:	Adeno-associated virus
AAVS1:	Adeno-associated virus integration site 1
ABC:	ATP-binding cassette
Ad:	Adenovirus
Ad5:	Adenovirus serotype 5
ASL:	Airway surface liquid
ATP:	Adenosine triphosphate
BCA:	Bicinchoninic acid
BSA:	Bovine serum albumin
C_{12}FDG:	5-dodecanoylaminofluorescein di- β-D-galactopyranoside
cAMP:	Cyclic adenosine monophosphate
CAR:	Coxsackievirus and adenovirus receptor
cDNA:	Complementary DNA
CF:	Cystic fibrosis
CFTR:	Cystic fibrosis transmembrane conductance regulator
CPE:	Cytopathogenic effect
CRISPR:	Clustered Regularly Interspaced Short Palindromic Repeats
Ct:	Cycle threshold
CtIP:	CtBP-interacting protein
DAPI:	4′,6-diamidino-2-phenylindole

DMEM: Dulbecco's Modified Eagle's Medium

DSB: Double-stranded break

E1a: Adenovirus early region 1A

E1b: Adenovirus early region 1B

E2: Adenovirus early region 2

E3: Adenovirus early region 3

E4: Adenovirus early region 4

ENaC: Epithelial sodium channel

ESC: Embryonic stem cell

EXO1: Exonuclease I

F508del: Deletion of phenylalanine residue at position 508 of CFTR

FBS: Fetal bovine serum

FDG: Fluorescein di-β-D-galactopyranoside

FG-Ad: First generation adenoviral vector

FITC: Fluorescein isothiocyanate

FIV: Feline immunodeficiency virus

FLASH: Fast ligation-based automatable solid-phase high-throughput method

FLIPR: Fluorescent imaging plate reader

FSC: Forward scatter

FSK: Forskolin

G1 phase: Gap 1 phase of cell cycle

G2 phase: Gap 2 phase of cell cycle

G551D: Substitution of glycine to aspartic acid at position 551 of CFTR

GFP:	Green fluorescent protein
GL67A:	Genzyme lipid 67A
GP64:	Glycoprotein 64
hCFTR:	Human CFTR
HD-Ad:	Helper-dependent adenoviral vectors
HDR:	Homology directed repair
HEK 293:	Human embryonic kidney cell 293
HEPES:	4-(2-hydroxyethyl)-1-piperazineethanesulfonic acid
HV:	Helper virus
IgG:	Immunoglobin G
iPSC:	Induced pluripotent stem cell
ITR:	Inverted terminal repeat
K18:	Promoter of the keratin 18 gene
Ku:	Ku70/Ku80 heterodimer
L1:	Adenovirus late region 1
L5:	Adenovirus late region 5
LHA:	Left homology arm
LIG4:	DNA ligase IV
LTR:	Long terminal repeat
MEM:	Eagle's Minimal Essential Medium
MOI:	Multiplicity of infection
MRN:	Protein complex consisting of Mre11, Rad50, and Nbs1
MCS:	Multiple cloning site

MSD1:	Membrane spanning domain 1
NBD:	Nucleotide binding domain
NG163:	Helper virus
NGS:	Next-generation sequencing
NHEJ:	Non-homologous end joining
NLS:	Nuclear localization signal
OD:	Optical density
PBS:	Phosphate-buffered saline
PCR:	Polymerase chain reaction
PETG:	Phenyl-ethyl β-D-thiogalactopyranoside
PEx:	Pulmonary exacerbation
PKA:	Protein kinase A
PPP1R12C:	Protein phosphate 1 regulatory subunit 12C
qPCR:	Quantitative PCR
R domain:	Regulatory domain
REAL:	Restriction enzyme digestion and ligation
RHA:	Right homology arm
RIPA:	Radioimmunoprecipitation assay
RVD:	Repeat variable di-residue
SDS-PAGE:	Sodium dodecyl sulfate polyacrylamide gel electrophoresis
S phase:	Synthesis phase in cell cycle
SG-Ad:	Second generation adenoviral vector
siRNA:	Small interfering RNA

SV40:	Simian vacuolating virus 40
T7E1:	T7 endonuclease I
TALE:	Transcription activator-like effector
TALEN:	Transcription activator-like effector nuclease
TBS:	Tris-buffered saline
TCAG:	The Centre for Applied Genomics
TE:	Tris-EDTA buffer
TMD:	Transmembrane spanning domain
UBC:	Ubiquitin C promoter
US FDA:	United States Food and Drug Administration
UV:	Ultraviolet
W1282X:	Nonsense mutation at position 1282 of CFTR
X-gal:	5-bromo-4-chloro-3-indolyl-β-D-galactopyranoside

1 Introduction

1.1 Cystic fibrosis

Cystic fibrosis (CF) is an autosomal recessive genetic disorder characterized by epithelial secretory dysfunctions in multiple organs. The disease is caused by mutations in the cystic fibrosis transmembrane conductance regulator (CFTR) gene located on human chromosome 7. The CFTR protein belongs to the ATP-binding cassette (ABC) transporter superfamily. It is a protein kinase A (PKA) and cyclic adenosine monophosphate (cAMP)-regulated chloride and bicarbonate channel primarily expressed in ciliated epithelial cells and submucosal glands[1,2]. Beyond its role as an anion channel, several other cellular functions of CFTR were described including regulating sodium transport[3], potassium channels, exocytosis, and the expression of many other gene products[4]. The protein is composed of two transmembrane domains (TMDs), two nucleotide-binding domains (NBDs), and a regulatory (R) domain[1,5-7].

Defective CFTR function can lead to pulmonary failure, pancreas insufficiency, intestinal obstruction, and infertility in male[8]. CF occurs most commonly within the Caucasians population, affecting about 70,000 people worldwide. In Canada, CF occurs in one out of every 3,600 new births by estimation[8,9]. Although the disease is less likely to be found among non-white populations, the mutation screening and early diagnosis in varied ethnic groups still need future optimizations[10].

Over the decades since CF has been discovered, the median age of survival in CF patients has substantially increased because of the improved care delivery, the better nutrient status, and the effect of new drugs[1,8,9]. Yet, respiratory-related conditions are considered as the leading cause of death accounting for more than 80% of patients[11].

1.1.1 CF lung pathology

The CF pulmonary disease is characterized by mucosal obstruction, persistent bacterial infection, and chronic inflammation in lung. Episodes of acute worsening of symptoms, termed pulmonary exacerbation (PEx), usually mark the chronic development of the pulmonary disease[12]. Thickening of the airway mucus is an initiating lesion of CF lung pathogenesis as the mucociliary clearance is impaired in the presence of abnormally viscous, elastic, and adhesive mucus[13]. Following the damage of the mucosal barrier between the airway epithelium and the external environment, chronic colonization of microorganisms such as *Pseudomonas aeruginosa* and *Burkholderia cepacia* — which are usually innocuous in healthy individuals — often leads to severe infections and progressive loss of lung functions in patients with CF[14–16]. Up-regulation of pro-inflammatory cytokines and reduced levels of anti-inflammatory cytokines are another hallmark of the disease seen in the airways of CF patients. Repeated pulmonary inflammation in CF is dominated by neutrophils releasing oxidants and proteases, which also contributes to the onset of bacterial infection and the destruction of the organ[16–18].

The mechanism behind CF pulmonary complications at the molecular level remains controversial despite extensive research of the disease. A long-established hypothesis termed the low-volume model explains that the absence of CFTR regulation in CF epithelia results in over-activity of the epithelial sodium channel (ENaC). Hyperabsorption of Na^+ leads to an abnormal increase in the uptake of Cl^- via passive channels and the subsequent water flow from the apical airway surface liquid (ASL) into the cells. Depletion of the ASL diminishes the normal mucociliary transport and initiates the mucosal obstruction[19]. On the other hand, Smith *et al.* purposed the high-salt model, arguing that Cl^- cannot be reabsorbed by the cells

without the CFTR channel and the ASL becomes excessively salty. The group showed through several *in vitro* experiments that the airway epithelial cells produce apical bactericidal factors[20]. The high salt condition inactivates these natural antibiotics in the ASL, which makes patients with CF vulnerable to bacterial infections in the airway[20,21]. Although the two disease models sharply different, it is remarkable that both demonstrated the important role of CFTR channel in maintaining the normal chloride secretion in airway epithelia.

1.1.2 Types of CFTR mutation

Reported in 2015, 90% of individuals with CF in Canada carry at least one deletion mutation at the phenylalanine 508 residue (F508del). However, more than 2,000 different mutations have been identified at the CFTR locus[9,11], posing a major challenge to the treatment of the disease.

CFTR mutations are traditionally divided into six categories based on the type of CFTR protein defect[22–24]. Class I mutations refer to protein synthesis defects and are usually resulted from nonsense, frameshift, or RNA splicing mutations. Class II describes mutations that affect the processing and trafficking of CFTR protein to the apical membrane, usually caused by missense mutation or amino acid deletion. Notably, the most common F508del falls into this category, therefore the correction of protein folding and delivery becomes the target of many potential therapeutic strategies. In Class III mutations, a normal amount of CFTR proteins are transported to the cell surface, but the mutant nucleotide binding domains fail to bind ATP to activate channel function[25,26]. Class I, II, and III mutations are considered to cause more severe CF phenotypes as there is virtually no functional CFTR in the apical membrane. In Class IV, V, and VI mutations, however, certain residual CFTR function is still present at the cell surface

and the phenotype is usually milder. Class IV mutations are located in the MSD1 domain which contributes to the formation of pore[27]. This class of mutations is characterized by insufficient CFTR channel conductance. Class V mutations are caused by splicing defects, promoter mutations, or inefficient transport, resulting in a decreased amount of CFTR synthesis and trafficking to the apical membrane[28–30]. Class VI mutations are characterized by functional but unstable CFTR at the cell surface, usually caused by C-terminal truncation of CFTR[31].

Classification of CFTR mutations provides a point of reference on disease severity and potential drug targets. More recently, different methods to classify CFTR mutations have been on the basis of therapeutic strategy or a combination of protein defect, approaches, and clinical features[32,33]. Nevertheless, some of the mutations cannot be classified because of their heretofore unknown effects on CFTR protein[9].

1.1.3 Established therapies for CF lung disease

The life expectancy and quality of those with CF lung disease have been greatly improved with a wide spectrum of available therapies and drugs, from antibiotics and anti-inflammatory therapies to mucolytic agents to more recently developed CFTR modulators.

Antimicrobial drugs have been a long-established approach to combat pulmonary infections in CF patients. They are used for four purposes including prophylaxis, early stage eradication, management of chronic infections, and treatment of pulmonary exacerbation. Many studies have shown positive outcomes from the inhalation of nebulized tobramycin[34], colistin[35], and aztreonam[36,37] against *P. aeruginosa* infection which occurs in most CF patients[11]. Although several novel antibiotic treatments such as liposomal amikacin[38,39] and

levofloxacin[40] are still being tested, concerns and controversies over the risk of bacterial antibiotic resistance have been raised especially from the prophylactic use of anti-staphylococcal antibiotics[41].

It is mentioned earlier in Section 1.1.1 that inflammatory response is another important aspect of the pathogenesis of CF lung disease. Persistent inflammation is closely associated with the bacterial burden and leads to bronchiectasis[42]. Effective anti-inflammatory drugs recommended for long-term management of CF lung inflammation are relatively limited. High-dose ibuprofen treatment has shown clinical benefits in younger patients[43,44], but the long-term side effects are of concern and the proper dosing needs further investigations[45]. On the other hand, some antimicrobial agents are reported to have anti-inflammatory properties although the mechanisms are not clear. An example of such antibiotics is azithromycin, which has been found to reduce neutrophil counts as well as serum inflammatory markers in patients uninfected with *P. aeruginosa*[46].

Mucus in the airway is normally cleared by airflow and ciliary interactions[47]. In the airway of CF patients, thickened mucus impairs normal mucociliary clearance, which contributes to chronic pulmonary inflammation and infections[13]. Several mucolytic agents are available for helping CF lung clearance. Dornase alfa, a recombinant human DNase, has been shown to aid airway clearance by digesting the excessive extracellular DNA from the breakdown of neutrophils[48–50]. Another effective, safe, and affordable agent is hypertonic saline which temporarily rehydrates the airway surface to restore the mucociliary clearance[41,51].

A remarkable revolution in CF therapies is the development of CFTR modulator therapies as they target CFTR protein defects instead of downstream symptoms. Three major categories of CFTR modulators are being studied, including potentiators, correctors, and

production correctors (also called read-through agents). Potentiators aim to enhance the CFTR chloride channel function only if it can be correctly located on the cell surface. Correctors target the protein processing and trafficking defects, while production correctors help the ribosome to read-through a premature termination codon to translate a full-length CFTR protein.

Ivacaftor (commercialized as Kalydeco, Vertex Pharmaceuticals) represents a significant advance in the potentiator development. As the first CFTR modulator approved by the US Food and Drug Administration and European Commission, its efficacy has been confirmed through clinical trials for the most common class III mutation G551D and some other gating mutations[52–54] Despite the compelling results, such mutations are relatively rare and the effect of ivacaftor only covers 5% of total CF patients. In patients with two copies of F508del mutation, accounting for about 50% of total patients, potentiators are less likely to be effective due to insufficient CFTR protein on the cell surface[55]. This drives the further studies of combination therapies with multiple CFTR modulators.

Lumacaftor is a corrector that facilitates intracellular trafficking of CFTR protein, however, it showed little clinical benefit in patients homozygous for F508del because the protein transported to the cell membrane is not functional[39]. Therefore, a mechanism was proposed that when lumacaftor is combined with ivacaftor, it will increase the CFTR protein trafficking to the cell surface where ivacaftor will restore the protein function. In 2015, an ivacaftor/lumacaftor medication (Orkambi, Vertex Pharmaceuticals) was approved by the US FDA for the treatment of homozygous F508del mutation. The drug was confirmed to improve lung function and reduce sweat chloride in patients with such mutation, although the effect may be suboptimal possibly due to drug-drug interactions[56,57].

Numerous CFTR modulators and combination therapies are still under investigation or in different phases of clinical studies in order to benefit more patients in a safer and more effective way. Recently, clinical trials of triple combination therapies VX-659 in combination with tezacaftor and ivacaftor, and VX-445 in combination with tezacaftor and ivacaftor are stepping into Phase 3 studies. In early studies, both of them have demonstrated significant improvement in lung function of the participants[58].

1.1.4 Genetic therapies for CF lung disease

Gene therapy as an emerging treatment is an appealing future option in addition to the established therapies and drugs for CF lung disease because of its great potentials in target specificity, safety, cost-effectiveness, and long-term efficacy.

Since the identification of CFTR gene in 1989, more research in the field has been focusing on novel approaches to replace the CFTR gene — the primary underlying cause of CF[59]. Besides its monogenic nature, several characteristics of CF lung disease have made it a great candidate for genetic therapy. First, airway epithelial cells expressing CFTR have a relatively easy access through non-invasive routes such as aerosol and nebulizer delivery. Studies also showed that although a higher CFTR correction rate might be beneficial to host defense defects, as few as 6-10% corrected cells in a CF airway epithelial sheet could restore the normal chloride channel functions[60,61]. Moreover, unlike CFTR modulators, genetic therapy-based approaches could be effective for virtually all types of CFTR defect. Research into pluripotency in basal cells and myoepithelial cells in the airway further accelerates the development of CFTR replacement strategies targeting these progenitor cells in order to achieve a long-lasting CFTR expression in the airway[62–65]. Despite promising advances and

years of intensive research, CF lung gene therapies face numerous challenges, for instance in efficient gene delivery to the target cells, transgene integration for long-term expression, and host immune responses before it can be brought to the clinic.

1.2 Vector systems for CF lung disease genetic therapies

1.2.1 Non-viral vectors

Non-viral vectors deliver the therapeutic gene to the target cells either as naked nucleic acid or with macromolecule complex to facilitate transfection. They offer major advantages in a low immunogenicity and packaging capacity for large molecules, but a downside is the limited *in vivo* gene transfer efficiency[66,67].

Plasmid-based strategies with liposomal vectors have been widely used for gene delivery to the lung. Positively charged liposomes are able to spontaneously interact with negatively charged DNA molecules as well as cell membranes to enhance entrance through membrane fusion or endocytosis[68]. A recent Phase I/IIa clinical study using the GL67A liposome for the delivery of CpG-deleted pGM169 demonstrated a small improvement in lung functions and highlighted the good safety profile even of repeated dosing. However, the study also reported inflammatory responses at higher doses likely due to the cationic lipid formulation[69]. Therefore, improving the delivery efficiency and lowering the dose required for sufficient expression is critical for future studies. A related strategy is to form nanoparticles which nucleic acids are complexed with a single-layer lipid or polymers. Variation in the composition of nanoparticles gives them different properties. For example, chitosan nanoparticles are mucoadhesive and therefore are suitable for lung gene therapy, whereas solid lipid nanoparticles effectively protect the degradation of unstable nucleic acids by nucleases[70].

Alternatives to plasmid DNA vectors are also being developed and optimized using small circular or linear DNA, also called DNA minicircles and ministrings respectively, that are depleted of bacterial sequences to reduce the immunogenicity[71–73]. A study in 2016 showed correction of a CF splicing mutation by delivering single-stranded DNA oligonucleotides that hybridized to the pre-mRNA[74]. Small interfering RNA (siRNA) has also been used for CF recently to inhibit the upregulated ENaC[75].

1.2.2 Lentiviral vectors

The RNA genome of lentiviruses is reverse-transcribed into double-stranded DNA and randomly integrated to the host genome, while in contrast to other members of retroviruses, they are able to infect both dividing and non-dividing cells[76]. Because of these features, lentiviral vectors came into the picture as an option for CF gene therapy aiming for long-term CFTR expression *in vivo*[77]. Several improvements have been made to optimize lentiviruses for gene transfer applications. Wild-type lentiviruses contain a 9.7 kb genome, whereas lentiviral vectors are able to package up to 8 kb of transgene cassette due to the partial removal of viral genes[78]. Pseudotyped lentiviruses allow them to be recognized by apical receptors in the airway epithelia which lack affinity for the wild-type ones[79–81]. Moreover, the oncogenic risk resulting from random chromosomal integration can be greatly reduced with the careful design of lentiviral vectors, for example by eliminating some strong viral long terminal repeat (LTR) promoters[82].

In a recent *in vivo* study of a feline immunodeficiency virus (FIV)-based lentiviral vector pseudotyped with the GP64 envelope protein, the authors reported the correction of CFTR channel function and an increase in bacterial killing in the airways of vector-treated CF

pigs[83]. However, there is a need for further studies to reveal the long-term safety profile of lentiviral vectors in human lungs. The application of lentiviruses in CF gene therapy remains challenging also due to the difficulty in large-scale production and purification[67].

1.2.3 Adeno-associated virus (AAV) vectors

Recombinant AAV serotype 2 (rAAV2) is a nonenveloped virus with a small linear single-stranded DNA genome of approximately 4.7 kb[84]. Similar to lentiviruses, they are able to infect quiescent cells. The life cycle of AAV in human hosts can follow either the lytic or the lysogenic pathway. The former will occur in the presence of adenovirus or herpesvirus in the host cell. Otherwise, AAV will undergo latency and integrate to a variety of preferential genomic sites, including AAVS1 locus on chromosome 19. Yet, integration of AAV occurs at an extremely low frequency and most of their genome stay episomal[85,86]. The most outstanding advantage of recombinant AAV vectors is their safety profile: they do not cause any known disease in human hosts[86].

In late 2017, the first gene therapy drug using an AAV vector (Luxturna, Spark Therapeutics) was approved by the US FDA for clinical use in the treatment of vision loss caused by inherited retinal disease[87]. However, AAV vectors have not yet been applied in CF gene therapies due to the small packaging capacity[86].

1.2.4 Adenoviruses (Ads)

Adenovirus was first isolated from human adenoid tissues in 1953 and has gained popularity as vectors for foreign gene delivery in mammalian cells due to their high gene transfer efficiency *in vivo*, their natural tropism for the respiratory tract, the ability to infect

both dividing and nondividing cells, and the ease to be produced and purified in large quantities[88–90]. Among the 67 reported human Ad serotypes, type 5 (Ad5) is the most extensively studies for gene therapy applications[91]. Ad5 uses Coxsackie-Adenovirus Receptors (CAR) at the basolateral membrane of airway epithelial cells as the primary receptors for cell entry[92,93]. After the internalization, they escape from the endosomes to the cytoplasm, travel to the nuclear core complex, and release the genetic material to the nucleus[94]. Ad5 has a linear double-stranded DNA genome of ~36 kb enclosed in an icosahedral, non-enveloped capsid. The genome of Ad5 contains early viral gene regions E1a, E1b, E2, E3, and E4 which are expressed before viral replication. E1a is a central gene responsible for regulating the transcription of other viral genes for replication and reprogramming the host mitogenic activities, while E1b work to prevent the host cell from apoptosis[95–97]. The late viral genes L1 to L5 that encode structural and other regulatory components are expressed after viral DNA replication[89].

The first generation of recombinant Ads (FG-Ad) for gene transfer have been developed by deleting the E1 region to introduce viral replication deficiency and the E3 region to make room for the transgene. This allows the vectors to package an 8 kb transgene expression cassette[98]. During the viral vector production, the essential functions for viral replication are complemented *in trans* by a human embryonic kidney (HEK) 293-based producer cell line[90,99]. In the second-generation Ads (SG-Ad), the removal of early viral genes E2 and/or E4 in addition to the E1 and E3 regions has reduced viral antigen expression and generated a larger cloning capacity ranging from 10 to 13 kb[100,101]. However, first and second-generation Ads both evoke relatively strong host immune responses against the viral genes in animals and humans at a high dose, which shortens the expression of the transgene to 2 to 3 weeks[102–104].

1.2.5 Helper-dependent adenoviral (HD-Ad) vectors

To overcome the immunological barriers of adenoviral vectors, a helper-dependent adenovirus (HD-Ad), or gutted adenovirus, has been developed. HD-Ad vectors are devoid of all viral coding sequences, left with only the viral inverted terminal repeats (ITRs) required for DNA replication (~500 bp) and a packaging signal. Thus, they exhibit greatly reduced immunogenicity and a maximized DNA packaging capacity of ~36 kb[105].

Studies showed that *in vivo* delivery with HD-Ad vectors to airway epithelial cells in mice resulted in significantly reduced inflammation, and the transgene expression lasted longer compared to the first-generation Ads[106]. In pig models with lung anatomy more similar to humans, human CFTR transgene can be efficiently delivered and expressed in both airway epithelial cells and submucosal glands by HD-Ad vectors, without showing systemic toxicity[107]. These studies suggested that airway delivery by HD-Ad could be an advance in clinical strategies for CF lung gene therapy.

Shown in Figure 1-1, the propagation of HD-Ad vectors in 293 producer cells requires complementary functions of an E1-deleted helper virus (HV). In order to eliminate the propagation of helper virus during HD-Ad preparation, the Cre/loxP system has been applied in the production system to remove the packaging signal (Ψ) from the helper virus. The modified helper virus carries two loxP sites flanking the packaging signal. In an engineered 293 cell line (293Cre) where Cre recombinase is constitutively expressed, the helper virus is able to replicate its DNA and express essential viral genes for HD-Ad propagation, yet its genome will not be packaged because of Cre/*loxP*-mediated excision of Ψ[105]. Further modifications of the 239Cre producer cell line resulted in the generation of 116 cell line, which allows both adherent and suspension growth for efficient production in large scale. It has also

been shown that the 293Cre-derived 116 cells have a higher level of Cre recombinase expression than 293Cre, marking an improvement in Ψ excision efficiency[108]. Helper virus contamination, which is a major concern in HD-Ad applications, can be reduced to 0.1% - 0.001% of total virus particles HD-Ad preparation with this system[109].

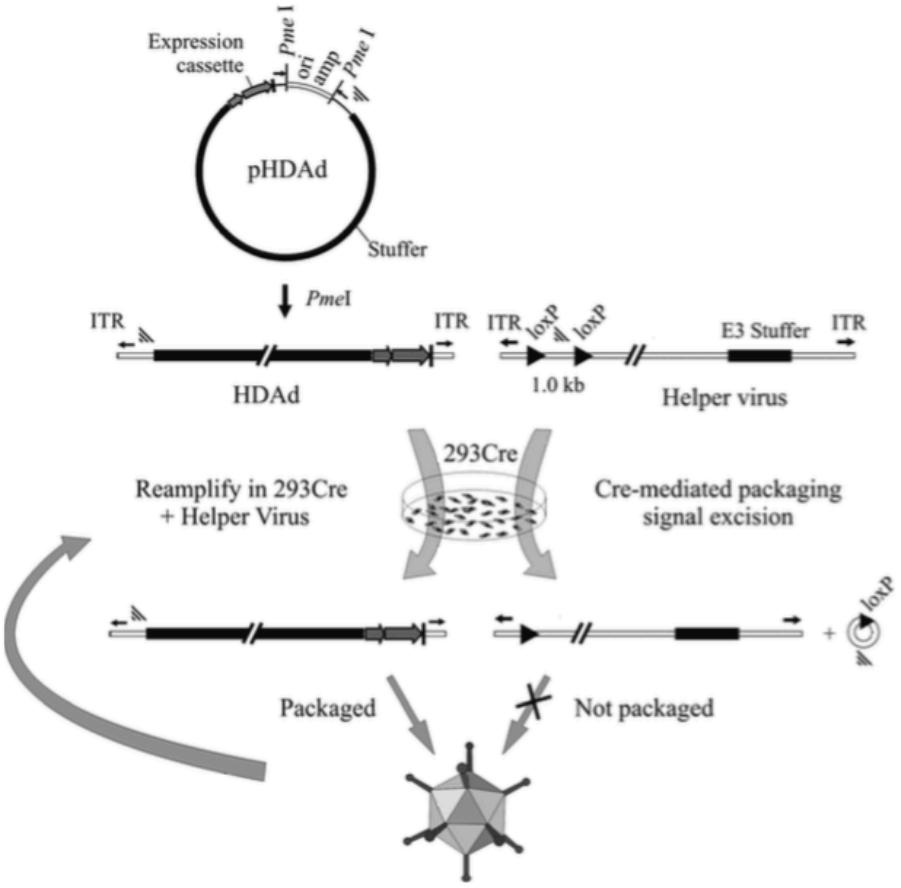

Figure 1-1. Rescue and propagation of HD-Ad vectors in the 293Cre cell line

The bacterial plasmid pHD-Ad carrying the HD-Ad genome is linearized by restriction enzyme digestion. The linearized DNA is transfected into Cre expressing 293 cells, and cells are infected with the HV. The noncoding E3 stuffer DNA is inserted in order to avoid packaging of replication competent $E1^+$ Ad generated by homologous recombination between the HV and the Ad sequence in the 293Cre genome. The Cre-mediated recombination between the two loxP sites results in excision of the Ψ. The titre of HD-Ad vectors is increased by serial coinfections of 293Cre cells with the HD-Ad and the HV. Adapted from Palmer and Ng[110].

1.3 The AAVS1 safe harbour for gene integration

As mentioned in Section 1.2.3, the adeno-associated virus integration site 1 (AAVS1) is a preferential integration site of wild-type AAV. The AAVS1 site is located within the intron 1 of protein phosphatase 1, regulatory subunit 12C (PPP1R12C) gene in human chromosome 19 (19q13.43) [111].

Although it has been found that latent AAV infection does alter the phenotypes and the expression of certain cellular genes as the research goes deeper, disruption of the region is not associated with any known human disease[112,113]. The AAVS1 locus is still considered as a preferable safe harbour for transgene integration. Remarkably sustained transgene expression has been shown in previous studies assessing the AAVS1 locus within several types of human cells including embryonic stem cells (ESC), induced pluripotent stem cells (iPSC), and fibroblasts[114–116].

1.4 TALEN: A site-specific gene editing technology

Transcription activator-like effector nucleases (TALENs) are a class of highly specific and easily engineered endonucleases for gene editing by introducing targeted double-strand breaks (DSBs). TALENs bind and cleave the target DNA as heterodimers. Each TALEN unit is composed of a FokI endonuclease domain artificially fused to a customizable domain responsible for recognition and binding of the target sequence. This domain is derived from transcription activator-like effectors (TALEs) secreted by the Gram-negative plant-pathogenic bacteria *Xanthomonas spp*. These pathogens inject TALEs through the type III secretion system to their host plant cells, targeting the genes related to disease resistance and host susceptibility[117–119].

TALEs in the *Xanthomonas* bacteria are made up of three major regions: A C-terminal nuclear localization signal (NLS), a domain that activates the target gene transcription, and a central DNA-binding domain. The DNA-binding domain contains arrays, or monomers, of highly conserved amino acid repeats with the exception of two hypervariable residues at position 12 and 13 in each array, termed the repeat variable di-residues (RVDs). RVDs in each individual array recognize a single DNA nucleotide. The most commonly used RVDs — NN, NI, HD, and NG — are able to recognize G, A, C, and T, respectively[119–121]. Naturally occurring TALEs consist of an average number of 17 RVDs in each arm, recognizing 34 nucleotides at the target site[122]. The target sequence bound by TALE monomers usually contains a 5' thymine, which affects the binding efficiency[123]. Site-specific binding of TALEs to the target allows the subsequent target DNA cleavage by the FokI nucleases. Once the TALEN-induced DSB is generated, non-homologous end-joining or homology-direct repair (See Section 1.5) can lead to alterations at the designated target site[124]. Figure 1-2 shows TALEN that binds to the target site as heterodimers and the basic structure of a TALEN monomer.

TALEs can be engineered with standard restriction enzyme digestion and ligation (REAL) method[125], but assembly of the individual monomer is laborious. With the Golden Gate cloning techniques[126], fast ligation-based automatable solid-phase high-throughput (FLASH) method[127], or more recently developed unit assembly strategies[128], customized TALENs can be relatively easily customized and assembled to target virtually any DNA sequence. Engineered TALENs have been widely applied to sequence-specific editing in plants, animals, and a variety of human cells. Its advantages in the cleavage specificity and efficiency with minimal cytotoxicity have been confirmed by many studies[116,129–131].

a.

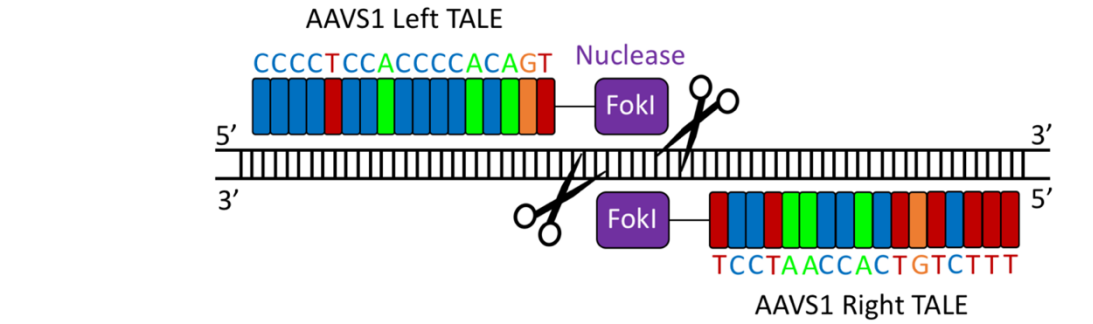

AAVS1 target 5' – **CCCCTCCACCCCACAGT**ggggccactagggac**AGGATTGGTGACAGAAA** – 3'

b.

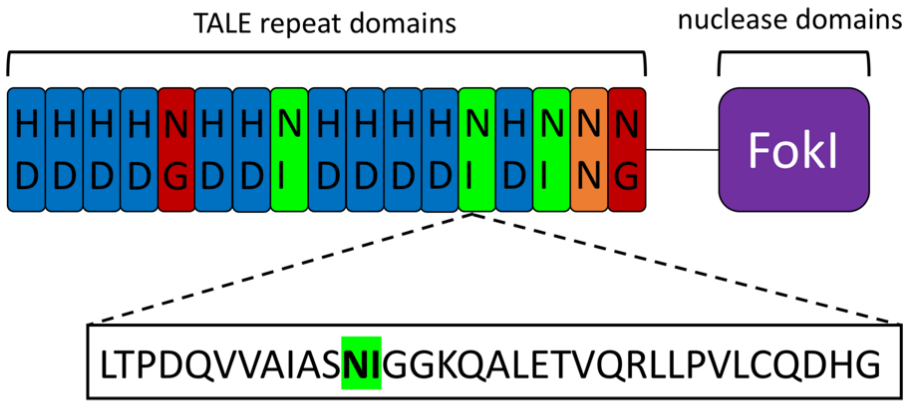

Figure 1-2. TALEN targeting the AAVS1 site

a. Schematic diagram of TALEN heterodimers binding to the AAVS1 locus. Each arm recognizes and binds to 17 target nucleotides. DNA cleavage by FokI occurs in the spacer sequence between binding sites of the two TALEN units. **b.** Schematic diagram of a TALEN unit. Letters in each repeat represent the RVDs at positions 12 and 13. N-terminal and C-terminal domains of TALE are not shown in the figure, but they are also required for DNA binding.

1.5 DNA repair pathways and transgene integration

Eukaryotic cells undergo DNA repair when a DSB is generated through either non-homologous end joining or homology-directed repair. The two pathways have been intensively studied because they lead to different outcomes at the break and therefore may be adopted for different applications for gene editing.

1.5.1 Non-homologous end joining (NHEJ)

The NHEJ pathway is characterized by the absence of 5' end resection and direct ligation of the DBS ends. This process is mediated by the Ku70-Ku80 heterodimer (Ku) which holds the ends close to each other and protects them from resection, ligase IV (LIG4) which is responsible for the ends ligation, and a range of different regulatory factors[132]. NHEJ is active throughout the cell cycle, although it occurs more frequently in G1 cells[133,134]. NHEJ is an error-prone mechanism that often results in small (1-10 bp) but very heterogeneous insertions, deletions, or substitutions at the break site. Approximately two-thirds of them will lead to a frameshift mutation[132]. Therefore, the pathway is widely used for generating gene knock-outs.

1.5.2 Homology-directed repair (HDR)

Unlike the error-prone NHEJ pathway, HDR results in high-fidelity repair by using a homologous donor template for DNA synthesis. HDR occurs at a lower frequency than NHEJ, predominantly in S and G2 phases during which the sister chromatid can be used as the template[133,134]. The HDR pathway is more desired for applications in accurate gene knock-in, where a repair donor template with upstream and downstream homologous arms can be provided in the form of a single-stranded oligonucleotide for small insertions or double-

stranded plasmid DNA for larger insertions. At the beginning of HDR, the break site resection is mediated by helicases and nucleases such as MRN, CtIP, and EXO1, creating 3' single-stranded overhangs. The overhangs are then bound by RAD51 recombinase to invade the homologous double-stranded DNA[135]. The mechanism by which the cells make choice between the competing NHEJ and HDR pathways is still unclear, but apparently, it is heavily regulated and influenced not only by the cell cycle, but also by the concentration of donor templates, the length of homologous overlaps, and expression of regulatory genes[136–138].

1.6 Model cell line for CF research

The study of human diseases, especially genetic diseases like CF greatly relies on the development of immortalized cell lines. *In vitro* cell models for CF not only help researchers to better understand the physiological, molecular, and biochemical mechanism of the disease, but also provide valuable insight for subsequent *in vivo* tests of therapeutic strategies. The IB3-1 cell line was derived from primary human CF bronchial epithelial cells heterozygous for F508del and a nonsense mutation W1282X, immortalized by adeno-SV40 hybrid virus transformation[139,140]. For this thesis, the CFTR-defective IB3-1 cell line is an appropriate model because it largely represents the primary *in vivo* target in the airway. On the other hand, an IB3-1 derived 8-3-7 inducible cell line was generated previously in our lab by transfection of a reverse tetracycline-inducible transcription activator (rtTA) expression cassette and a CFTR expression cassette with tetracycline response element. In the presence of doxycycline, a derivative of tetracycline, rtTA is expressed and it turns on CFTR expression by binding to the tetracycline response element[141]. Nevertheless, immortalized cell lines are isolated clones from the mixed population of primary epithelial cells and grown in altered conditions. They

may not always have the same phenotypic characteristics of the original culture. The IB3-1 cells used in this thesis also lack differentiated features such as tight junction and cilia formation[139]. These limitations of *in vitro* models should be taken into consideration when extrapolating the results to *in vivo* studies.

1.7 Hypothesis and objectives

Permanent integration of a wild-type human CFTR gene expression cassette into the genome of airway epithelial cells is essential for CF lung gene therapy, as it reduces the risk of host immune responses caused by repeated administration. The utilization of TALEN system allows targeted DSB at the AAVS1 site, where a CFTR expression cassette can be integrated by HDR. The large packaging capacity (36 kb) of HD-Ad makes the delivery of a pre-established TALEN system together with a CFTR cDNA expression cassette and two 4 kb homology arms possible in one single vector. An overview of the strategy used for this thesis is shown in Figure 1-3.

I hypothesize that **efficient TALEN-mediated integration of human CFTR gene into the AAVS1 locus in cultured airway epithelial cells can be achieved by delivery of the TALEN system along with the donor CFTR expression cassette using HD-Ad vectors.**

Two aims of the research are described in this thesis:

1. To determine the integration efficiency of a UBCLacZ reporter expression cassette in cultured IB3-1 airway epithelial cells and
2. To determine expression and functional correction of a K18CFTR expression cassette in IB3-1 cells.

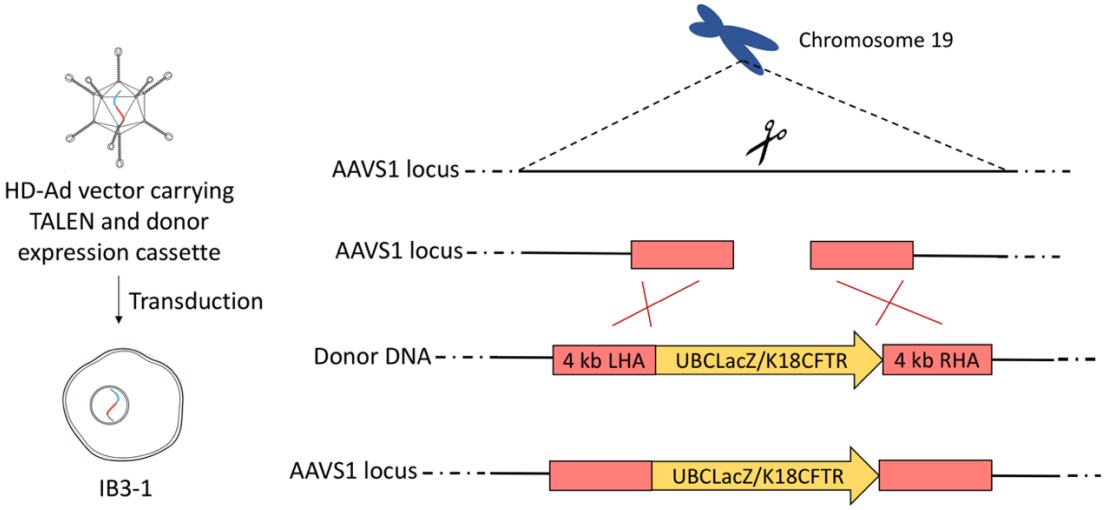

Figure 1-3. Strategy overview

HD-Ad vectors carrying TALEN and the donor expression cassette are produced from corresponding HD-Ad plasmids and transduced into IB3-1 cells. TALEN-mediated DBS is generated at the designated target site in the AAVS1 locus. The 4 kb homology arms on the donor DNA allow the integration of transgene expression cassettes to the target site through HDR. LHA, left homology arm. RHA, right homology arm.

2 Integration efficiency of a UBCLacZ reporter expression cassette in IB3-1 cells

2.1 Rationale

The first step to evaluate our strategy *in vitro* is to determine how efficiently a transgene will be integrated to the designated target site for long-term, stable expression in the airway epithelial cells. Therefore, we delivered TALEN and a LacZ expression cassette as a reporter gene with homology arms to IB3-1. The LacZ gene encodes the β-galactosidase protein, which mediates the cleavage of X-gal (5-bromo-4-chloro-3-indolyl-β-D-galactopyranoside) and yields a blue and insoluble product[142]. Thus, the expression of LacZ can be easily visualized through the staining method. We fused the LacZ gene under a human ubiquitin C (UBC) promoter which has been used by previous studies to drive a strong *in vivo* LacZ expression in airway basal cells[143]. The cassette also includes an upstream nuclear localization signal (NLS) to restrict LacZ expression to the nucleus. The UBCLacZ expression cassette is flanked by a right and a left homology arm for HDR at the target site. Each of the homology arms is about 4 kb in length for optimal efficiency. The overall design allows us to determine the integration efficiency by counting LacZ positive rate after passing the transduced cells to dilute the residual vectors.

2.2 Material and Methods

2.2.1 Basic molecular techniques

Basic molecular techniques described in this section were routinely applied for molecular cloning, verification of the plasmid constructs, sample collection, and sample analysis. Same protocols were followed throughout this thesis unless otherwise specified.

Restriction enzyme digestion. All restriction digestions were performed with New England Biolabs enzymes following the manufacturer's protocol. Incubations for enzyme

digestions were performed in 37°C water bath and the reactions were heat-inactivated on a Thermomixer Compact (Eppendorf).

Agarose gel electrophoresis. Depending on purpose of the experiment, 0.6 – 2% agarose gels were made with UltraPure Agarose (Invitrogen) in TAE buffer (40 mM Tris-acetate, 1 mM EDTA, pH 8.3). RedSafe Nucleic Acid Staining Solution (FroggaBio) was added before pouring the gel. DNA samples were prepared by adding Gel Loading Dye (New England Biolabs) and were loaded to the wells. Agarose gels were run in TAE buffer, pH 8.3 at 100 V for approximately 1 hour.

DNA fragment purification from agarose gel. One percent agarose gels were used to separate the desired DNA fragment for purification from the gel. The bands of interest were observed and cut out from the gel under long wavelength UV light, then transferred to 1.5 mL microtubes. The DNA fragments were then purified with QIAquick Gel Exaction Kit (QIAGEN) following the manufacturer's protocol.

Ligation. Ligation reactions were performed with the Rapid DNA Ligation Kit (Thermo Fisher Scientific) according to the manufacturer's protocol. The mixtures were stored at 4°C until use.

Transformation. A desired amount of plasmid DNA or ligation reaction was added to 100 μL of thawed Stellar Competent Cells (Clontech) and incubated on ice for 20 minutes. After incubation, the mixture was heat shocked at 42°C for 50 seconds and immediately cooled on ice. Aseptically, 1 mL of SOC medium (Clontech) was added to the cells, and the cells were allowed to recover in a 37°C shaker for 45 minutes. The cells were then plated on 2x YT agar (16 g tryptone, 10 g yeast extract, 5 g sodium chloride, 15 g bacteriological agar in 1 L distilled water) plates with 100 μg/mL ampicillin and incubated at 37°C overnight.

Mini-prep plasmid isolation. Bacterial colonies were picked from the plates, and each colony was aseptically inoculated into sterile tubes containing 1.5 mL of 2x YT broth medium (16 g tryptone, 10 g yeast extract, 5 g sodium chloride in 1 L distilled water) with 100 μg/mL ampicillin. The tubes were incubated at 37°C overnight with shaking and aeration. The cells were then centrifuged fat 8000 rpm for 2 minutes and resuspended in 150 μL of P1 buffer (50 mM Tris-HCl, pH 8.0, 10 mM EDTA). Then, 150 μL of P2 buffer (0.2 M NaOH, 1% SDS) was added and the tubes were inverted for several times. When an increased viscosity was observed, 150 μL of P3 buffer (3 M potassium acetate, pH 5.5) was added to the mixture and the tubes were incubated on ice for 10 minutes. When the incubation was done, the tubes were centrifuged at 14000 rpm for 10 minutes at 4°C, and the supernatant in each sample was transferred to a clean 1.5 mL microtube. 900 μL of 100% ice-cold ethanol was added to each sample. The tubes were inverted for several times and centrifuged at 14000 rpm for 5 minutes at room temperature. The supernatant was removed from each tube, and the DNA pellets were washed with 1 mL of ice-cold 70% ethanol. The resulting DNA pellets were air-dried and re-dissolved in 40 μL of TE buffer (10 mM Tris-HCl, 1mM EDTA, pH 8.0). The mini-prep plasmid DNA samples were stored at -20°C until use.

Midi-prep plasmid isolation. Bacterial colonies were picked from the plates and aseptically inoculated into sterile tubes containing 1.5 mL of 2x YT broth medium with 100 μg/mL ampicillin. The tubes were cultured at 37°C for 8 hours with shaking and aeration. After incubation, 300 μL of broth culture from each tube was transferred aseptically into a sterile flask containing 100 mL of fresh 2x YT broth medium with 100 μg/mL ampicillin and incubated at 37°C overnight with shaking and aeration. On the next day, the broth cultures were poured into centrifuge bottles and centrifuged at 4800 rpm for 15 minutes. The cell pellets

were re-suspended in 7 mL of P1 buffer and transferred to 50 mL Falcon tubes, followed by the addition of 7 mL of P2 buffer to each sample. The tubes were inverted for several times, and 7 mL of P3 buffer was added to each sample. Next, the tubes were incubated on ice for 10 minutes and centrifuged at 4800 rpm for 10 minutes. The resulting supernatant was transferred to clean 50 mL tubes, and 13.5 mL of isopropanol was added to each sample allowing the DNA to precipitate. The tubes were centrifuged at 4800 rpm for 10 minutes, and then the crude DNA pellets were re-suspended in 400 μL of TE buffer and transferred to clean 1.5 mL microtubes. Two hundred microliters of 7.5 M ammonium acetate was added to each tube. The tubes were incubated on ice for 5 minutes and centrifuged at 4°C for 5 minutes. Then, the supernatant was transferred to clean microtubes and 800 μL of ice-cold 100% ethanol was added to each sample for the DNA to precipitate. The tubes were centrifuged at 14000 rpm for 5 minute, and the DNA pellet was re-dissolved in 400 μL of TE buffer. Ten microliters of 10 mg/mL RNase A was added to each sample and incubated at 37°C for 1 hour before proceeding to the phenol chloroform purification (methods were described below). The purified midi-prep plasmid DNA samples were stored at -20°C until use.

Phenol chloroform purification. To each plasmid or genomic DNA samples, an equal volume of UltraPure Phenol:Chloroform:Isoamyl Alcohol 25:24:1, v/v (Invitrogen) was added and mixed thoroughly with vortex. The mixtures were centrifuged at 14000 rpm for 5 minutes. After centrifugation, the upper aqueous layer was collected and transferred to a clean microtube without disturbing the interphase. Next, 0.5 volume of 7.5 M ammonium acetate and 2 volumes of ice-cold 100% ethanol was added to each sample. The tubes were inverted for several times allowing the DNA to precipitate and then centrifuged at 14000 rpm for 5 minutes at room temperature. Then, the supernatant was removed and the DNA pellets were

washed with 1 mL of ice-cold 70% ethanol. The pellets were then air-dried and re-dissolved in a desired amount of TE buffer.

Genomic DNA isolation from adherent cells. The adherent cell cultures in 6-well plates were gently washed with PBS, pH 7.4 for two times and lysed in 400 μL of Tail Lysis Buffer (100 mM Tris-HCl, pH 8.0, 5 mM EDTA, 0.2% SDS, 200 mM NaCl) and 10 μL of proteinase K (Thermo Fisher Scientific) at 50°C for 2 hours with shaking. Next, the proteinase K was heated inactivated at 65°C for 20 minutes and 10 μL of 10 mg/mL RNase A was added to each sample. The RNA was digested at 37°C for 10 minutes, and then the samples were subjected to phenol chloroform purification as described above. The purified genomic DNA samples were stored at -20°C until use.

DNA quantification. The concentration and purity of plasmid or genomic DNA samples were determined from the OD readings on a SimpliNano Spectrophotometer (GE Healthcare Life Sciences). Proper blanks were used for different samples before the measurements.

Sanger sequencing. Sanger sequencing reactions for the DNA samples described in this thesis were performed by The Center for Applied Genomics (TCAG) at the Hospital for Sick Children. The samples to be sequenced were prepared by mixing 200 – 300 ng of DNA in a volume of 7 μL with 5 ng of desired primer in a volume of 0.7 μL. Primers used for sequencing were synthesized by ACGT Corporation.

2.2.2 Construction of pHD-Ad-UBCLacZ-TALEN

TALEN used for this thesis was generated by Dr. Bo Zhang's lab (Peking University, Beijing, China) using the Unit Assembly method, carried by a pBSII-SK(+) backbone with a

CMV-EGFP marker[128]. The RVDs HD-HD-HD-HD-NG-HD-HD-NI-HD-HD-HD-HD-NI-HD-NI-NN-NG and NG-NG-NG-HD-NG-NN-NG-HD-NI-HD-HD-NI-NI-NG-HD-HD-NG recognize a region in the AAVS1 site within the human chromosome 19 with a 15-nucleotude spacer. Generation of the UBCLacZ expression cassette carried by pBSII-SK(+) backbone plasmids was described in the previous study[144]. Left and right homology arms (4kb) were amplified from human cell line A549 (CCL-185) obtained from American Type Culture Collection (ATCC), and the sequences were fused to expression cassettes using the In-Fusion HD Cloning Kit (Clontech Laboratories). The UBCLacZ expression cassette with homology arms was cloned into an HD-Ad backbone plasmid pC4HSU (NotI/SalI)[145]. The PmeI sites on the resulting vectors were switched to PacI sites using infusion cloning. The assembled UBCLacZ plasmid pC4HSU-UBCLacZ-L4-R4 was linearized with NheI followed by blunt end treatment with T4 DNA polymerase (New England Biolabs), then digested with NsiI. The TALEN insert was cleaved from the backbone by FspI and Nsil digestion, then ligated to the linearized vector. The resulting vector was denominated as pHD-Ad-UBCLacZ-TALEN.

2.2.3 Production of HD-Ad-UBCLacZ-TALEN

Methods for HD-Ad viral production were modified from Ng et al[110].

Cell culture. 116 cells were cultured in MEM medium (Life Technologies) supplemented with 10% heat inactivated FBS (Wisent), 100 U/ml penicillin streptomycin, and 0.1 mg/ml hygromycin B (BioShop). 116 cells were grown at 37°C with 5% CO2 in humidified air and split 1:5 twice a week. Same growth media and conditions were used for 116 cells throughout the study unless otherwise specified.

Rescue. Ten micrograms of pHD-Ad-UBCLacZ-TALEN was linearized by PacI digestion to expose the terminal ITR. The linearized plasmid was purified by phenol chloroform extraction and dissolved in sterile TE, pH 8.0. 116 cells were seeded into a 6 cm dish and transfected with the linearized DNA upon 70% confluency using the jetPRIME Versatile DNA/siRNA Transfection Reagent (Polyplus Transfection) according to the manufacture's protocol. After 24 hours, the growth medium was aspirated and replaced by 0.5 ml of warm serum-free, antibiotic-free MEM. NG163 helper virus was added to the cells at 5 multiplicity of infection (MOI) and allowed for absorption at 37°C with occasional shaking for 1 hour. Then, fresh medium was added to a final volume of 3 ml. The cells displayed cytopathic effect (CPE) 48 hours after the addition of helper virus and were collected together with the medium into 15 mL Falcon tubes. Sucrose was added to the cells to a final concentration of 4% for long-term storage at -80°C.

Amplification. The harvested cells were lysed through three freeze-thaw cycles on 37°C water bath and dry ice. To amplify the viral vectors, freshly seeded 116 cells in a 6 cm plate was co-transduced with the cell lysate and NG163 upon 70% confluency. Before transduction, the old growth media was aspirated from the plate. One milliliter of the cell lysate and NG163 at 2 MOI were added to the cell monolayer. Again, the cells were incubated at 37°C with occasional shaking for 1 hour, and then fresh growth medium was added to a final volume of 3 ml. The cells were harvested 48-hour post-transduction upon CPE in 15 mL Flacon tubes with 4% sucrose and were stored at -80°C. The co-transduction was repeated for four more passages to increase the viral titre. For the later passages, one 10 cm dish, one 15 cm dish, eight 15 cm dishes, and ten 15 cm dishes of 116 cells respectively were co-transduced

with cell lysate from the previous passage and NG163 at 2 MOI. The final cell lysate was collected in a 50 mL Falcon tube with 4% sucrose and were stored at -80°C.

Large-scale amplification. 116 cells were grown in thirteen 15 cm plates to 90% confluency and seeded into a 3 L spinner flask (Bello biotechnology) containing 1 L of growth media. The speed of spinner flask was set to 75 rpm. 500 mL of growth media was added to the spinner flask 24 hours and 48 hours after seeding respectively. One liter of growth media was added to the flask on the third day. On the fourth day, the cells were poured into nine 500 mL centrifuge bottles and were centrifuged at 2000 rpm for 10 minutes at 4°C. After centrifugation, the cell pellets were re-suspended with 20 mL of conditioned growth media then transferred to a 250 mL spinner flask. The cell lysate from the latest amplification passage was frozen and thawed for 3 times in 37°C water bath and dry ice, then added to the 250 mL spinner flask. NG163 was added to the mixture at 1 MOI. The 250 mL spinner flask were set to stir at 75 rpm and were incubated at 37°C for 2 hours. After incubation, the mixture and additional 460 mL of conditioned growth media was transferred to a 3 L spinner flask containing 1.5 mL of pre-warmed viral transduction media (5% heat-inactivated FBS, 100 U/ml penicillin streptomycin, and 0.1 mg/ml hygromycin B in MEM). The final mixture was incubated at 37°C with stir at 75 rpm for 3 days. After 3 days, 5 mL of the suspension culture was collected in a 15 mL Falcon tube for orcein staining of inclusion body, and the rest was harvested by centrifugation at 2000 rpm for 10 minutes at 4°C. The cell pellets were re-suspended in 17 mL of sterile 10 mM Tris-HCl, pH 8.0 in a 50 mL Falcon tube. Sucrose was added to a final concentration of 4% for long-term storage at -80°C.

Orcein staining of inclusion body. This protocol is adapted from Graham and Prevec[146]. The collected cells were centrifuged at 1000 rpm for 10 minutes at room temperature.

The cell pellet was re-suspended with 0.5 mL of 1% sodium citrate and incubate for 10 minutes at room temperature. The cells were fixed for 10 minute at room temperature by adding 0.5 mL of Carnoy's fixative solution (3:1 methanol to glacial acetic acid). Then, 1 mL of 1% sodium citrate was added and the cells were centrifuged at 1000 rpm for 10 minutes at room temperature. The cell pellet was re-suspended in 150 μL of 1% sodium citrate. One drop of the cell suspension was added onto a glass slide (VWR) and thoroughly air dried. One drop of Orcein staining solution (2% Orcein and 50% glacial acetic acid in) was added on the top of dried cells. A cover slip (VWR) was placed on the cells before examining the inclusion bodies under the bright field microscope.

Purification. One and a half milliliters of 5% sodium deoxycholate in 10 mM Tris-HCl, pH 8.0 was added to the cells harvested from the large-scale amplification. The cells were incubated for 30 minutes on a tube rotator at room temperature. Ten microliters of 250 U/μL benzonase DNase (EMD Millipore) and magnesium chloride at a final concentration of 2 mM were added to the cell lysate and incubated for another 30 minutes under the same conditions. After incubation, the mixture was centrifuged at 5500 rpm for 15 minutes at 4°C. The supernatant was collected and added to 14 x95 mm ultracentrifuge tubes (Beckman) on top of the cesium chloride concentration gradients. Each tube contains 0.5 mL of 1.5 g/mL cesium chloride at the bottom, 3 mL of 1.35 g/mL cesium chloride in the middle layer, and 3 mL of 1.25 g/ mL cesium chloride at the top. The balanced tubes were secured in ultracentrifuge tube buckets and placed to the rotor. The tubes were centrifuged at 35000 rpm for 1 hour at 4°C. After ultracentrifugation, the virus band at the interface of 1.35 g/mL and 1.25 g/mL cesium chloride was withdrawn from the tubes with a 20 gauge needle and collected in a 15 mL Falcon tube. For the second purification, the collected band was loaded to new ultracentrifuge tubes

containing 7 mL of 1.35 g/mL cesium chloride and centrifuged at 35000 rpm overnight at 4°C. On the next day, the virus band was collected from the tube and injected to a 3 mL 10K MWCO Slide-A-Lyzer dialysis cassette (Thermo Fisher Scientific).The cassette was dialyzed in 10 mM Tris-HCl buffer, pH 8.0 for 24 hours, with the buffer changed every 8 hours. The dialyzed viral prep was withdrawn from the cassette with a 18 gauge needle. For spectrophotometer quantification, 2.5 μL of the viral prep was saved in a clean microtube, and the rest was supplemented with glycerol to a final concentration of 10% and aliquoted to sterile microtubes for long-term storage at -80°C.

Alternatively, the cell lysate from the large-scale amplification may be quickly purified with the Adenovirus Standard Purification ViraKit (VIRAPUR) following the manufacturer's protocol. The eluted virus in the buffer provided in the kit were supplemented with glycerol to a final concentration of 10% and stored at -80°C.

Viral quantification. Saved purified vectors were diluted in distilled water for spectrophotometer quantification at 260 nm. Final virus particle number = OD_{260} x dilution factor x 0.9 x 10^{12}. In addition to the spectrophotometric assessment, qPCR was applied for quantification of the viral preparations with primers that bind specifically to the adenovirus packaging signal 5' CAG GAA GTG ACA ATT TTC GCG C 3' (forward primer) and 5' CGC GCT ATG AGT AAC ACA AAA TTA TTC AG 3' (reverse primer). The qPCR was performed with Power SYBR Green PCR Master Mix (Thermo Fisher Scientific) on a QuantStudio 3 Thermal Cycler (Applied Biosystems).

2.2.4 HD-Ad transduction

Cell culture. IB3-1 cells (ATCC CRL-2777) were grown in DMEM medium (Life Technologies) containing 10% heat inactivated FBS (Wisent) and 100 U/ml penicillin streptomycin (Life Technologies). The cells were cultured at 37°C with 5% CO2 in humidified air and split 1:7 twice a week. Same growth media and conditions were used for IB3-1 cells throughout the study unless otherwise specified.

Transduction. IB3-1 cells were seeded in 6-well dishes and cultured until 70% confluency. Before transduction, the cells were washed once with warm PBS, pH 7.4. The cells were transduced with 50 MOI and 100 MOI of HD-Ad-UBCLacZ-TALEN vectors in 0.5 mL of serum-free, antibiotic-free DMEM. Controls were transduced with 100 MOI of HD-Ad-UBCLacZ vectors. Cells were incubated for 1 hour with rocking per 10 min. Warmed regular medium was added to the cells to a final volume of 2 ml per well.

Passage. Transduced IB3-1 cells were cultured for 5 days before the first passage. After the first passage, the cells were split twice per week at a ratio of 1:7.

2.2.5 T7E1 assay

Cleavage efficiency analysis. Cells transduced with HD-Ad-UBCLacZ-TALEN or HD-Ad-UBCLacZ control vectors were collected and lysed in 50 μL Cell Lysis Buffer with Protein Degrader from the GeneArt Genomic Cleavage Detection Kit (Life Technology) according to the manufacturer's instructions 72 h post-transduction. A 644 bp region covering the TALEN target site was amplified with the AmpliTaq Gold 360 Master Mix (Life Technology). Sequences of the primers are: 5' GAT CCT CTC TGG CTC CAT CGT AAG CAA AC 3' (forward primer) and 5' GAT GGC CTT CTC CGA CGG ATG TCT C 3' (reverse

primer). Two hundred nanograms of PCR product in each sample was mixed with 2 μl of 10X NEBuffer 2 and nuclease-free water to a final volume of 19 μL. The PCR products were denatured at 95°C for 5 min, followed by re-annealing at a ramp rate of -2°C/s from 95-85°C and -0.1°C/s from 85-25°C. Ten units of T7 endonuclease I (New England Biolabs) was added to the annealed PCR products immediately. For T7E1-negative control reactions, 1 μL of nuclease-free water were added instead. The mixtures were incubated at 37°C for 30 min before the reactions were terminated by adding 1.5 μL of 0.25 M EDTA. The reactions were visualized on a 2% agarose gel. The band intensities were analyzed with ImageJ, and the cleavage efficiency was quantified according to the following formula for assessment of TALEN-induced NHEJ[147]: % cleavage efficiency = 100 x sum of cleaved products / (cleaved products + parent peak).

Off-target analysis. The same methods were applied except that the PCR was designed to amplify regions around the top 3 off-target sites predicted by TALENoffer (http://galaxy.informatik.uni-halle.de/root?tool_id=TALENoffer). Sequences of primers sequences and the corresponding length of the amplicons are: 5' GTA CAG CAA TCT AAG GAA GTA GAC TCT TAG G 3' (forward primer) and 5' GTT TCA CTA TGT TGG TCA GGC TGC TC 3' (reverse primer) for off-target site #1 (738 bp), 5' GTC TGA TTG TGC AGG TTG TGT AGG ATC 3' (forward primer) and 5' CAC CCA AGT GCT GAC CTT ACT GC 3' (reverse primer) for off-target site #2 (687 bp), and 5' CAG CAG TCA GGG TTG TTC AGT TTG TTC 3' (forward primer) and 5' CCT AAA CCT TGG TGG CTA AAC ACA GTA AAA G 3' (reverse primer) for off-target site #3 (763 bp).

2.2.6 Junction PCR analysis.

Genomic DNA of cells transduced with TALEN viral vectors or control vectors were collected 5-day post-transduction. Junction PCR was performed on a SimpliAmp Thermal Cycler (Applied Biosystems). The sequences of primer sets used and the size of amplicons are as follows: UBCLacZ left junction, 4.5 kb amplicon, 5' CAT CAG CGA TGC AAT GAT GCT TGG GTT TGC ACC AAT G 3' (forward primer), 5' TCC TTC TGC TGA TAC TGG GGT TCT AAG GCC GAG TC 3' (reverse primer); UBCLacZ right junction, 4.4 kb amplicon, 5' GGT TTT TCA CAG ACC GCT TTC TAA GG 3' (forward primer), 5' GTT GGA GGA GGA AGG AGA CAG AAT CC 3' (reverse primer). Eight microliters of each PCR reaction was visualized on a 0.8% agarose gel. PCR products were purified using the NucleoSpin Gel and PCR Clean-up Kit (Macherey-Nagel) following the manufacturer's instructions. Three hundred nanograms of purified products were subjected to EcoRV or AfeI digestion (New England Biolabs) at 37°C for 2 h. The reactions were run on 1% agarose gels. Sanger sequencing was performed by the TCAG Sequencing Facility at the Hospital for Sick Children.

2.2.7 β-galactosidase staining

IB3-1 cells to be stained were washed with PBS, pH 8.0 and fixed in 0.5% glutaraldehyde in PBS for 15 min. After PBS washing, β-galactosidase staining solution (0.1% X-gal, 2 mM $MgCl_2$, 5 mM K-ferricyanide, 5 mM K-ferrocyanide in PBS) was added to cover the cell monolayer. The cells were incubated at 37°C overnight in dark. To terminate the reaction, the staining solution was removed from the dish and the cells were washed with PBS. To count the transduction efficiency, IB3-1 cells were stained 3 days post-transduction. To count the integration efficiency, IB3-1 cells were passed for 18 passages before staining. 20

images were taken randomly for each well under a bright field microscope at 100x magnification. The number of LacZ positive cells and the total number of cells in each image was recorded with ImageJ. The transduction and integration efficiencies were calculated according to the following formulas: % transduction = 100 x sum of LacZ positive cells from all 20 images / sum of total number of cells from all 20 images. % integration = 100 x sum of LacZ positive cells from all 20 images / (sum of total number of cells from all 20 images x transduction efficiency).

2.2.8 Single cell colonies

Transduced IB3-1 cells were cultured for 12 passages before single cell sorting. Upon 70% confluency, the cells were suspended in ice-cold PBS, pH 7.4 containing 1% FBS. The cells were incubated on ice in the dark with viability marker 7-aminoactinomycin D (7-AAD, BioLegend) at a concentration of 100 ng per million cells for 10 minutes. Live singlet cells were sorted on a MoFloXDP BRV/UV sorter (Beckman) directly to 96-well plates containing 100 μL of warm DMEM supplemented with 20% heat-inactivated FBS and 100 U/ml penicillin streptomycin. Sorted cells were incubated at 37°C with 5% CO2 in humidified air for approximately 2 weeks until they developed into colonies. The cells were then subjected to β-galactosidase staining before examining under a bright field microscope.

2.2.9 SCR7 treatment

The NHEJ inhibitor SCR7 (Xcess Biosciences) was added at desired concentrations directly to the IB3-1 cells 20 hours post-transduction. Treated cells were cultured until day 5 after the transduction and passaged as normal.

2.2.10 Flow cytometry

Cells were cultured in 6-well plates until 90% confluency for flow cytometry analysis. The cells were gently washed with PBS, pH 7.4, scraped from the plates in 1 mL of PBS, and spun down at 400 rpm for 1 minute at room temperature. The resulting cell pellet was resuspended in 300 μL of DMEM, high glucose, HEPES, no phenol red (Life Technologies) with 3 μL of 30 mM chloroquine diphosphate and incubated at 37°C for 30 minutes. Next, 3.3 μL of 1:10 diluted ImaGene Green C_{12}FDG substrate reagent (Invitrogen) was added to each sample and incubated at 37°C for 45 minutes in dark. After incubation, the cells were collected by centrifugation at 400 rpm for 1 minute. Each cell pellet was resuspended in 500 μL of the phenol red-free DMEM with 5 μL of 50 mM phenyl-ethyl β-D-thiogalactopyranoside (PETG) reagent (Invitrogen) and 3 μL of 7-AAD (BioLegend). The cell suspension was filtered into 5 mL Falcon polystyrene round bottom tubes and incubated on ice for 10 minutes in dark. Live singlet cells were run on a LSRII-CFI, VBGR 15-colour analyzer (Becton Dickinson). The flow cytometry data was analyzed with the FlowJo software (FlowJo, LLC, Ashland, OR).

2.2.11 Statistical analysis

GraphPad Prism software (GraphPad, La Jolla, CA) was used to analyze difference between groups. Unpaired student's t-test was used for the comparison between means of two groups. A p value less than 0.05 was considered statistically significant. Error bars were shown in standard error of the mean (SEM).

Table 2-1. Plasmid constructs used for Aim 1

Plasmid	Size (bp)	Details
pBSII-SK(+)	2961	Contains Amp resistance gene and MSC
pBSII-SK(+)-UBCLacZ-Neo	9366	Modified pBSII-SK(+) with UBCLacZ-Neo expression cassette inserted into MSC
pBSII-SK(+)-UBCLacZ-Neo-L4-R4	17198	Modified pBSII-SK(+)-UBCLacZ-Neo with left and right homology arms flanking the UBCLacZ-Neo expression cassette
pBSII-SK(+)-TALEN	13269	Modified pBSII-SK(+) with genes encoding for left and right TALEN units flanking a GFP expression cassette
pC4HSU-PN	16278	HD-Ad backbone plasmid containing ITR and ψ
pC4HSU-PNE-U	9544	Modified pC4HSU-PN containing ITR and ψ, stuffer DNA partially removed
pC4HSU-UBCLacZ-Neo-L4-R4	27356	Modified pC4HSU-PNE-U with UBCLacZ-Neo-L4-R4 inserted
pHD-Ad-UBCLacZ-TALEN	33424	Final construct modified from pC4HSU-UBCLacZ-Neo-L4-R4 containing Amp resistance gene, ITR, ψ, TALEN, and UBCLacZ-Neo expression cassette flanked by left and right homology arms

Table 2-2. HD-Ad vectors used for Aim 1

Vector	Details
HD-Ad-UBCLacZ-TALEN	Carries GFP-labeled, TALEN-encoding sequences targeting the AAVS1 site, and UBCLacZ-Neo expression cassette flanked by a 4 kb left homology arm and a 4 kb right homology arm
HD-Ad-UBCLacZ	Carries a UBCLacZ-Neo expression cassette

Table 2-3. Oligonucleotide primers used for Aim 1

Primer	Sequence (5'-3')	Purpose
Infusion-U-LHA-F	CCAGCGGTGGCGGCCAGGTCGACGGTATCG	Forward primer for inserting left homology arm flanking LacZ-Neo reporter through In- Fusion
Infusion-U-LHA-R	GGAGGCCGAGCGGCCCCTAGTTATCAGCCAAGTC	Reverse primer for inserting left homology arm flanking LacZ-Neo reporter through In- Fusion
Infusion-U-RHA-F	TCAGCTTTGCACAAGGAATAGTCAACGAGC	Forward primer for inserting right homology arm flanking LacZ-Neo reporter through In- Fusion
Infusion-U-RHA-R	ATCCACTAGTTCTAGCTCTAAAGCTTCAGCCCAG	Reverse primer for inserting right homology arm flanking LacZ-Neo reporter through In- Fusion
Ad5-F	CAGGAAGTGACAATTTTCGCGC	Forward primer amplifying sequence near ψ for detection of HD-Ad vector
Ad5-R	CGCGCTATGAGTAACACAAAATTATTCAG	Reverse primer amplifying sequence near ψ for detection of HD-Ad vector
Hexon-F	GAGGATACTGCGTACTCGTAC	Forward primer amplifying sequence in *hexon* gene for detection of HV
Hexon-R	CAGGGCGTTGTAGGCAGTG	Reverse primer amplifying sequence in *hexon* gene for detection of HV
T7E1-F	GATCCTCTCTGGCTCCATCGTAAGCAAAC	Forward primer amplifying sequence near AAVS1 target site for T7E1 assay

T7E1-R	GATGGCCTTCTCCGACGGATGTCTC	Reverse primer amplifying sequence near AAVS1 target site for T7E1 assay
JPCR-UL-F	CATCAGCGATGCAATGATGCTTGGGTTTGCACCAATG	Forward primer for left arm junction PCR analysis of UBCLacZ integration
JPCR-UL-R	TCCTTCTGCTGATACTGGGGTTCTAAGGCCGAGTC	Reverse primer for left arm junction PCR analysis of UBCLacZ integration
JPCR-UR-F	GGTTTTTCACAGACCGCTTTCTAAGG	Forward primer for right arm junction PCR analysis of UBCLacZ integration
JPCR-UR-R	GTTGGAGGAGGAAGGAGA CAGAATCC	Reverse primer for right arm junction PCR analysis of UBCLacZ integration
JPCR-Seq-UL-in	GTAAGAGGTTCCAGTCAGAGG	Primer for sequencing of junction PCR product at the left homology arm of UBCLacZ, proximal junction
JPCR-Seq-UL-out	TGCACCAATGATATGCAGG	Primer for sequencing of junction PCR product at the left homology arm of UBCLacZ, distal junction
JPCR-Seq-UR-in	ACTGCTGTGTTCCAGAAG	Primer for sequencing of junction PCR product at the right homology arm of UBCLacZ, proximal junction
JPCR-Seq-UR-out	CCTAAAACAGGACCACTGG	Primer for sequencing of junction PCR product at the right homology arm of UBCLacZ, distal junction
OT1-F	GTACAGCAATCTAAGGAAGTAGACTCTTAGG	Forward primer amplifying off-target site #1 on chromosome 3 for T7E1 assay

OT1-R	GTTTCACTATGTTGGTCAGGCTGCTC	Reverse primer amplifying off-target site #1 on chromosome 3 for T7E1 assay
OT2-F	GTCTGATTGTGCAGGTTGTGTAGGATC	Forward primer amplifying off-target site #2 on chromosome 22 for T7E1 assay
OT2-R	CACCCAAGTGCTGACCTTACTGC	Reverse primer amplifying off-target site #2 on chromosome 22 for T7E1 assay
OT3-F	CAGCAGTCAGGGTTGTTCAGTTTGTTC	Forward primer amplifying off-target site #3 on chromosome 5 for T7E1 assay
OT3-R	CCTAAACCTTGGTGGCTAAACACAGTAAAAG	Reverse primer amplifying off-target site #3 on chromosome 5 for T7E1 assay

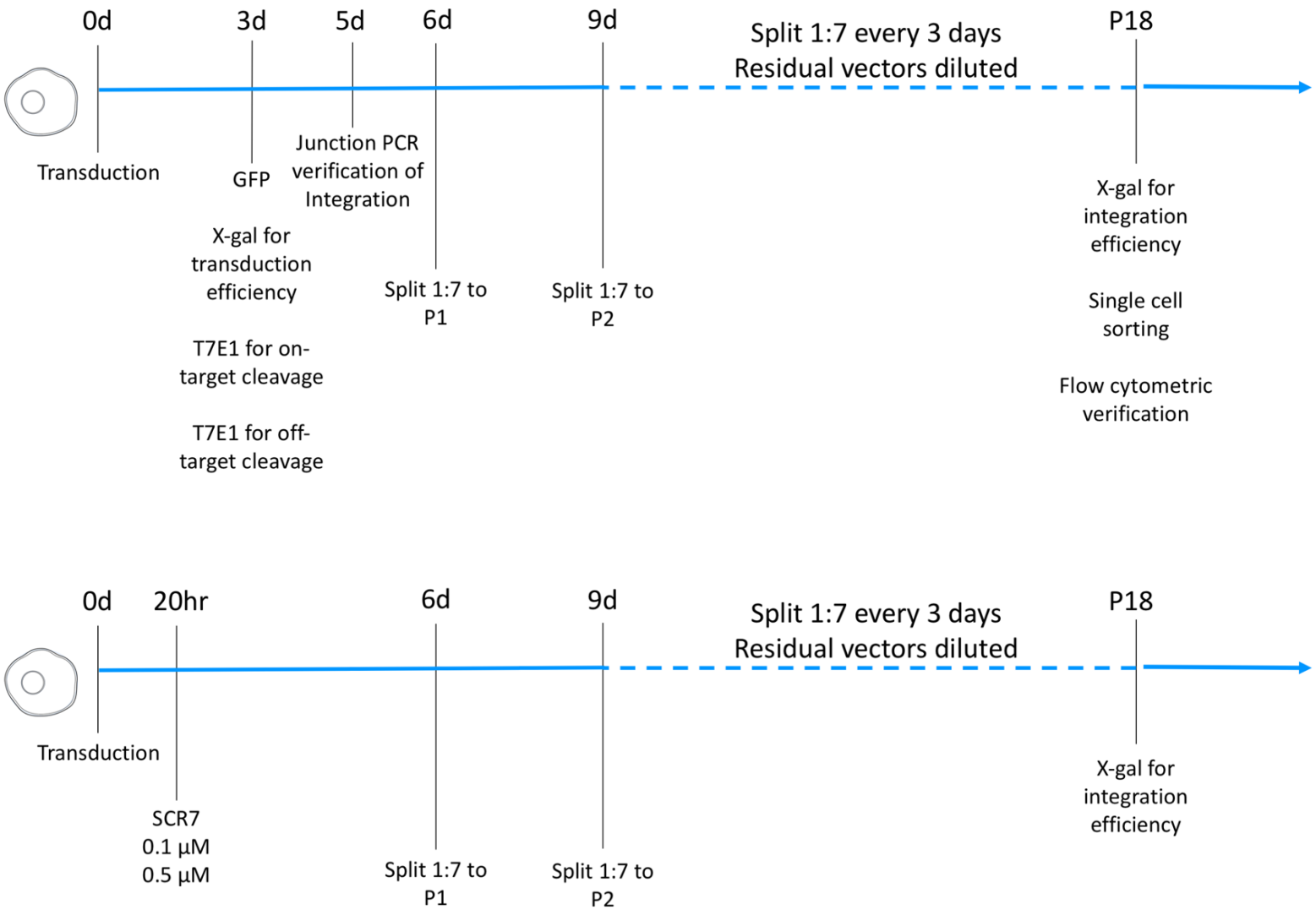

Figure 2-1. A schematic timeline on experimental design for Aim 1

2.3 Result

2.3.1 Verifying the pHD-Ad-UBCLacZ-TALEN construct

We built the pHD-Ad-UBCLacZ-TALEN plasmid construct by conventional molecular cloning for the subsequent viral production in 116 producer cells. To determine whether the plasmid construct was correctly built before proceeding to the next step, restriction enzyme digestions by PacI, BstBI, and BstZ17I were performed for verification. Location of the resulting fragments on gel matched the expecting size (Figure 2-2b). To further determine whether the important reporter LacZ and GFP genes on the construct can be properly expressed, we transfected IB3-1 cells with 2 μg of the plasmid DNA in 6-well plates. Three days after transfection, both GFP and LacZ expression were observed in transfected cells (Figure 2-2c).

a.

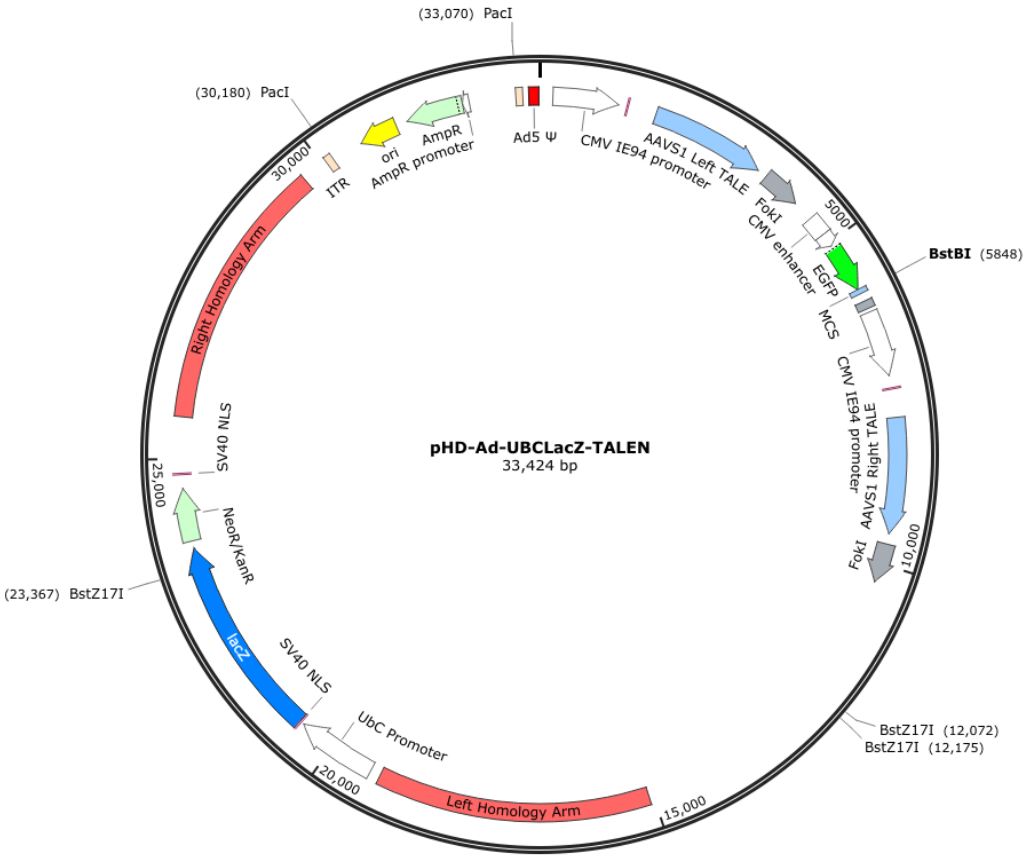

b.

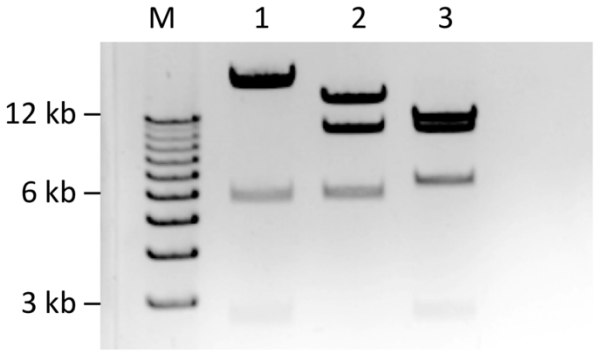

Size (kb)	24.3	15.8	12.3
	6.2	11.1	11.1
	2.9	6.2	6.8
		0.1	2.9
			0.1

c.

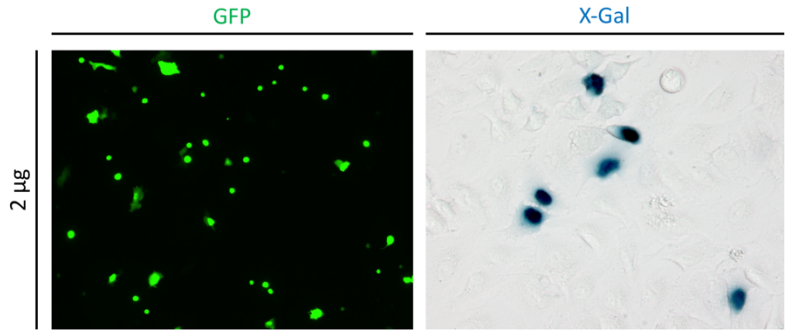

Figure 2-2. Verification of the pHD-Ad-UBCLacZ-TALEN construct

a. Schematic diagram of the 33 kb pHD-Ad-UBCLacZ-TALEN plasmid vector (generated in SnapGene). Restriction sites used for verification were labelled with their locations on the plasmid. **b.** Restriction enzyme digestion of the plasmid construct. Lane 1, PacI and BstBI. Lane 2, BstBI and BstZ17I. Lane 3, BstZ17I and PacI. M, DNA maker. Expected size of the resulting DNA fragments were listed below each lane. The 0.1 kb bands are not visible on this gel. **c.** IB3-1 cells under fluorescent microscope and subjected to β-galactosidase staining 3 days after transfection with the pHD-Ad-UBCLacZ-TALEN plasmid.

2.3.2 Producing the HD-Ad-UBCLacZ-TALEN vectors

To produce HD-Ad vectors, we first linearized the pHD-Ad-UBCLacZ plasmid construct with PacI to remove the bacterial sequences and expose the ITRs. The HD-Ad was rescued by transfecting 116 cells with the linearized pHD-Ad-UBCLacZ-TALEN, followed by helper virus NG163 transduction. In order to monitor the transfection and viral amplification, we observed the GFP expression and the morphological change of the producer cells before harvest (usually 48-hour post helper virus transduction). By this time, transduced 116 cells underwent cytopathic effect (CPE) as a result of virus invasion. The cells became round in shape and started to detach from the plate. At passage 0, high levels of GFP expression from plasmid DNA were found in the producer cells. We observed a sharp decrease of GFP from passage 0 to passage 1 as a result of plasmid DNA degradation over time. To amplify HD-Ad-UBCLacZ-TALEN, 116 cells were co-transduced with HD-Ad from the cell lysate and HV for 5 passages. Increasing levels of GFP expression from passage 1 to 5 indicate the propagation of HD-Ad vectors (Figure 2-3a). We obtained a maximum HD-Ad titre in passage 5 and proceeded to the large-scale amplification. In 3 L large-scale culture, inclusion bodies formed within the virus-producing cells, which were visualized by Orecin red staining (Figure 2-3b). After the first CsCl gradient ultracentrifugation, a white viral band was observed in each tube at the interphase, below the cellular debris. After the second purification, only the viral band is visible in the ultracentrifuge tube (Figure 2-3c). The final yield from the large-scale amplification and ultracentrifuge purification is 5.8×10^{11} viral particles. To quickly obtain a satisfactory amount of viral vectors, one tenth of the cell lysate from the large-scale amplification were directly purified with a membrane-based adenovirus purification kit. We achieved a final yield of 1.8×10^{11} viral particles from the purification kit.

To determine whether the purified viral vectors have proper activity for the future experiments, we transduced IB3-1 cells at 50 MOI and 100 MOI (Figure 2-4). Three days after transduction, we observed high levels of GFP and LacZ expression in transduced cells. The transduction efficiency was determined to be 96.7% at 50 MOI and 98.4% at 100 MOI by staining. The control vector HD-Ad-UBCLacZ transduced 98.3% of the cells at 100 MOI.

a.

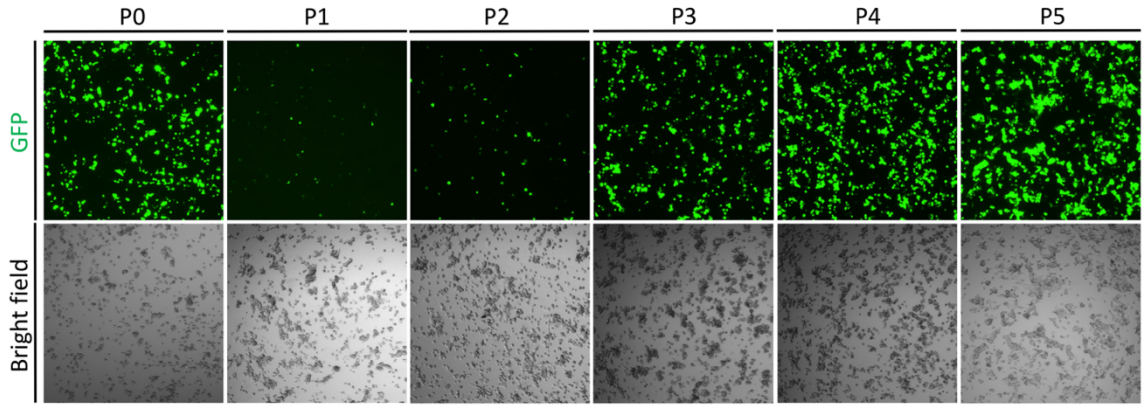

b.

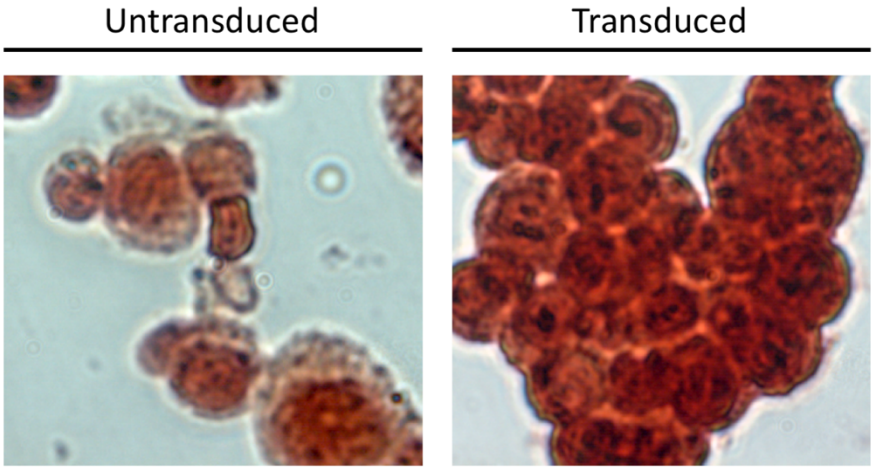

c.

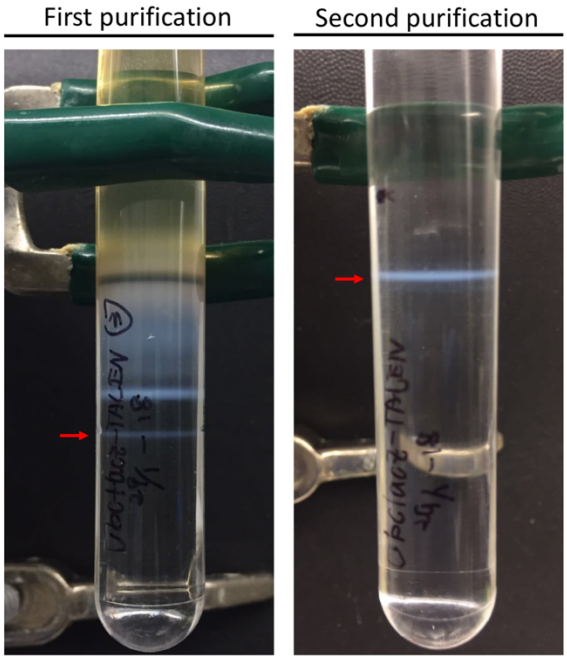

Figure 2-3. HD-Ad-UBCLacZ-TALEN amplification and purification

a. GFP expression in 116 cells 48-hour post NG163 transduction (512 nm) from passage 0 to passage 5 (P0-P5) and cells under normal light (bright field). **b.** Orcein red staining of untransduced and transduced 116 cells from the 3 L large-scale culture. **c.** Viral bands after the first and second CsCl gradient ultracentrifugation indicated by the red arrows.

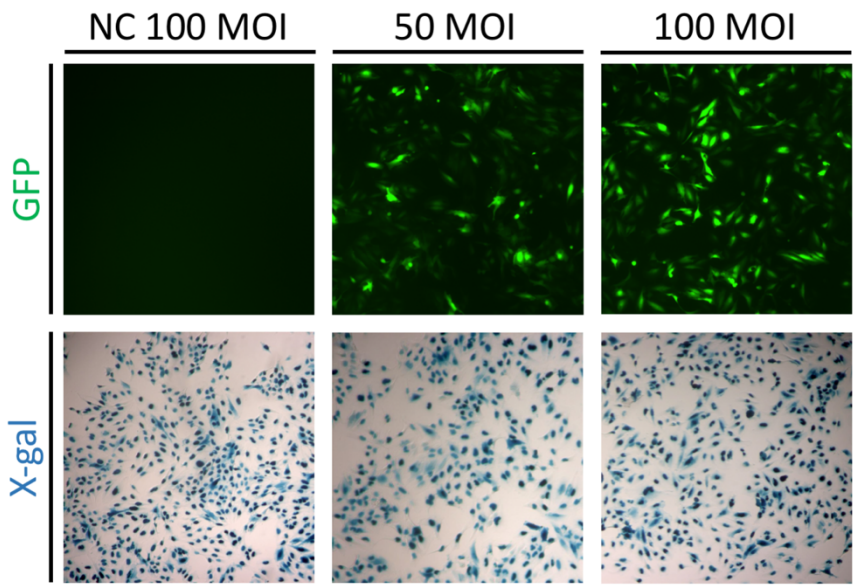

Figure 2-4. Transduction of IB3-1 cells with HD-Ad-UBCLacZ-TALEN

GFP expression in IB3-1 cells 3 days after transduction with HDAd-UBCLacZ-TALEN at 50 MOI and 100 MOI. LacZ expression was visualized by β-galactosidase staining (X-gal) 3-day post-transduction. NC, IB3-1 transduced with 100 MOI of HDAd-UBCLacZ.

2.3.3 Validating TALEN activity at AAVS1

We assessed the genomic cleavage efficiency of TALEN at the designated target site in the transduced cells using the T7 endonuclease (T7E1) assay (Figure 2-5). Short PCR products (~650 bp) at the target site formed hetero-duplexes after denaturation and reannealing, which were then recognized and cleaved by T7E1. After normalizing the band intensities to the negative control, we observed a cutting efficiency (NHEJ) of 36% in IB3-1 cells transduced by 50 MOI of HDAd-UBCLacZ-TALEN and 66% in cells transduced with 100 MOI of the

virus. In cells transduced with the control vector, there was no detectable cleavage at the AAVS1 site.

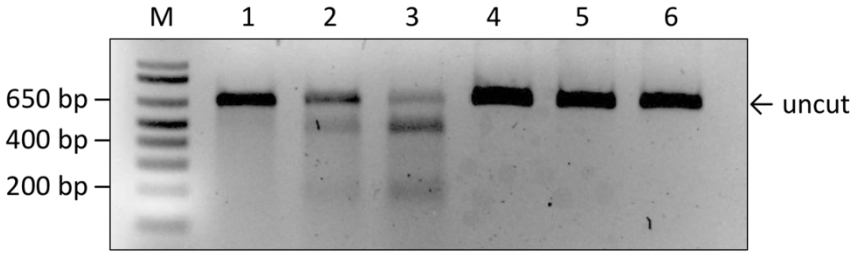

Figure 2-5. Assessment of on-target NHEJ induced by TALEN in IB3-1 cells

Lane 1 and 4, cells transduced with 100 MOI of control vector. Lane 2 and 5, 50 MOI of HD-Ad-UBCLacZ-TALEN. Lane 3 and 6, 100 MOI of HD-Ad-UBCLacZ-TALEN. Lane 1-3, with T7E1 treatment. Lane 4-6, without T7E1 treatment. M, DNA marker. Indicated by the arrow, the topmost band in each lane is the uncut parental band. The two lower bands in each lane represent the fraction of mismatched DNA.

2.3.4 Validating UBCLacZ integration at AAVS1

To detect integration of the UBCLacZ expression cassette at the proposed target site, we then performed junction PCR at both homology arms. At each junction, the forward primer was designed to bind the AAVS1 sequence immediately upstream to the target site, whereas the reverse primer bound to the expression cassette near the 5' junction region. Shown in Figure 2-6, we have obtained PCR products from cells transduced with 100 MOI of HD-Ad-UBCLacZ-TALEN at both homology arms, indicating transgene integrations at the correct location. In comparison, there was no detectable integration at the target site in cells transduced with 100 MOI of HD-Ad-UBCLacZ control vectors. The products obtained from junction PCR were further verified by restriction enzyme digestion and Sanger sequencing at the junctions.

Undesired gene modifications at off-target sites with highly similar sequences to the designed target is a major concern in gene editing studies. Cleavage at off-target sites was usually effectively detected with T7E1-based methods[148]. In this study, we predicted the potential off-target sites of the designed TALEN using an online program TALENoffer (http://galaxy.informatik.uni-halle.de/root?tool_id=TALENoffer). The top 3 potential sites with the highest scores were selected for the off-target analysis (Table 2-1). None of the three off-target site is located in the exon. Shown in Figure 2-7, we observed non-specific smears below the uncut bands in all samples treated with the T7E1 enzyme, while cleaved fragments of expected sizes were not detectable.

a.

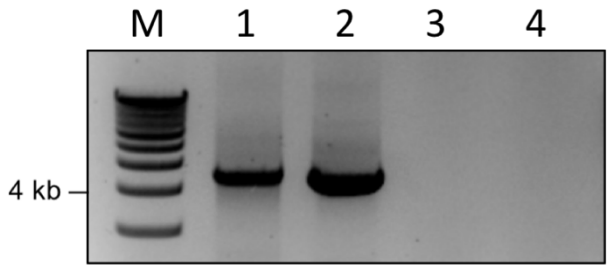

b.

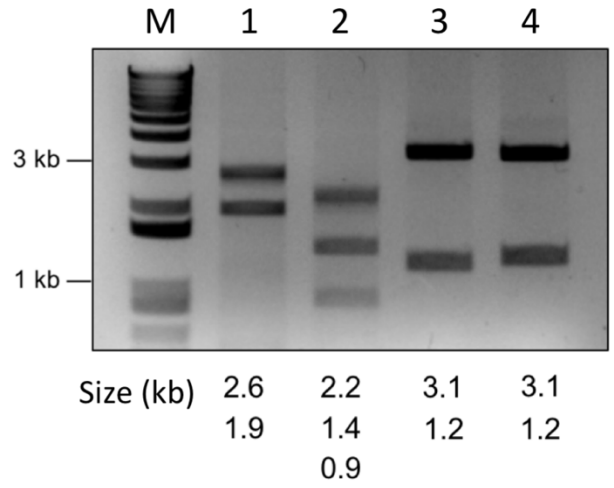

c.

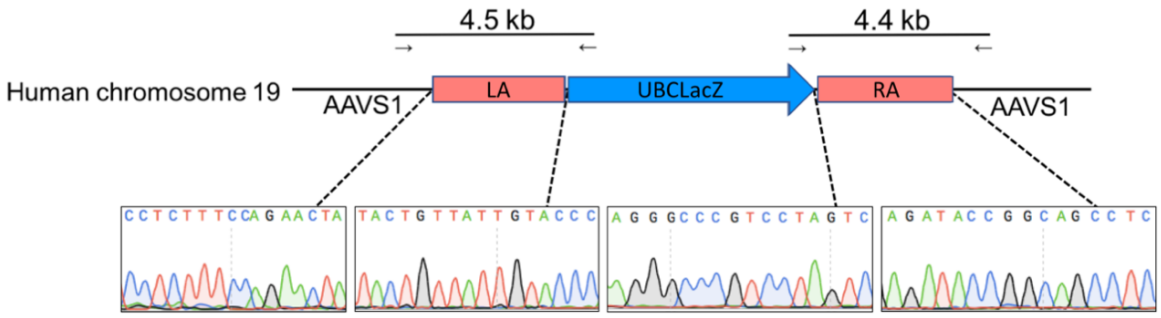

Figure 2-6. Validation of UBCLacZ gene integration by junction PCR

a. Junction PCR detection of UBCLacZ integration in IB3-1 cells transduced with 100 MOI of HD-Ad-UBCLacZ-TALEN at left (lane 1) and right (lane 2) homology arms. The expected PCR products are 4.5 kb and 4.4 kb, respectively. Lane 3, PCR at the left homology arm in cells transduced with 100 MOI of HD-Ad-UBCLacZ control vector. Lane 4, PCR at the right homology arm in cells transduced with 100 MOI of HD-Ad-UBCLacZ control vector. M, DNA marker. **b.** Restriction enzyme digestion of junction PCR products using EcoRV and AfeI. The expected fragment lengths are indicated below each lane. Lane 1, left arm PCR product digested by EcoRV. Lane 2, left arm PCR product digested by AfeI. Lane 3, right arm PCR product digested by EcoRV. Lane 4, right arm product digested by AfeI. M, DNA marker. **c.** Schematic diagram of the integrated expression cassette at AAVS1 and Sanger sequencing analysis at the junctions.

Table 2-4. Off-target sites predicted by TALENoffer

Site	Location	Exon	Full site sequence	Score
AAVS1	Chromosome 19	No	TTTTCTGTCACCAATCCTgtccctagtggccccACTGTGGGGTGGAGGGGA	0
#1	Chromosome 3	No	ATTTCTGTCAAAAATCCTtgtccactgtataagaatAGTATTAGTGAAAGACAA	-0.375
#2	Chromosome 22	No	CTCCCCCCACCCCCCAAAaaaatccatttccgggacTGGAGTGGGGACAGAAAA	-1.300
#3	Chromosome 5	No	TACTCCCCACCCCACAGAtaatctgtggtcaatgACTGTTGGATGCAGGGGA	-1.383

The location, sequence, and score of the AAVS1 target site and the top 3 off-target sites predicted by the TALENoffer online programme. Capital letters in the site sequences indicate the possible regions recognized and bound by TALE arms. Potential spacer regions are indicated by lowercase letters. A score closer to zero indicates a higher possibility that the TALEN will bind to the site.

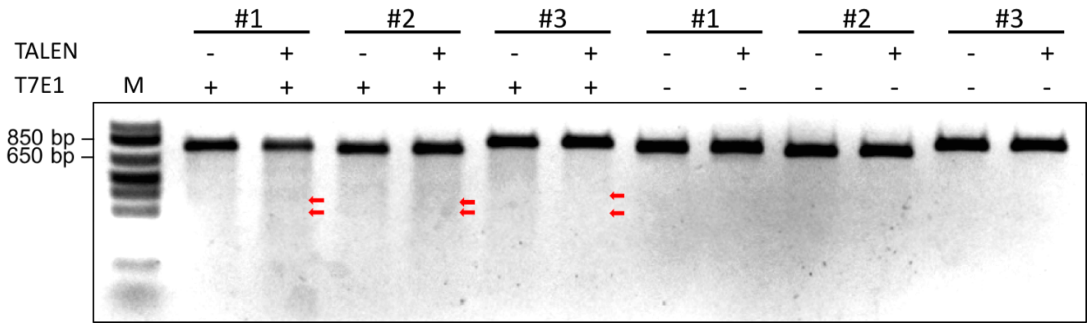

Figure 2-7. T7E1 detection of off-target NHEJ induced by TALEN in IB3-1 cells

IB3-1 cells were transduced with either 100 MOI of HD-Ad-UBCLacZ control virus or HD-Ad-UBCLacZ-TALEN. PCR products at selected off-target sites #1, #2, and #3 were subjected to T7E1 digestion. Positions of potential cleaved fragments are indicated by the arrows. M, DNA marker.

2.3.5 Determining the UBCLacZ integration efficiency

A stable transgene expression depends on the integration frequency of our expression cassette at the purposed locus. To assess the transgene integration efficiency, we transduced IB3-1 cells with 50 and 100 MOI of HD-Ad-UBCLacZ-TALEN or 100 MOI of the control vector, and we cultured the cells for 18 passages to dilute the transient LacZ expression by non-integrated vectors. Shown in Figure 2-8a, formation of LacZ-positive IB3-1 colonies in late passages can be observed as a result of UBCLacZ integration. By cell counting, a 2.87% integration efficiency was found in cells transduced with 50 MOI of the HD-Ad vector. In those transduced with 100 MOI of the virus, the efficiency was 5.21% (Figure 2-8c). Significant differences in the integration rate were observed at both viral doses tested comparing to the no TALEN control (50 MOI, n=3, p=0.0407; 100 MOI, n=3, p<0.0001).

To isolate cells with transgene integration, we sorted individual cells into 96-well plates by flow cytometry. The single cells were cultured until they developed into colonies, and then they were subjected to β-galactosidase staining for LacZ expression. We observed positive colonies with uniformly stained nuclei (Figure 2-8b). From the single cell sorting, we also obtained an estimate of integration efficiency. At 100 MOI, 6 out of 113 single cell colonies displayed positive LacZ signals. The integration efficiency was determined to be 5.59% after normalization to the transduction efficiency, which was consistent with the result from cell counting. No colony with integration was observed in the HD-AD-UBCLacZ control group (0 LacZ positive out of 125 colonies).

We further verified the LacZ positive rate using a flow cytometric method with the ImaGene Green C_{12}FDG LacZ Gene Expression Kit (Invitrogen) which produces fluorescence when cleaved by β-galactosidase. Live singlet cell population was gated to exclude any cell aggregates or debris. The cells were analyzed on fluorescein isothiocyanate (FITC) versus forward scatter (FSC) density plots (Figure 2-9). We set the gate to include the population with strong fluorescence. We also noticed a low level of background fluorescence in untransduced IB3-1 cells (Figure 2-9a). After normalization to the untransduced control, we found a similar trend with slightly higher LacZ positive rate at each condition comparing to the results from the cell counting method. In cells transduced with 100 MOI of no TALEN control vector, approximately 2% of the population produced florescence (Figure 2-9b). In cells transduced with HD-Ad-UBCLacZ-TALEN, the rate was about 5% at 50 MOI (Figure 2-9c) and 7% at 100 MOI (Figure 2-9d).

Previous work on DNA repair pathways showed that a small molecule SCR7 inhibits DNA ligase IV, a major enzyme involved in the NHEJ pathway[149]. To further enhance

transgene expression cassette integration by HDR, we treated the transduced cells with 0.1 μM and 0.5 μM of SCR7 (Figure 2-10). In cells transduced with 100 MOI of the vector and supplemented with 0.1 μM of SCR7, we observed a slight but not statistically significant increase in the integration efficiency (n=3, p=0.1923). A significant increase from 5.21% to 7.07% was found between the untreated transduced cells and those supplemented with 0.5 μM of SCR7 (n=3, p=0.0033).

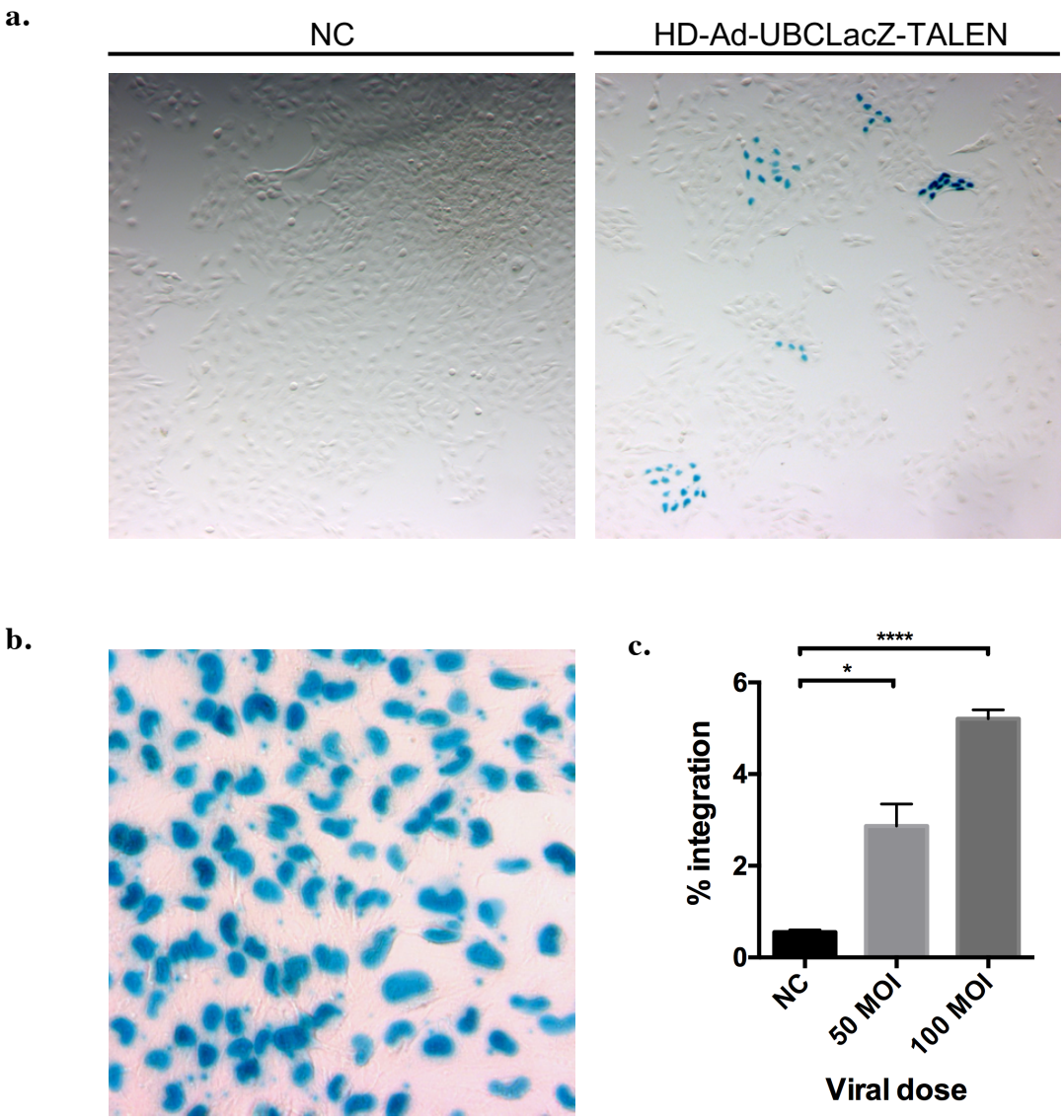

Figure 2-8. UBCLacZ integration visualized by β-galactosidase staining

a. β-galactosidase staining of IB3-1 cells transduced with HD-Ad-UBCLacZ control vectors (NC) or HD-Ad-UBCLacZ-TALEN at 100 MOI and cultured for 18 passages. **b.** β-galactosidase staining of a representative LacZ positive IB3-1 colony derived from a single cell with integrated UBCLacZ transgene. **c.** Integration efficiency of IB3-1 cells transduced with 50 MOI and 100 MOI of HD-Ad-UBCLacZ-TALEN (n=3). NC, cells transduced with 100 MOI of HD-Ad-UBCLacZ control vector. Error bars were calculated with the standard deviation of the mean. *p<0.05, ****p<0.0001.

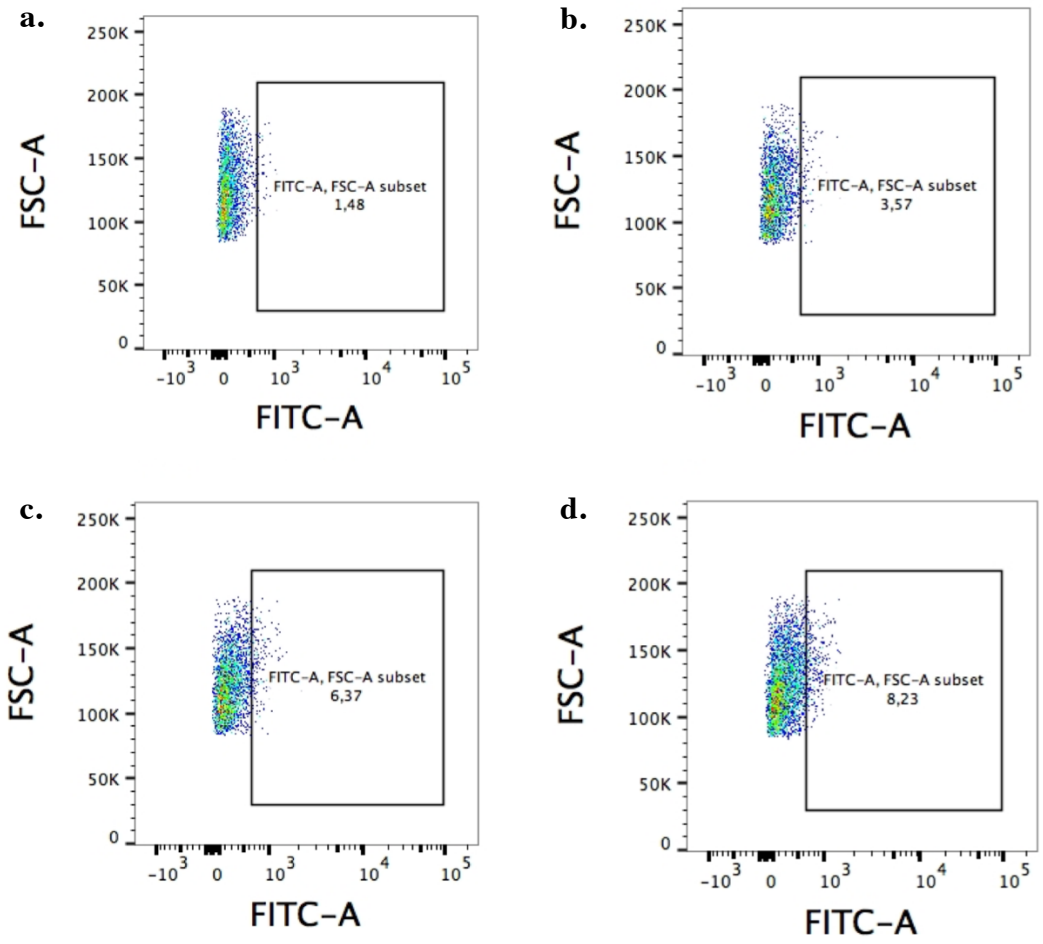

Figure 2-9. Flow cytometry of C_{12}FDG stained IB3-1 cells

a. FITC vs FSC density plot of untransduced IB3-1 cells. **b.** FITC vs FSC density plot of IB3-1 cells transduced with 100 MOI of HD-Ad-UBCLacZ control vector and cultured for 18 passages. **c.** FITC vs FSC density plot of IB3-1 cells transduced with 50 MOI of HD-Ad-UBCLacZ-TALEN and cultured for 18 passages. **d.** FITC vs FSC density plot of IB3-1 cells transduced with 100 MOI of HD-Ad-UBCLacZ-TALEN and cultured for 18 passages.

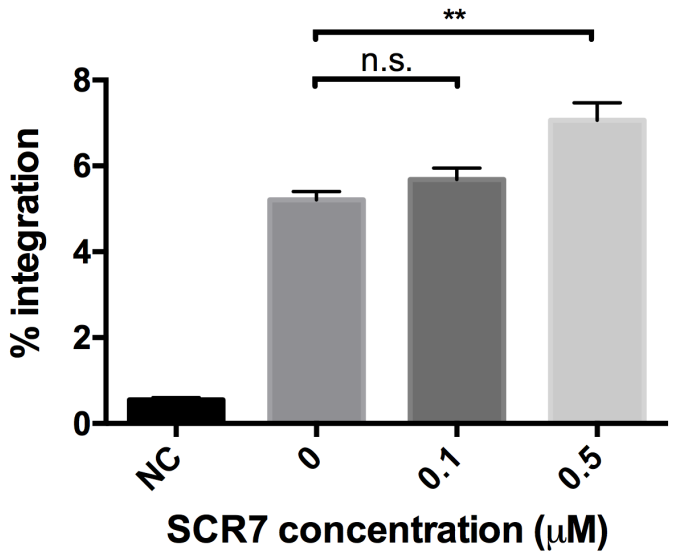

Figure 2-10. Enhancement of integration efficiency by SCR7 treatment

Integration efficiency of IB3-1 cells transduced by 100 MOI of HD-Ad-UBCLacZ-TALEN, without and with SCR7 treatment at 0.1 μM and 0.5 μM. NC, cells transduced with 100 MOI of HD-Ad-UBCLacZ control vector (n=3). Error bars were calculated with the standard deviation of the mean. n.s., not significant, $p>0.05$, **$p<0.01$.

2.4 Discussion

The increased interest in precise gene editing technology as a therapeutic modality for genetic disorders has highlighted the need for safe and efficient delivery vectors. In this thesis, we described a novel strategy that allows us to package the TALEN gene editing system, the therapeutic gene expression cassette, and the homology arms for transgene integration into one single HD-Ad vector for delivery.

Although production of HD-Ad vectors in large quantities is usually simple and highly efficient within the 116 Cre/loxP platform, packaging of TALEN that targets human genome remains challenging. We found it more difficult to obtain a good yield of HD-Ad-TALEN vectors from 116 cells, but the reason remains unclear. We speculate that TALEN could lead to modifications in the genome of 116 producer cells because the cell line is also derived from human cells, which may somehow negatively affect viral production in the cells. Earlier in this study, we found that the genomic DNA of 116 cells was cleaved during viral production and LacZ integration at the AAVS1 site was detected by junction PCR (data not shown). Further investigation may be needed to improve the viral production. To overcome this limitation, we adjusted the passage number for viral amplification and the viral titre for transduction before proceeding to the large-scale production. The membrane-based purification kit also offered the possibility to quickly isolate a smaller but sufficient amount of HD-Ad vector that may not form a visible band after the ultracentrifugation. The purified HD-Ad vector showed a superior efficiency in delivering the TALEN-transgene system to the nucleus, indicated by high levels of GFP and LacZ expression in transduced cells (Figure 2-4). This highlighted the value of high-capacity HD-Ad vectors to our study, because nuclear delivery efficiency by traditional plasmid-based transfection is greatly reduced with increasing construct size[150].

An advantage of TALEN gene editing technology is its high level of target specificity. DNA binding domains of the two TALE units used in this study recognize a total of 34 nucleotides at the target site, while they could be customized for an even higher specificity by increasing the length of the target sequence. In this chapter, we present that the delivered TALEN system was able to produce substantial on-target cleavage and undetectable off-target cleavage. However, a limitation of the off-target study by T7E1 assay is that only predicted

sites could be tested. In order to screen off-target cleavage at the whole genome level, additional methods such as next generation sequencing (NGS) are need.

We determined the UBCLacZ integration efficiency primarily by counting the β-galactosidase staining because of the high sensitivity of this method. In addition, the stained cell colonies can be directly and clearly observed by eye under a light microscope. Despite the advantages of β-galactosidase staining, the result could be greatly affected by bacterial contamination which produces considerable levels of false positive signals. Thus, routine use of antibiotics such as penicillin/streptomycin during the passages is important for generating reliable data. The morphology of stained cells also provided key information. Because the expression cassette includes a NLS, true signals from integrated UBCLacZ were located only in the cell nuclei (Figure 2-8a, b) but not in the cytoplasm. In late passages, because the residual vectors were fully diluted, cells carrying integrated expression cassette usually appear as independent blue colonies. The level of LacZ expression may be different from colony to colony depending on whether the integration was heterozygous or homozygous, but the expression levels were roughly the same within each colony.

We further confirmed the integration efficiency in viable cells by flow cytometry. The fluorescent β-galactosidase substrate C_{12}FDG carries a lipophilic fluorescein that allows the substrate to enter the cell membrane. Once cleaved by β-galactosidase, the fluorescent product stays within the cell membranes and is readily detected by flow cytometry[151]. Interestingly, we observed slightly higher positive rate in the no TALEN control and at the two viral dosages comparing to the cell counting results, probably due to the higher sensitivity of flow cytometry. However, the method does not allow us to quickly distinguish true nuclear signals from the cytoplasmic background. Although the endogenous β-galactosidase was inhibited by

chloroquine diphosphate treatment, bacterial infection would potentially be a great problem affecting the results. In addition, the fluorescent intensity also depends on the substrate incubation time which requires further optimization.

The NHEJ inhibitor SCR7 has been shown to enhance the efficiency of precise gene editing both *in vitro* and *in vivo*. Application of 0.5 μM of SCR7 in this study has significantly improved the integration efficiency at 100 MOI from about 5% to 7% in IB3-1 (Figure 2-10). Although not tested for this thesis, a higher SCR7 concentration may further boost the HDR efficiency. In a previous study, as high as 5-100 μM of SCR7 was used and showed little adverse effect in mouse embryos[152]. Thus, SCR7 treatment at appropriate dosages could be extended to future *in vivo* studies of our HD-Ad-TALEN vectors. Considering the small amount of wild-type CFTR required for normal chloride ion transport, we here conclude that the approach described in this thesis led to efficient transgene integration for sustainable expression *in vitro*.

3 Functional correction by a donor K18CFTR expression cassette in IB3-1 cells

3.1 Rationale

Following the delivery of a K18CFTR expression cassette with the HD-Ad-TALEN system, we would like to investigate whether functional CFTR can be expressed. The K18CFTR (K18mTECFTag2-i6x7pA) expression cassette contains 2.5 kb of the genome upstream of the human keratin 18 (K18) promoter, the K18 promoter, the first intron of K18, the downstream translational enhancer, the human CFTR cDNA, and the following 3' untranslated region and the polyadenylation signal[153]. The K18 promoter restricts expression of CFTR within epithelial cells, allowing future test of the vector in primary cells or *in vivo*. In this section, we examined the CFTR mRNA and protein expression, as well as the ion channel function in transduced IB3-1 cells.

3.2 Material and Methods

3.2.1 Basic Molecular Techniques

The assembly of HD-Ad-K18CFTR-TALEN construct involved the application of same basic molecular protocols as described in Section 2.2.1.

Total RNA isolation from adherent cells. All RNA samples were collected with the PureLink RNA Mini Kit (Invitrogen) following the manufacturer's protocol. Before purification, cells in 6-well plates were gently washed with PBS, pH 7.4.

RNA quantification. The concentration and purity of RNA samples were determined from the OD readings on a SimpliNano Spectrophotometer (GE Healthcare Life Sciences). Proper blanks were used for different samples before the measurements.

Total protein isolation from adherent cells. Cells in 6-well plates were gently washed with ice-cold PBS, pH 7.4 then scraped from the bottom of the plate with a cell scraper in 1

mL of ice-cold PBS. The cells were transferred to a clean microtube and centrifuged down at 14000 rpm for 20 seconds at 4°C. The resulting cell pellet was re-suspended on ice in 30 μL of RIPA buffer (1% Triton X-100, 0.1% SDS, 150 mM NaCl, 20 mM Tris HCl, and 0.5% sodium deoxycholate) supplemented with cOmplete Protease Inhibitor Cocktail (Roche). The cells were lysed on ice for 20 minutes with occasional vortex. Then, the lysate was centrifuged at 14000 rpm for 20 minutes at 4°C. Five microliters of the supernatant was saved on ice for protein quantification, and the rest was collected and transferred to a clean microtube. To each protein sample, an equal volume of 4x Laemmli protein sample buffer for SDS-PAGE (Bio-Rad) supplemented with 2-mercaptoethanol was added. The samples were thoroughly mixed and stored at -80°C until use.

Protein quantification by BCA assay. The protein sample was mixed with an equal volume of ddH_2O. Standards were replicates consisting of 10, 5, 2.5, 1.25, 0.625, 0.3125, and 0 mg/mL BSA in PBS, pH 7.4. In a 15 mL Falcon tube, Pierce BCA Protein Assay Reagent A was mixed by vortex with Reagent B (Thermo Scientific) at a ratio of 50:1. 200 μL of the mixture was added to each well on a flat bottom clear 96-well plate. Then, 1 μL of the protein sample or the BSA standards were added to each well containing the reagent. The 96-well plate was incubated in dark for 30 minutes and then the OD was read at 562 nm. The protein concentration was determined by comparing the OD readings to the standard.

3.2.2 Construction of pHD-Ad-K18CFTR-TALEN

The same methods as described in Section 2.2.2 were used to add the 4 kb homology arms to the K18CFTR expression cassettes carried by pBSII-SK(+) backbone plasmid. Similarly, the expression cassette and the homology arms were cloned into pC4HSU backbone

(NotI/SalI). TALEN was inserted to the pC4HSU-K18CFTR-L4-R4 by AscI digestion and ligation. The resulting plasmid was denominated as pHD-Ad-K18CFTR-TALEN.

3.2.3 Production of HD-Ad-K18CFTR-TALEN

The same methods as described in Section 2.2.3 were used to produce HD-Ad-K18CFTR-TALEN from the pHD-Ad-K18CFTR-TALEN plasmid vector.

3.2.4 Transduction of IB3-1 cells

The same methods as described in Section 2.2.4 were used to transduce IB3-1 cells with purified HD-Ad-K18CFTR-TALEN vectors.

3.2.5 Junction PCR

Genomic DNA of cells transduced with HD-Ad-K18CFTR-TALEN vectors or HD-Ad-K18CFTR control vectors were collected 5-day post-transduction. Junction PCR was performed on a SimpliAmp Thermal Cycler (Applied Biosystems). The sequences of primer sets used are as follows: K18CFTR left junction, 4.6 kb amplicon, 5’ CAT CAG CGA TGC AAT GAT GCT TGG GTT TGC ACC AAT G 3’ (forward primer), 5’ GGC AGA GCA CAG ATA AAG AGC CTG AGC CTG GAT TG 3’ (reverse primer); K18CFTR right junction, 4.7 kb amplicon, 5’ GAA TTC GAT GTG CTG GGA TCA GGA G 3’ (forward primer), 5’ GTT GGA GGA GGA AGG AGA CAG AAT CC 3’ (reverse primer). Eight microliters of each PCR reaction was visualized on a 0.8% agarose gel. PCR products were purified using the NucleoSpin Gel and PCR Clean-up Kit (Macherey-Nagel) following the manufacturer’s instructions. 300 ng of purified products were subjected to EcoRV or AfeI digestion (New

England Biolabs) at 37°C for 2 h. The reactions were run on 1% agarose gels. Sanger sequencing was performed by the TCAG Sequencing Facility at the Hospital for Sick Children.

3.2.6 Immunodetection of CFTR

Cells were seeded onto collagen-coated round glass cover slips in 6-well plates 3 days prior to staining. At confluency, the cells were washed in PBS, pH 7.4, fixed in ice-cold methanol for 10 minutes, and permeabilized with 0.5% Triton-100 in PBS. The cells were then blocked for 1 hour in block solution (5% goat serum, 0.5% BSA, 0.05% Triton-100 in PBS). The cells were incubated with mouse monoclonal antibodies against the human CFTR R-domain MAB1660 and C-terminus MAB25031 (R&D Systems) at 1:500 dilution overnight at 4°C, washed in PBS with 0.05% Triton-100, and then incubated in dark for 1 hour in 1:750 diluted CF555 goat anti-mouse IgG (H+L). After washes in dark, cells on the glass slips were taken out from the 6-well plates, and mounted with one drop of VECTASHIELD Hardset Antifade Mounting Medium with DAPI (Vector Laboratories).

3.2.7 Detection of CFTR mRNA expression by RT-qPCR

Total RNA of IB3-1 cells transduced with 100 MOI of HD-Ad-K18CFTR-TALEN or the control vector were harvested and purified with the PureLink RNA Mini Kit (Life Technologies) following the manufacturer's instructions at 3 days, 6 passages, 12 passages, and 18 passages post-transduction. One microgram of each RNA sample was subjected to DNase I (Invitrogen) digestion at room temperature for 15 minutes. Reverse transcription was performed with the SuperScript VILO Master Mix (Invitrogen) according to the manufacturer's protocol on a SimpliAmp Thermal Cycler (Applied Biosystems). The resulting

cDNA samples were diluted in DEPC-treated water, and 10 ng of each sample was used for quantitative PCR analysis. The qPCR was performed with Power SYBR Green PCR Master Mix (Applied Biosystems) on a QuantStudio 3 Thermal Cycler (Applied Biosystems). The primers for detecting human CFTR mRNA level are 5' CCT GAG TCC TGT CCT TTC TC 3' (forward primer) and 5' CGC TGT CTG TAT CCT TTC CTC 3' (reverse primer). GAPDH mRNA levels were measured as the internal control using primers 5' GTT CGA CAG ACA GCC GTG TG 3' (forward primer) and 5' ATG GCG ACA ATG TCC ACT TTG C 3' (reverse primer). The relative hCFTR mRNA expression was calculated according to the formula: Relative expression = $2^{-\Delta\Delta CT}$, in which $-\Delta\Delta Ct = [(Ct_{treatment} - Ct_{internal\ control}) - (Ct_{standard} - Ct_{internal\ control})]$.

3.2.8 Detection of CFTR protein expression by Western blotting

SDS-PAGE. Protein samples collected were thawed and incubated at room temperature for 10 minutes to allow protein denaturation. Polyacrylamide gel with 4% stacking gel and 6% separating gel was placed in the running cassette and submerged by running buffer (25 mM Tris base, 0.2 M glycine, 0.1% SDS). One hundred micrograms of the total protein sample was loaded to each lane and run at 100 V for 90 minutes.

Immunoblot. The gel was removed from the running cassette and soaked in chilled transfer buffer (25 mM Tris base, 0.2 M glycine, 20% methanol, 0.01% SDS) for 10 minutes before setting up the transfer cassette. The assembled transfer cassette was then placed in a running tank with transfer buffer and ice pack. The protein was transferred onto the nitrocellulose membrane at 85 V for 90 minutes on ice. When the transfer was done, total protein on the nitrocellulose membrane was visualized in Ponceau S solution (BioShop), and

then the membrane was roughly washed with water and blocked in 5% skim milk in TBS-T (0.1% Tween 20 in TBS, pH 7.4) for 2 hours at room temperature with shaking. After blocking, the membrane was cut into 2 pieces based on the marker such that one piece contained the CFTR protein, and the other contained the GAPDH protein. The membrane pieces were incubated in separate containers with primary mouse anti-CFTR antibody MAB 596 (Chapel Hill, University of North Carolina) 1:1000 diluted in 5% skim milk or primary rabbit anti-GAPDH antibody ab9485 (Abcam) 1:2000 diluted in 5% skim milk overnight at 4°C. On the next day, the primary antibody was removed and the membranes were washed 5 times with TBS-T for 10 minutes. Then, Goat Anti-Mouse IgG (H+L)-HRP Conjugate secondary antibody (Bio-Rad) was diluted 1:3000 in 5% skim milk and added to the membrane with CFTR. Goat Anti-Rabbit IgG (H+L)-HRP Conjugate secondary antibody (Bio-Rad) was diluted 1:3000 in 5% skim milk and added to the membrane with GAPDH. The membranes were incubated in the secondary antibodies for 2 hours at room temperature, then washed 5 times with TBS-T for 10 minutes. After washing, Western Lightning Plus-ECL Solution A was mixed with an equal volume of Solution B (PerkinElmer) and dipped onto the membranes. The membranes were incubated for 1 minute and visualized in ChemiDoc XRS+ (Bio-Rad).

3.2.9 Detection of CFTR function with FLIPR membrane potential assay

The protocol for membrane potential assay was adapted from Ahmadi *et al*[154]. Cells were seeded to black-walled, clear-bottom 96-well plates and cultured until 100% confluency. The blue membrane potential dye (Molecular Devices) was dissolved in a chloride-free buffer (150 mM NMDG-gluconate, 3 mM KCl, 10 mM HEPES, pH 7.35, osmolarity 300 mOsm) and loaded to the cells. The plates were incubated at 37°C with 5% CO_2 and humidified air for

30 minutes, then transferred to the i3 multi-well microplate reader (Molecular Devices). The reader was heated to 37°C and set to fluorescence whole well scan with multiple points being read at the center. Eleven baseline reads were made, followed by addition of 2.5 μL forskolin per well. After adding the drug, 31 reads were made. Then, 21 scans were made after the reaction was terminated by addition of 10 μM CFTRinh-172. For negative controls, 2.5 μL of DMSO was added instead of forskolin.

Table 3-1. Plasmid constructs used for Aim 2

Plasmid	Size (bp)	Details
pBSII-SK(+)	2961	Contains Amp resistance gene and MSC
pK18CFTR	11586	Contains Amp resistance gene and K18CFTR expression cassette
pK18CFTR-L4-R4	19719	Modified pK18CFTR with left and right homology arms flanking the K18CFTR expression cassette
pBSII-SK(+)-TALEN	13269	Modified pBSII-SK(+) with genes encoding for left and right TALEN units flanking a GFP expression cassette
pC4HSU-PN	16278	HD-Ad backbone plasmid containing ITR and ψ
pC4HSU-PNE-K	12323	Modified pC4HSU-PN containing ITR and ψ, stuffer DNA partially removed
pC4HSU-K18CFTR-L4-R4	22402	Modified pC4HSU-PNE-K with K18CFTR-L4-R4 inserted
pHD-Ad-K18CFTR-TALEN	32896	Final construct modified from pC4HSU-K18CFTR-L4-R4 containing Amp resistance gene, ITR, ψ, TALEN, and K18CFTR expression cassette flanked by left and right homology arms

Table 3-2. HD-Ad vectors used for Aim 2

Vector	Details
HD-Ad-K18CFTR-TALEN	Carries GFP-labeled, TALEN-encoding sequences targeting the AAVS1 site, and K18CFTR expression cassette flanked by a 4 kb left homology arm and a 4 kb right homology arm
HD-Ad-K18CFTR	Carries a K18CFTR expression cassette

Table 3-3. Oligonucleotide primers used for Aim 2

Primer	Sequence (5'-3')	Purpose
Infusion-K-LHA-F	TTTAAACGTGAGAGCAGGTCGACGGTATCG	Forward primer for inserting left homology arm flanking K8CFTR through In- Fusion
Infusion-K-LHA-R	ACAATTCGGTACAGCCCTAGTTATCAGCCAAGTC	Reverse primer for inserting left homology arm flanking K8CFTR reporter through In- Fusion
Infusion-K-RHA-F	ATCGATAAGCTTGATGCTCTAGAACTAGTGGATCCC	Forward primer for inserting right homology arm flanking K8CFTR reporter through In- Fusion
Infusion-K-RHA-R	CTGCAGGAATTCGATCTCCTCTATCCTACCTCTAAAGC	Reverse primer for inserting right homology arm flanking K8CFTR reporter through In- Fusion
Ad5-F	CAGGAAGTGACAATTTTCGCGC	Forward primer amplifying sequence near ψ for detection of HD-Ad vector
Ad5-R	CGCGCTATGAGTAACACAAAATTATTCAG	Reverse primer amplifying sequence near ψ for detection of HD-Ad vector
Hexon-F	GAGGATACTGCGTACTCGTAC	Forward primer amplifying sequence in *hexon* gene for detection of HV
Hexon-R	CAGGGCGTTGTAGGCAGTG	Reverse primer amplifying sequence in *hexon* gene for detection of HV
JPCR-KL-F	CATCAGCGATGCAATGATGCTTGGGTTTGCACCAATG	Forward primer for left arm junction PCR analysis of K18CFTR integration

JPCR-KL-R	GGCAGAGCACAGATAAAGAGCCTGAGCCTGGATTG	Reverse primer for left arm junction PCR analysis of K18CFTR integration
JPCR-KR-F	GAATTCGATGTGCTGGGATCAGGAG	Forward primer for right arm junction PCR analysis of K18CFTR integration
JPCR-KR-R	GTTGGAGGAGGAAGGAGACAGAATCC	Reverse primer for right arm junction PCR analysis of K18CFTR integration
JPCR-Seq-KL-in	ACTGTCAAGTTGGGCAG	Primer for sequencing of junction PCR product at the left homology arm of K18CFTR, proximal junction
JPCR-Seq-KL-out	GGTACAACACAAACTTTTCCC	Primer for sequencing of junction PCR product at the left homology arm of K18CFTR, distal junction
JPCR-Seq-KR-in	GTTACAGTCTTGGTGATGCC	Primer for sequencing of junction PCR product at the right homology arm of K18CFTR, proximal junction
JPCR-Seq-KR-out	GCTCCCGAACCTCAGATC	Primer for sequencing of junction PCR product at the right homology arm of K18CFTR, distal junction
qPCR-hCFTR-F	CCTGAGTCCTGTCCTTTCTC	Forward primer for amplifying human CFTR cDNA
qPCR-hCFTR-R	CGCTGTCTGTATCCTTTCCTC	Reverse primer for amplifying human CFTR cDNA
qPCR-GAPDH-F	GTTCGACAGACAGCCGTGTG	Forward primer for amplifying human GAPDH cDNA
qPCR-GAPDH-R	ATGGCGACAATGTCCACTTTGC	Reverse primer for amplifying human GAPDH cDNA

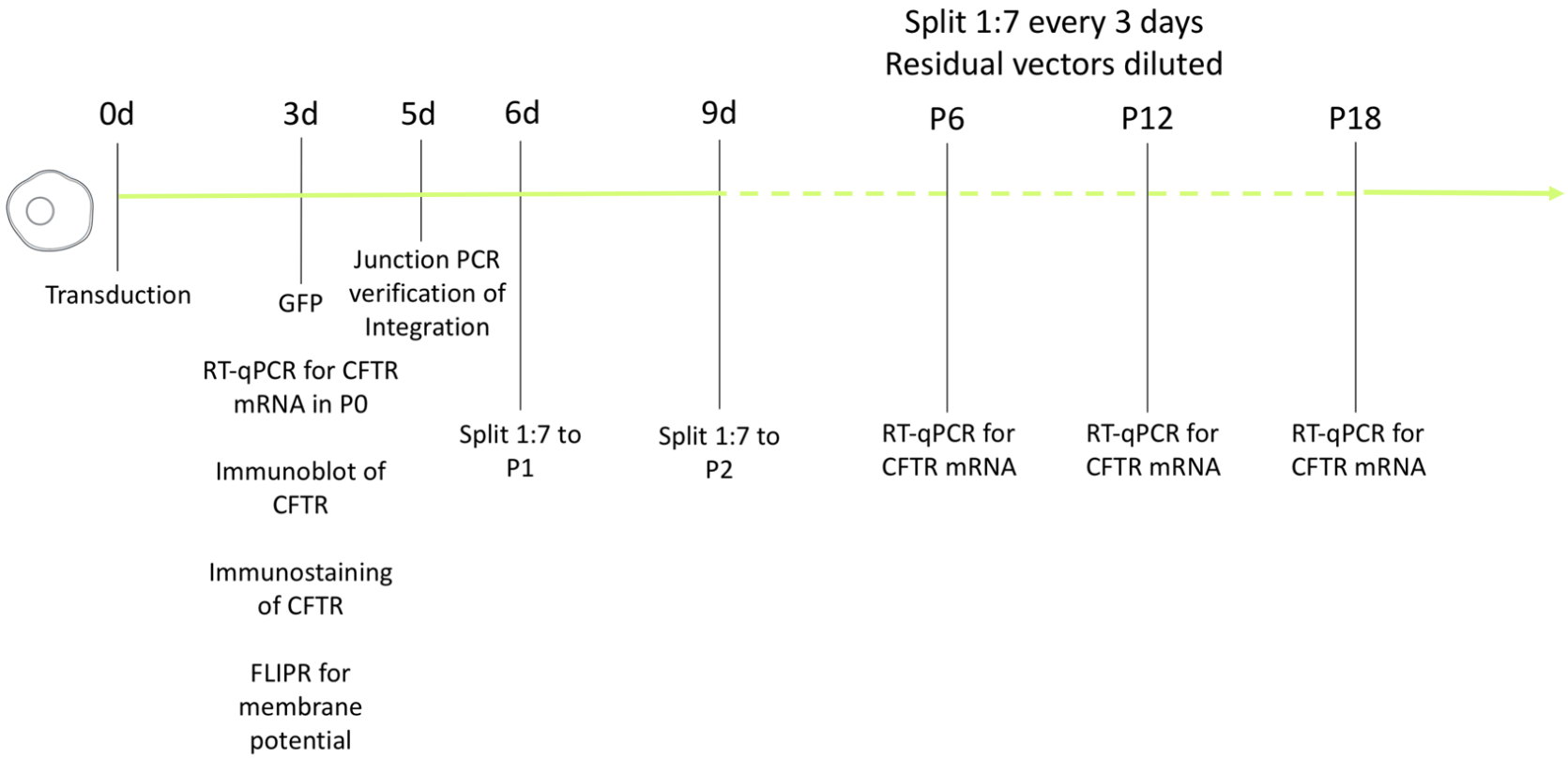

Figure 3-1. A schematic timeline on experimental design for Aim 2

3.3 Results

3.3.1 Verifying the pHD-Ad-K18CFTR-TALEN construct

The pHD-Ad-K18CFTR-TALEN plasmid construct was built by conventional molecular cloning for the viral production (Figure 3-2a). Again, we digested the final construct with restriction enzyme PacI, HpaI, AscI, EcoRV, BstZ17I, and BglII for verification. The locations of the resulting fragments on gel matched the expecting size (Figure 3-2b). To further determine whether the GFP gene on the construct can be properly expressed, we transfected IB3-1 cells with 2 μg of the plasmid DNA in 6-well plates. Three days after transfection, GFP expression was observed in transfected cells (Figure 3-2c).

a.

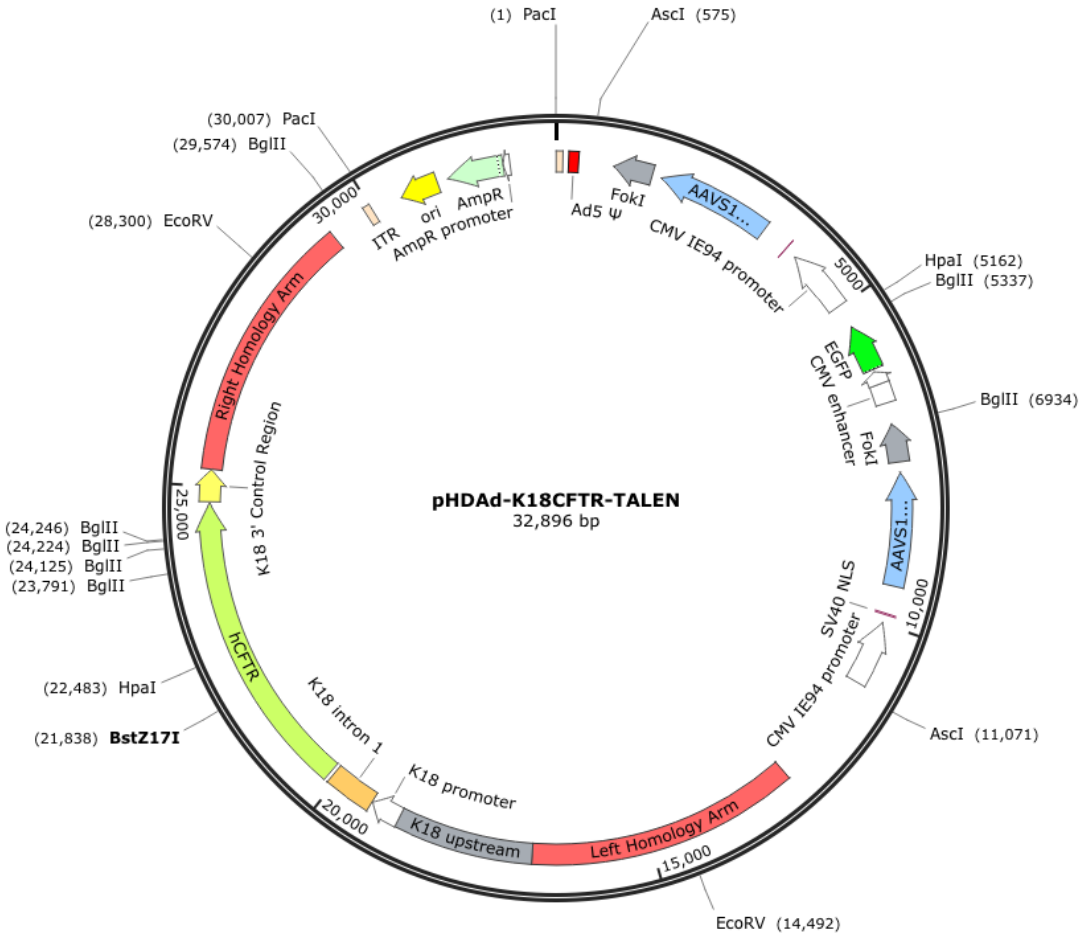

b.

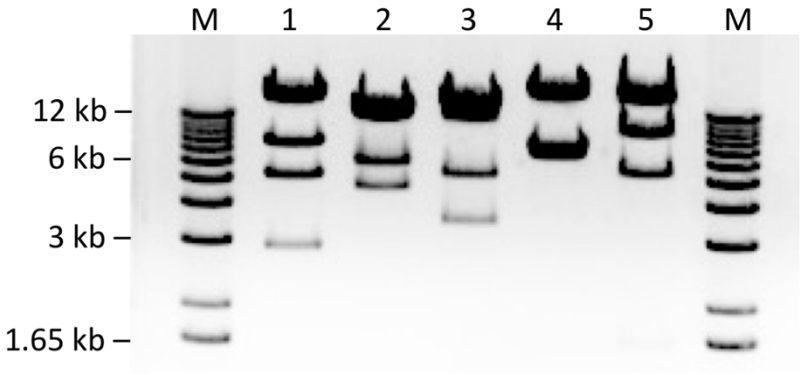

Size (kb)	17.3	11.4	13.8	19.1	16.9
	7.5	11.0	10.5	7.3	8.7
	5.2	5.9	5.2	6.5	5.3
	2.9	4.6	3.4		1.6
					0.3
					0.1
					0.02

c.

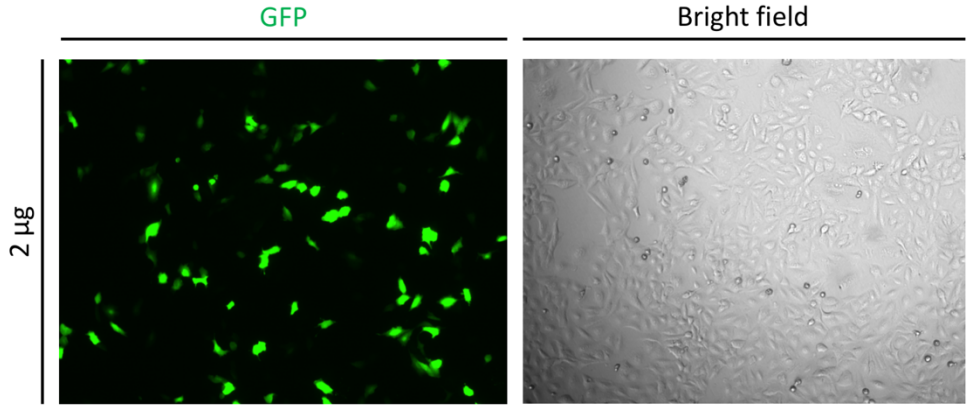

Figure 3-2. Verification of the pHD-Ad-K18CFTR-TALEN construct

a. Schematic diagram of the 33 kb pHD-Ad-K18CFTR-TALEN plasmid vector (generated in SnapGene). Restriction sites used for verification were labelled with their locations on the plasmid. **b.** Restriction enzyme digestion of the plasmid construct. Lane 1, PacI and HpaI. Lane 2, HpaI and AscI. Lane 3, AscI and EcoRV.

Lane 4, EcoRV and BstZ17I. Lane 5, BglII. M, DNA maker. Expected size of the resulting DNA fragments were listed below each lane. The 0.3 kb, 0.1 kb, and 0.02 kb bands are not visible on this gel. **c.** IB3-1 cells under fluorescent and bright field microscope 3 days after transfection with 2 μg of pHD-Ad-K18CFTR-TALEN plasmid.

3.3.2 Producing the HD-Ad-K8CFTR-TALEN vectors

Similarly to the production of HD-Ad-UBCLacZ-TALEN vector described in Section 2.3.2, we linearized the pHD-Ad-K18CFTR-TALEN plasmid construct with PacI and transfected 116 cells, followed by helper virus NG163 transduction. We observed CPE in each passage by 48 hours post helper virus transduction. Although the GFP expression increased from P1 to P5, we noticed that the viral amplification was less efficient compared to the HD-Ad-UBCLacZ-TALEN vector. To prevent the vectors in the cell lysate from being lost in the CsCl concentration gradient, we directly proceed to membrane-based purification after large-scale production. We achieved a final yield of 2.6×10^{11} viral particles from the purification kit.

With the purified HD-Ad-K18CFTR-TALEN vectors, we looked at the viral transduction of IB3-1 cells (Figure 3-4). Three days after transduction, we observed GFP expression in transduced cells. The GFP level is higher in cells transduced with 100 MOI of virus comparing to those transduced at 50 MOI. The control vector HD-Ad-K18CFTR does not carry GFP and there was no signal in the transduced cells.

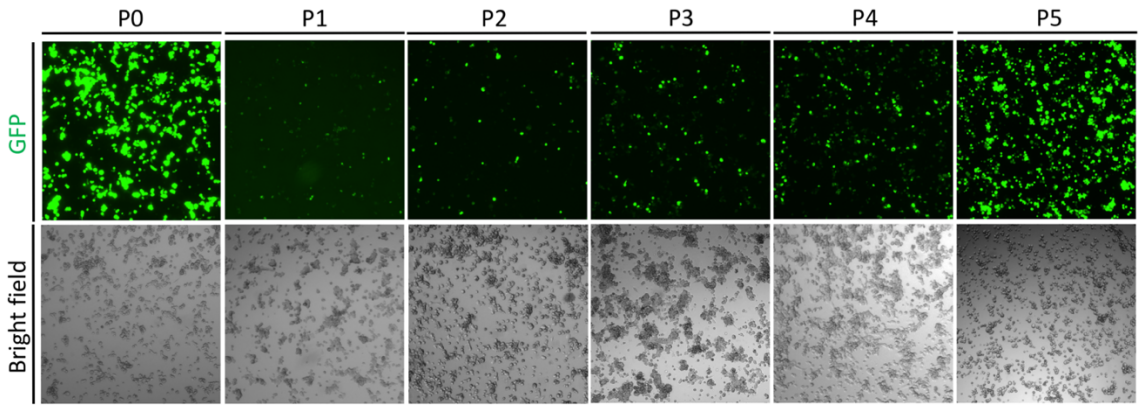

Figure 3-3. HD-Ad-K18CFTR-TALEN amplification and purification

GFP expression in 116 cells 48-hour post NG163 transduction (512 nm) from passage 0 to passage 5 (P0-P5) and cells under normal light (bright field).

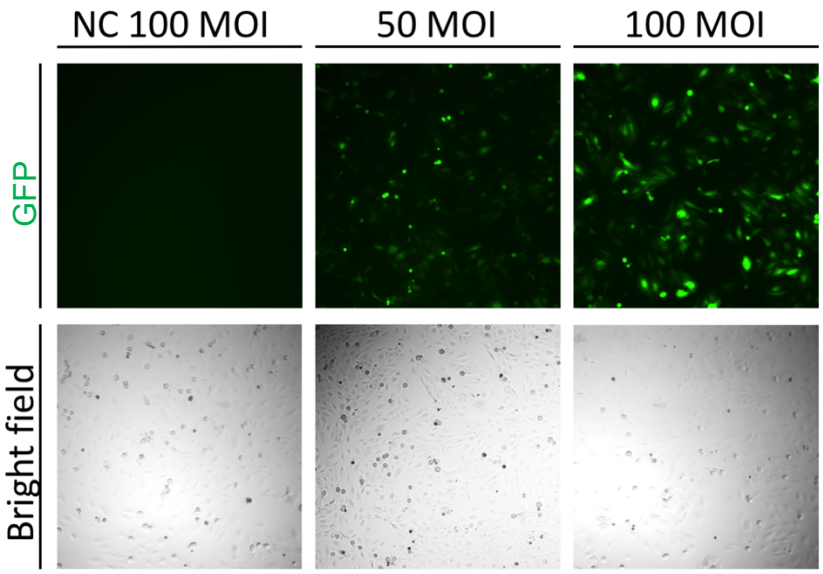

Figure 3-4. Transduction of IB3-1 cells with HD-Ad-K8CFTR-TALEN

GFP expression in IB3-1 cells 3 days after transduction with HD-Ad-K8CFTR-TALEN at 50 MOI and 100 MOI. NC, IB3-1 transduced with 100 MOI of HD-Ad-K18CFTR.

3.3.3 Validating K8CFTR integration at AAVS1 locus

To detect on-target integration of the K18CFTR expression cassette, we transduced IB3-1 cells with HD-Ad-K18CFTR-TALEN or HD-Ad-K18CFTR control vector at 100 MOI and performed junction PCR at both homology arms. We obtained the expected 4.6 kb and 4.7 kb PCR products at the left and right junction in cells transduced with 100 MOI of HD-Ad-K18CFTR-TALEN, but not in those transduced with control vector (Figure 3-5a). The PCR products were verified by restriction enzyme digestion with EcoRV and AfeI (Figure 3-5b) and Sanger sequencing (Figure 3-5c).

a.

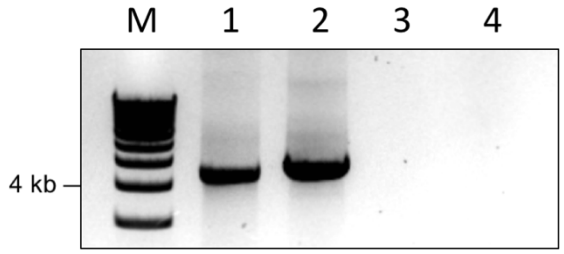

b.

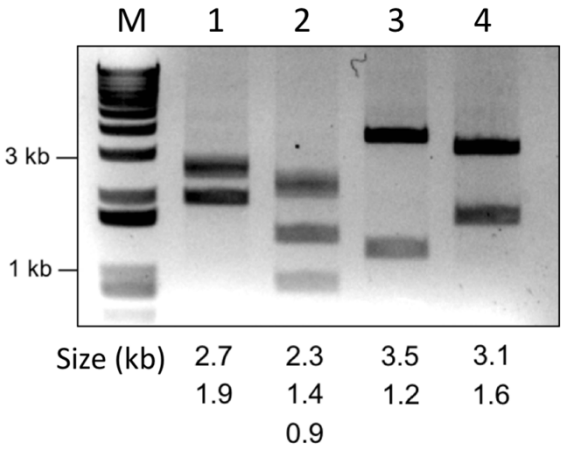

c.

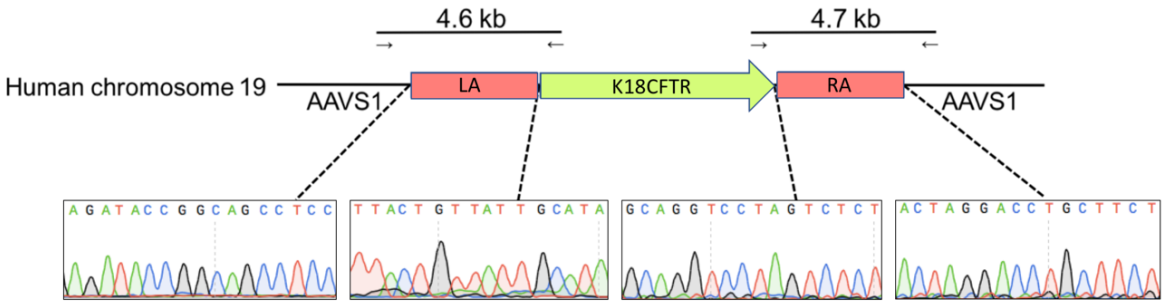

Figure 3-5. Validation of K18CFTR gene integration by junction PCR

a. Junction PCR detection of K18CFTR integration in cells transduced with 100 MOI of HD-Ad-K18CFTR-TALEN at left (Lane 1) and right (Lane 2) homology arms. The expected PCR products are 4.6 kb and 4.7 kb, respectively. Lane 3, PCR at the left homology arm in cells transduced with 100 MOI of HD-Ad-HDAd-K18CFTR control vector. Lane 4, PCR at the right homology arm in cells transduced with 100 MOI of HDAd-K18CFTR control vector. M, DNA marker. **b.** Restriction enzyme digestion of junction PCR products using EcoRV and AfeI. The expected fragment lengths are indicated below each lane. Lane 1, left arm PCR product digested by EcoRV. Lane 2, left arm PCR product digested by AfeI. Lane 3, right arm PCR product digested by EcoRV. Lane 4, right arm product digested by AfeI. M, DNA marker. **c.** Schematic diagram of the integrated expression cassette at AAVS1 and Sanger sequencing analysis at the junctions.

3.3.4 Examining CFTR expression in transduced cells

To determine whether a steady human CFTR mRNA expression from the integrated K18CFTR transgene could be achieved, total RNA from passages 0, 6, 12, and 18 of IB3-1 cells transduced with 100 MOI of HD-Ad-K18CFTR-TALEN or HD-Ad-K18CFTR control vector was isolated for mRNA quantification by RT-qPCR. The relative expression was compared to the baseline CFTR mRNA level in passage 18 cells transduced with the control vector. Shown in Figure 3-6, the human CFTR mRNA expression in IB3-1 transduced with

the HD-Ad-K18CFTR-TALEN came to a stable level after passage 6. At passage 18, the expression level is approximately 3 folds higher compared to the control. The initial CFTR mRNA expression level in cells transduced with the control vector at P0 was approximately 2 times higher than that in the cells transduced with the HD-Ad-K18CFTR-TALEN vector, probably due to the different viral activities between the two preparations.

In order to determine whether wild type CFTR protein was expressed in IB3-1 cells transduced with the HD-Ad-TALEN vector carrying the K18CFTR expression cassette, we performed immunofluorescent staining of the CFTR protein in IB3-1 post-transduction and confirmed the expression by Western blotting. In Figure 3-7a, untransduced IB3-1 cells showed a very low level of fluorescence due to endogenous CFTR expression. A higher level of CFTR was observed from the immunostaining (Figure 3-7b) 3 days after transduction with 100 MOI of HD-Ad-K18CFTR-TALEN. Mature and immature CFTR proteins can usually be separated on SDS-PAGE gels due to difference in their sizes. The normal CFTR c band locates at 180 kDa, whereas immature CFTR proteins form b band at 160 kDa. Shown in Figure 3-7d, a high level of normal CFTR protein was expressed in cells transduced with 100 MOI of HD-Ad-K18CFTR-TLAEN, while the endogenous CFTR protein was not detectable by Western blotting.

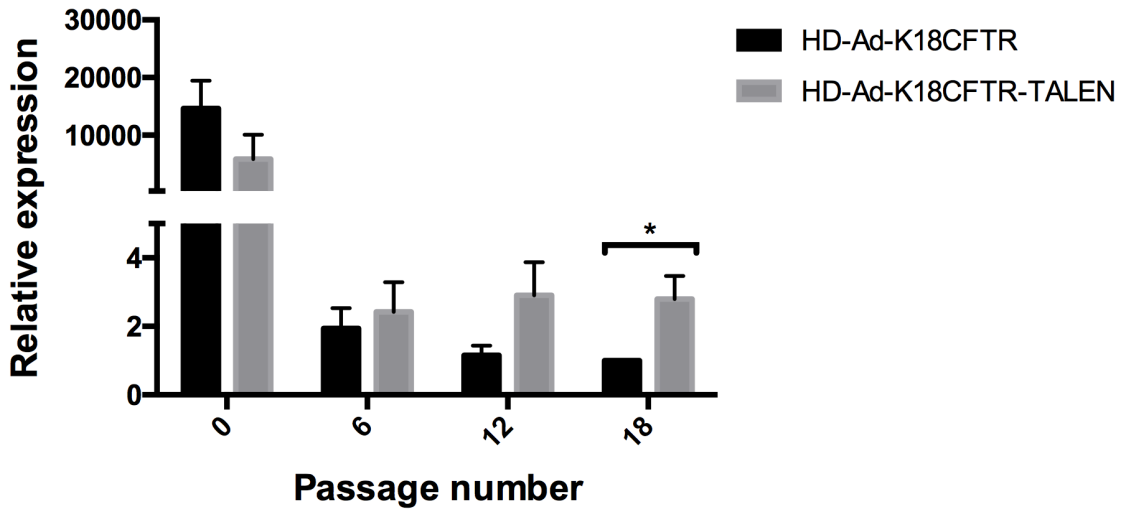

Figure 3-6. CFTR mRNA expression in IB3-1 cells

Levels of human CFTR mRNA expression are relative to the expression level in IB3-1 cells transduced with HD-Ad-K18CFTR control vectors at 100 MOI in passage 18 (n=3). Black bar, IB3-1 cells were transduced with HD-Ad-K18CFTR at 100 MOI. Gray bar, IB3-1 cells were transduced with HDAd-K18CFTR-TALEN at 100 MOI. Error bars were calculated with the standard deviation of the mean. *$p<0.05$.

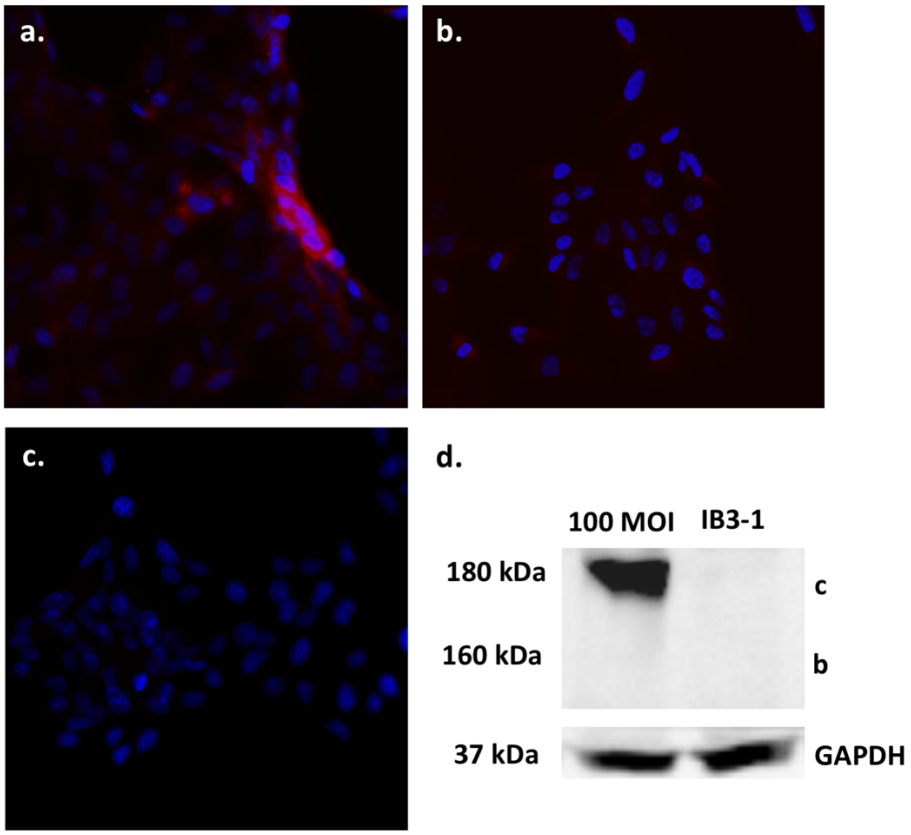

Figure 3-7. CFTR protein expression in transduced IB3-1 cells

a. Immunofluorescent staining of CFTR (red) in IB3-1 cells transduced with 100 MOI of HD-Ad-K18CFTR-TALEN at day 3. b. Immunofluorescent staining of CFTR (red) in untransduced IB3-1 cells. c. Untransduced IB3-1 cells without addition of the primary antibody. Nuclei were labeled in blue with DAPI. d. Western blotting of CFTR protein in IB3-1 cells transduced with 100 MOI of HD-Ad-K18CFTR-TALEN at day 3 and untransduced IB3-1 cells. c band, normal CFTR. b band, immature CFTR.

3.3.5 Examining CFTR function in transduced cells

To measure the functional response of CFTR expressed in IB3-1 from the K18CFTR expression cassette, we performed membrane potential assay with fluorescent imaging plate reader (FLIPR). In cells transduced with 100 MOI of HD-Ad-K18CFTR-TALEN, addition of forskolin (FSK) activated the CFTR channel, indicated by a robust depolarization shown in Figure 3-8a. This response was not observed in untransduced IB3-1 cells (Figure 3-8c) or those transduced with 100 MOI of HD-Ad-UBCLacZ-TALEN (Figure 3-8b). Shown in Figure 3-8d, significant differences in the maximum percentage change of fluorescence were found between cells transduced with HD-Ad-K18CFTR-TALEN and both control groups (LacZ, n=3, p=0.0205; IB3-1, n=3, p=0.0006). The results confirmed that the response to FSK was due to functional CFTR expressed from the transgene expression cassette.

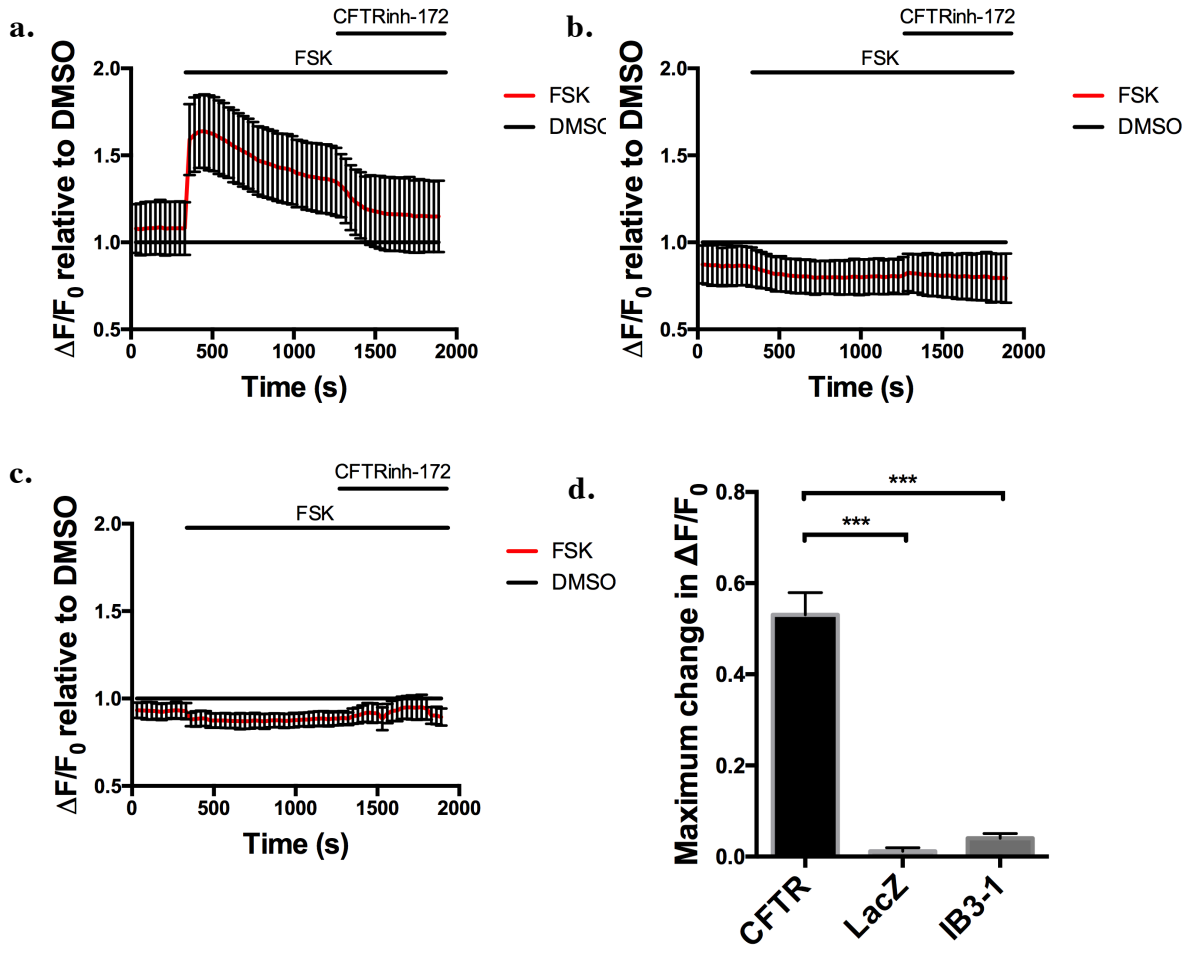

Figure 3-8. CFTR ion channel function in transduced IB3-1 cells

a. CFTR channel function in IB3-1 cells were measured 3 days after transduction with 100 MOI of HD-Ad-K18CFTR-TALEN (n=3). CFTR was activated by FSK (time=300 s) and inactivated by CFTRinh-172 (time=1200 s). Changes in fluorescence ($\Delta F/F_0$) were normalized to measurements in DMSO treated cells. **b.** IB3-1 cells were measured 3 days after transduction with 100 MOI of HD-Ad-UBCLacZ-TALEN. **c.** Untransfected IB3-1 cells were measured. **d.** Maximum percentage change in $\Delta F/F_0$ relative to baseline (F_0) fluorescence measurement (time=300 s). CFTR, IB3-1 transduced with 100 MOI of HD-Ad-K18CFTR-TALEN. LacZ, Ib3-1 transduced with 100 MOI of HD-Ad-UBCLacZ-TALEN. IB3-1, untransduced cells. Error bars were calculated with the standard deviation of the mean. ***p<0.001.

3.4 Discussion

In this chapter, we showed that the K18CFTR expression cassette delivered using our strategy expresses functional CFTR protein in the airway epithelial cell line. In late passages, only a few percentage of the cells with transgene integration will express wild type CFTR, and detection of such low levels of CFTR expression in a mixed population is a difficult task. An advantage of RT-qPCR is the high sensitivity to amplify low levels transcripts. However, we were not able to detect CFTR protein by Western blotting not only because the expression level was much lower comparing to that in early passages, but also due to the fact that CFTR proteins are highly prone to degradation. Typically, two forms of wild type CFTR protein are found in significant amounts in many previous studies, indicated by two separated bands[155,156]. A 180 kDa mature band (c band) represents the fully glycosylated CFTR, whereas a 160 kDa immature band (b band) represents the incompletely glycosylate CFTR. In cells carrying F508del, the mutant CFTR is mostly detected as incompletely glycosylated band b. In our study, the immature band was not detected. This method will need future optimizations such as adjusting the lysing conditions and using different anti-CFTR antibodies. Because of the limitations of detection methods for CFTR protein in late passages, the integration frequency of the UBCLacZ reporter expression cassette described in the previous chapter provides important information to our study. An assumption was made that in late passages, a similar percentage of the cell population as determined in the previous chapter would carry integrated K18CFTR expression cassette at the AAVS1 locus.

Yet, the immunostaining of CFTR protein revealed the expression of mutant CFTR in IB3-1 cells. Many CFTR mutations seen in patients, including the most frequently occurring F508del, lead to production of abnormal or immature CFTR protein. Since our strategy

described in this thesis targets the AAVS1 locus instead of the CFTR locus, mutant CFTR will always be present no matter whether the functional expression cassette is integrated or not. Although traditionally we consider absence of functional CFTR as the major cause of CF, some recent studies showed that aggregates of mutated CFTR did induce inflammation in the lung[157,158]. Therefore, targeting the CFTR locus may be an option in the future to ensure that the mutated CFTR is not expressed.

Measuring the CFTR function in not fully differentiated cell line has been another challenge to test our strategy. The Ussing chamber method is extensively used for studies of membrane potential, but it requires tight junction integrity which controls apical and basolateral membrane polarity. In this study, the FLIPR-base membrane potential assay allowed us to test CFTR channel function in the IB3-1 cell line which does not form tight junctions as in primary epithelial cultures. The assay also generates better data by minimizing possible cell perturbation from multiple washing steps that are usually required in conventional iodide efflux assay.

4 Summary and future directions

We have developed a novel approach using a single HD-Ad vector to deliver the TALEN gene editing system together with a CFTR expression cassette for site-specific integration into the AAVS1 locus. Two major questions were investigated in this thesis: How efficiently can the transgene be integrated into the target locus for long-term expression? Whether the transgene expression cassette can produce functional CFTR?

In Chapter 2, we investigated the first research question, focusing on the transgene integration efficiency. We produced an HD-Ad-TALEN vector carrying a UBCLacZ expression cassette and transduced IB3-1 cells at 50 MOI and 100 MOI. In transduced cells, we demonstrated the DNA cleavage and UBCLacZ integration at the AAVS1 target site. We also showed that cleavage at the predicted three off-target sites was not detectable. The integration efficiency was determined by direct cell counting, single cell sorting, and flow cytometry. Finally, we concluded that an 5-7% transgene integration efficiency was achieved by transducing the cells with 100 MOI of HD-Ad-UBCLacZ-TALEN, and the use of 0.5 μM SCR7 significantly enhanced integration by HDR.

In Chapter 3, the second research question on expression and function of CFTR was explored. We produced a similar HD-Ad-TALEN vector carrying a K18CFTR expression cassette and measured the CFTR mRNA expression, protein expression, and protein channel function in transduced IB3-1 cells. We concluded that stable expression of CFTR mRNA was achieved in cells transduced with 100 MOI of HD-Ad-K18CFTR-TALEN, and functional CFTR protein was expressed from the K18CFTR expression cassette.

The key findings of our work reported great potential in the HD-Ad-TALEN system as a novel therapeutic strategy to restore the long-term function of mutated CFTR gene in lungs. Needless to say, future work is required for optimization and further assessment of safety.

Besides SCR7 treatment, some key proteins involved in the HDR repair pathway were shown to promote HDR. The human CtIP protein is required during DNA end resection and it facilitates the recruitment of other protein factors in homologous recombination[159]. The EXO1 protein exhibits 5'-3' exonuclease activity and is therefore recruited for degradation of the 5' strand in dsDNA end resection[160]. We are now trying to incorporate CtIP and EXO1 into HD-Ad vectors and test their effects on the expression cassette integration.

In this study, we investigated the CFTR mRNA expression in transduced cells for 18 generations. However, it is also necessary to determine whether the CFTR protein expression level from integration is sufficient to offer any functional benefit. Therefore, detection of CFTR channel function in cells at late passages with the FLIPR membrane potential assay is an important next step we could take. In Chapter 2, we showed an increase in UBCLacZ integration efficiency from 5% to 7% with SCR7 treatment, which is statistically significant. For further research into K18CFTR integration, SCR7 could also be applied post HD-Ad-K18CFTR-TALEN transduction so that we could determine how significantly this treatment affects CFTR functions.

Pigs are important model animals for *in vivo* study of CF lung disease because their lung anatomy is closer to human compared to other commonly used models[161]. For study of HD-Ad in pigs, vectors that target the pig genome is essential. Several HD-Ad-CRISPR vectors targeting the pig GGTA1 locus were developed by former lab members and are currently being tested in primary pig epithelial cells as well as in pig models. Similar to TALEN, CRISPR gene editing tool is made up of a DNA recognizing and binding component (guide RNA) and a Cas9 endonuclease for DNA cleavage. Furthermore, the small size and ease of assembly of CRISPR make it possible to simultaneously target multiple sites along the genome. These

features are essential for strategies that target a non-disease locus such as AAVS1 and the CFTR locus to knock out mutant CFTR at the same time.

With HD-Ad vectors combined with gene editing systems, our long-term goal is to integrate functional CFTR gene to lung stem cells for permanent gene correction. In an recent study by our lab colleague, HD-Ad vectors have been successfully delivered to airway basal cells in mice and pigs in vivo and primary human airway basal cells *in vitro*[143]. The future work will be extended to investigate whether the functional expression cassette can be efficiently integrated in such settings.

References

1. **Rowe SM, Miller S, Sorscher EJ.** Cystic Fibrosis. *N Engl J Med*. 2005;352(19):1992-2001. doi:10.1056/NEJMra043184
2. **Bals R, Weiner DJ, Wilson JM.** The innate immune system in cystic fibrosis lung disease. *J Clin Invest*. 1999;103(3):303-307. doi:10.1172/JCI6277
3. **Kunzelmann K, Schreiber R, Nitschke R, Mall M.** Control of epithelial Na+ conductance by the cystic fibrosis transmembrane conductance regulator. *Pflugers Arch*. 2000;440(2):193-201. doi:10.1007/s004240000255
4. **Xu Y, Clark JC, Aronow BJ, Dey CR, Liu C, et al.** Transcriptional Adaptation to Cystic Fibrosis Transmembrane Conductance Regulator Deficiency. *J Biol Chem*. 2003;278(9):76
74-7682. doi:10.1074/jbc.M210277200
5. **Patrick AE, Thomas PJ.** Development of CFTR structure. *Front Pharmacol*. 2012;3 SEP. doi:10.3389/fphar.2012.00162
6. **Riordan JR.** ASSEMBLY OF FUNCTIONAL CFTR CHLORIDE CHANNELS. *Annu Rev Physiol*. 2005;67(1):701-718. doi:10.1146/annurev.physiol.67.032003.154107
7. **Vergani P, Lockless SW, Nairn AC, Gadsby DC.** CFTR channel opening by ATP-driven tight dimerization of its nucleotide-binding domains. *Nature*. 2005;433(7028):876-880. doi:10.1038/nature03313
8. **Spoonhower KA, Davis PB.** Epidemiology of Cystic Fibrosis. *Clin Chest Med*. 2016;37(1):1-8. doi:10.1016/j.ccm.2015.10.002
9. **Cystic Fibrosis Canada.** *The Canadian Cystic Fibrosis Registry 2015 Annual Report*. Toronto; 2017. https://www.google.ca/url?sa=t&rct=j&q=&esrc=s&source=web&cd=2&cad=rja&uact=8&ved=0ahUKEwilr7OG_pvaAhXk5IMKHdC8DP8QFgguMAE&url=http%3A%2F%2Fwww.cysticfibrosis.ca%2Fuploads%2FRegistry%2520Report%252202015%2F2015%2520Registry%2520Annual%2520Report%2520EN.pdf.
10. **Schrijver I, Pique L, Graham S, Pearl M, Cherry A, Kharrazi M.** The Spectrum of CFTR Variants in Nonwhite Cystic Fibrosis Patients: Implications for Molecular Diagnostic Testing. *J Mol Diagnostics*. 2016;18(1):39-50. doi:10.1016/j.jmoldx.2015.07.005
11. **Marshall, B.; Elbert, A.; Petren, K.; Rizvi, S.; Fink, A.; Ostrenga, J.; Sewall, A.; Loeffler D.** Patient Registry: Annual Data Report 2015. *Cyst Fibros Found Patient Regist*. 2016:94. https://www.cff.org/Our-Research/CF-Patient-Registry/2015-Patient-Registry-Annual-Data-Report.pdf.
12. **Flume PA, Mogayzel PJ, Robinson KA, et al.** Cystic fibrosis pulmonary guidelines: Treatment of pulmonary exacerbations. *Am J Respir Crit Care Med*. 2009;180(9):802-808. doi:10.1164/rccm.200812-1845PP
13. **Rubin BK.** Mucus structure and properties in cystic fibrosis. *Paediatr Respir Rev*. 2007;8(1):4-7. doi:10.1016/j.prrv.2007.02.004
14. **Wine JJ.** The genesis of cystic fibrosis lung disease. *J Clin Invest*. 1999;103(3):309-312. doi:10.1172/JCI6222
15. **Wyckoff TJO, Thomas B, Hassett DJ, Wozniak DJ.** Static growth of mucoid Pseudomonas aeruginosa selects for non-mucoid variants that have acquired flagellum-

dependent motility. *Microbiology*. 2002;148(11):3423-3430. doi:10.1099/00221287-148-11-3423

16. **Drevinek P, Mahenthiralingam E.** *Burkholderia cenocepacia* in cystic fibrosis: epidemiology and molecular mechanisms of virulence. *Clin Microbiol Infect*. 2010;16(7):821-830. doi:10.1111/j.1469-0691.2010.03237.x
17. **Sagel SD, Sontag MK, Wagener JS, Kapsner RK, Osberg I, Accurso FJ.** Induced sputum inflammatory measures correlate with lung function in children with cystic fibrosis. *J Pediatr*. 2002;141(6):811-817. doi:10.1067/mpd.2002.129847
18. **Koehler DR, Downey GP, Sweezey NB, Tanswell AK, Hu J.** Lung inflammation as a therapeutic target in cystic fibrosis. *Am J Respir Cell Mol Biol*. 2004;31(4):377-381. doi:10.1165/rcmb.2004-0124TR
19. **Mall M, Grubb BR, Harkema JR, O'Neal WK, Boucher RC.** Increased airway epithelial Na+ absorption produces cystic fibrosis-like lung disease in mice. *Nat Med*. 2004;10(5):487-493. doi:10.1038/nm1028
20. **Smith JJ, Travis SM, Greenberg EP, Welsh MJ.** Cystic fibrosis airway epithelia fail to kill bacteria because of abnormal airway surface fluid. *Cell*. 1996;85(2):229-236. doi:10.1016/S0092-8674(00)81099-5
21. **Zabner J, Smith JJ, Karp PH, Widdicombe JH, Welsh MJ.** Loss of CFTR chloride channels alters salt absorption by cystic fibrosis airway epithelia in vitro. *Mol Cell*. 1998;2(3):397-403. doi:10.1016/S1097-2765(00)80284-1
22. **Tsui LC.** The spectrum of cystic fibrosis mutations. *Trends Genet*. 1992;8(11):392-398. doi:10.1016/0168-9525(92)90301-J
23. **Zielenski J, Tsui LC.** Cystic fibrosis: genotypic and phenotypic variations. *Annu Rev Genet*. 1995;29(1):777-807. doi:10.1146/annurev.genet.29.1.777
24. **Welsh MJ, Smith AE.** Molecular mechanisms of CFTR chloride channel dysfunction in cystic fibrosis. *Cell*. 1993;73(7):1251-1254. doi:10.1016/0092-8674(93)90353-R
25. **Fulmer SB, Schwiebert EM, Morales MM, Guggino WB, Cutting GR.** Two cystic fibrosis transmembrane conductance regulator mutations have different effects on both pulmonary phenotype and regulation of outwardly rectified chloride currents. *Proc Natl Acad Sci*. 1995;92(15):6832-6836. doi:10.1073/pnas.92.15.6832
26. **McNicholas CM, Guggino WB, Schwiebert EM, Hebert SC, Giebisch G, Egan ME.** Sensitivity of a renal K+ channel (ROMK2) to the inhibitory sulfonylurea compound glibenclamide is enhanced by coexpression with the ATP-binding cassette transporter cystic fibrosis transmembrane regulator. *Proc Natl Acad Sci U S A*. 1996;93(July):8083-8088. doi:10.1073/pnas.93.15.8083
27. **Akabas MH, Kaufmann C, Cook TA, Archdeacon P.** Amino acid residues lining the chloride channel of the cystic fibrosis transmembrane conductance regulator. *J Biol Chem*. 1994;269(21):14865-14868. http://www.ncbi.nlm.nih.gov/entrez/query.fcgi?cmd=Retrieve&db=PubMed&dopt=Citation&list_uids=7515047.
28. **Highsmith WE, Burch LH, Zhou Z, et al.** A novel mutation in the cystic fibrosis gene in patients with pulmonary disease but normal sweat chloride concentrations. *N Engl J Med*. 1994;331(15):974-980. doi:10.1056/NEJM199410133311503
29. **De Braekeleer M, Allard C, Leblanc JP, Simard F, Aubin G.** Genotype-phenotype correlation in cystic fibrosis patients compound heterozygous for the A455E mutation. *Hum Genet*. 1997;101(2):208-211. doi:10.1007/s004390050616

30. **Sheppard DN, Ostedgaard LS, Winter MC, Welsh MJ.** Mechanism of dysfunction of two nucleotide binding domain mutations in cystic fibrosis transmembrane conductance regulator that are associated with pancreatic sufficiency. *EMBO J*. 1995;14(5):876-883. http://www.pubmedcentral.nih.gov/articlerender.fcgi?artid=398160&tool=pmcentrez&rendertype=abstract.
31. **Haardt M, Benharouga M, Lechardeur D, Kartner N, Lukacs GL.** C-terminal truncations destabilize the cystic fibrosis transmembrane conductance regulator without impairing its biogenesis. A novel class of mutation. *J Biol Chem*. 1999;274(31):21873-21877. doi:10.1074/jbc.274.31.21873
32. **De Boeck K, Amaral MD.** Progress in therapies for cystic fibrosis. *Lancet Respir Med*. 2016;4(8):662-674. doi:10.1016/S2213-2600(16)00023-0
33. **De Boeck K, Amaral MD.** Classification of CFTR mutation classes – Authors' reply. *Lancet Respir Med*. 2016;4(8):e39. doi:10.1016/S2213-2600(16)30189-8
34. **Konstan MW, Flume PA, Kappler M, et al.** Safety, efficacy and convenience of tobramycin inhalation powder in cystic fibrosis patients: The EAGER trial. *J Cyst Fibros*. 2011;10(1):54-61. doi:10.1016/j.jcf.2010.10.003
35. **Schuster A, Haliburn C, Döring G, Goldman MH.** Safety, efficacy and convenience of colistimethate sodium dry powder for inhalation (Colobreathe DPI) in patients with cystic fibrosis: A randomised study. *Thorax*. 2013;68(4):344-350. doi:10.1136/thoraxjnl-2012-202059
36. **Oermann CM, Retsch-bogart GZ, Quittner AL, et al.** An 18-month study of the safety and efficacy of repeated courses of inhaled aztreonam lysine in cystic fibrosis. *Pediatr Pulmonol*. 2010;45(11):1121-1134. doi:10.1002/ppul.21301
37. **Wainwright CE, Quittner AL, Geller DE, et al.** Aztreonam for inhalation solution (AZLI) in patients with cystic fibrosis, mild lung impairment, and P. aeruginosa. *J Cyst Fibros*. 2011;10(4):234-242. doi:10.1016/j.jcf.2011.02.007
38. **Ehsan Z, Wetzel JD, Clancy JP.** Nebulized liposomal amikacin for treatment of Pseudomonas aeruginosa infection in cystic fibrosis patients. *Expert Opin Investig Drugs*. 2014:743-749. doi:10.1517/13543784.2014.895322
39. **Clancy JP, Dupont L, Konstan MW, et al. P**hase II studies of nebulised Arikace in CF patients with Pseudomonas aeruginosa infection. *Thorax*. 2013;68(9):818-825. doi:10.1136/thoraxjnl-2012-202230
40. **Stuart Elborn J, Geller DE, Conrad D, et al.** A phase 3, open-label, randomized trial to evaluate the safety and efficacy of levofloxacin inhalation solution (APT-1026) versus tobramycin inhalation solution in stable cystic fibrosis patients. *J Cyst Fibros*. 2015;14(4):507-514. doi:10.1016/j.jcf.2014.12.013
41. **Mogayzel PJ, Naureckas ET, Robinson KA, et al.** Cystic fibrosis pulmonary guidelines: Chronic medications for maintenance of lung health. *Am J Respir Crit Care Med*. 2013;187(7):680-689. doi:10.1164/rccm.201207-1160OE
42. **Nichols D, Chmiel J, Berger M.** Chronic inflammation in the cystic fibrosis lung: Alterations in inter- and intracellular signaling. *Clin Rev Allergy Immunol*. 2008;34(2):146-162. doi:10.1007/s12016-007-8039-9
43. **Konstan MW, Byard PJ, Hoppel CL, Davis PB.** Effect of high-dose ibuprofen in patients with cystic fibrosis. *N Engl J Med*. 1995;332(13):848-854. doi:10.1056/NEJM1995033033
21303

44. **Lands LC, Milner R, Cantin AM, Manson D, Corey M.** High-Dose Ibuprofen in Cystic Fibrosis: Canadian Safety and Effectiveness Trial. *J Pediatr*. 2007;151(3):249-254. doi:10.1016/j.jpeds.2007.04.009
45. **Konstan MW.** Ibuprofen therapy for cystic fibrosis lung disease: Revisited. *Curr Opin Pulm Med*. 2008;14(6):567-573. doi:10.1097/MCP.0b013e32831311e8
46. **Ratjen F, Saiman L, Mayer-Hamblett N, et al.** Effect of azithromycin on systemic markers of inflammation in patients with cystic fibrosis uninfected with Pseudomonas aeruginosa. *Chest*. 2012;142(5):1259-1266. doi:10.1378/chest.12-0628
47. **Rubin BK.** Physiology of airway mucus clearance. *Respir Care*. 2002;47(7):761-768. http://www.ncbi.nlm.nih.gov/pubmed/12088546.
48. **Amin R, Subbarao P, Lou W, et al.** The effect of dornase alfa on ventilation inhomogeneity in patients with cystic fibrosis. *Eur Respir J*. 2011;37(4):806-812. doi:10.1183/09031936.00072510
49. **Konstan MW, Ratjen F.** Effect of dornase alfa on inflammation and lung function: potential role in the early treatment of cystic fibrosis. *J Cyst Fibros*. 2012;11(2):78-83. doi:10.1016/j.jcf.2011.10.003
50. **Paul K, Rietschel E, Ballmann M, et al.** Effect of treatment with dornase alpha on airway inflammation in patients with cystic fibrosis. *Am J Respir Crit Care Med*. 2004;169(6):719-725. doi:10.1164/rccm.200307-959OC
51. **Donaldson SH, Bennett WD, Zeman KL, Knowles MR, Tarran R, Boucher RC.** Mucus Clearance and Lung Function in Cystic Fibrosis with Hypertonic Saline. *N Engl J Med*. 2006;354(3):241-250. doi:10.1056/NEJMoa043891
52. **De Boeck K, Munck A, Walker S, et al.** Efficacy and safety of ivacaftor in patients with cystic fibrosis and a non-G551D gating mutation. *J Cyst Fibros*. 2014;13(6):674-680. doi:10.1016/j.jcf.2014.09.005
53. **Davies JC, Wainwright CE, Canny GJ, et al.** Efficacy and safety of ivacaftor in patients aged 6 to 11 years with cystic fibrosis with a G551D mutation. *Am J Respir Crit Care Med*. 2013;187(11):1219-1225. doi:10.1164/rccm.201301-0153OC
54. **Ramsey BW, Davies J, McElvaney NG, et al.** A CFTR potentiator in patients with cystic fibrosis and the G551D mutation. *N Engl J Med*. 2011;365(18):1663-1672. doi:10.1056/NEJMoa1105185
55. F**lume PA, Liou TG, Borowitz DS, et al.** Ivacaftor in subjects with cystic fibrosis who are homozygous for the F508del-CFTR mutation. *Chest*. 2012;142(3):718-724. doi:10.1378/chest.11-2672
56. **Wainwright CE, Elborn JS, Ramsey BW, et al.** Lumacaftor–Ivacaftor in Patients with Cystic Fibrosis Homozygous for Phe508del *CFTR*. *N Engl J Med*. 2015;373(3):220-231. doi:10.1056/NEJMoa1409547
57. **Veit G, Avramescu RG, Perdomo D, et al.** Cystic fibrosis: Some gating potentiators, including VX-770, diminish ΔF508-CFTR functional expression. *Sci Transl Med*. 2014;6(246). doi:10.1126/scitranslmed.3008889
58. **Davies JC, Colombo C, Tullis E, Mckee C, Desouza C, Waltz D, Savage J, Fisher M, Shilling R, Moskowitz S, Robertson S.** WS01. 6 Preliminary safety and efficacy of triple combination CFTR modulator regimens in cystic fibrosis. Journal of Cystic Fibrosis. 2018 Jun 30;17:S3.
59. **Kerem B, Rommens JM, Buchanan JA, et al.** Identification of the cystic fibrosis gene: genetic analysis. *Science*. 1989;245(4922):1073-1080. doi:10.1126/science.2570460

60. **Shah VS, Ernst S, Tang XX, et al.** Relationships among CFTR expression, HCO_3^- secretion, and host defense may inform gene- and cell-based cystic fibrosis therapies. *Proc Natl Acad Sci*. 2016;113(19):5382-5387. doi:10.1073/pnas.1604905113
61. **Johnson LG, Olsen JC, Sarkadi B, Moore KL, Swanstrom R, Boucher RC.** Efficiency of gene transfer for restoration of normal airway epithelial function in cystic fibrosis. *Nat Genet*. 1992;2(1):21-25. doi:10.1038/ng0992-21
62. **Hong KU, Reynolds SD, Watkins S, Fuchs E, Stripp BR.** Basal Cells Are a Multipotent Progenitor Capable of Renewing the Bronchial Epithelium. *Am J Pathol*. 2004;164(2):577-588. doi:10.1016/S0002-9440(10)63147-1
63. **Hong KU.** In vivo differentiation potential of tracheal basal cells: evidence for multipotent and unipotent subpopulations. *AJP Lung Cell Mol Physiol*. 2003;286(4):643L-649. doi:10.1152/ajplung.00155.2003
64. **Rock JR, Onaitis MW, Rawlins EL, et al.** Basal cells as stem cells of the mouse trachea and human airway epithelium. *Proc Natl Acad Sci U S A*. 2009;106(31):12771-12775. doi:10.1073/pnas.0906850106
65. **Thomas J. Lynch, Preston J. Anderson, Pavana G. Rotti, et al.** Submucosal Gland Myoepithelial Cells Are Reserve Stem Cells That Can Regenerate Mouse Tracheal Epithelium. *Cell Stem Cell*. 2018. https://www.cell.com/cell-stem-cell/fulltext/S1934-5909(18)30123-1.
66. **Al-Dosari MS, Gao X.** Nonviral Gene Delivery: Principle, Limitations, and Recent Progress. *AAPS J*. 2009;11(4):671-681. doi:10.1208/s12248-009-9143-y
67. **Nayerossadat N, Ali P, Maedeh T.** Viral and nonviral delivery systems for gene delivery. *Adv Biomed Res*. 2012;1(1):27. doi:10.4103/2277-9175.98152
68. **Ruozi B, Forni F, Battini R, Vandelli MA.** Cationic liposomes for gene transfection. *J Drug Target*. 2003;11(7):407-414. doi:10.1080/10611860310001655600
69. **Alton EW, Boyd AC, Porteous DJ, Davies G, Davies JC, Griesenbach U, Higgins TE, Gill DR, Hyde SC.** A Phase I/IIa Safety and Efficacy Study of Nebulized Liposome-mediated Gene Therapy for Cystic Fibrosis Supports a Multidose Trial. *Am J Respir Crit Care Med*. 2015;192(11):1389-1392.
70. **Ramamoorth M, Narvekar A.** Non viral vectors in gene therapy- an overview. *J Clin Diagn Res*. 2015;9(1):GE01-6. doi:10.7860/JCDR/2015/10443.5394
71. **Munye MM, Tagalakis AD, Barnes JL, et al.** Minicircle DNA Provides Enhanced and Prolonged Transgene Expression Following Airway Gene Transfer. *Sci Rep*. 2016;6. doi:10.1038/srep23125
72. **Nafissi N, Alqawlaq S, Lee EA, Foldvari M, Spagnuolo PA, Slavcev RA.** DNA ministrings: Highly safe and effective gene delivery vectors. *Mol Ther - Nucleic Acids*. 2014;3. doi:10.1038/mtna.2014.16
73. **Wong S, Lam P, Nafissi N, Denniss S, Slavcev R.** Production of Double-stranded DNA Ministrings. *J Vis Exp*. 2016;(108). doi:10.3791/53177
74. **Igreja S, Clarke LA, Botelho HM, Marques L, Amaral MD.** Correction of a Cystic Fibrosis Splicing Mutation by Antisense Oligonucleotides. *Hum Mutat*. 2016;37(2):209-215. doi:10.1002/humu.22931
75. **Manunta MDI, Tagalakis AD, Attwood M, et al.** Delivery of ENaC siRNA to epithelial cells mediated by a targeted nanocomplex: A therapeutic strategy for cystic fibrosis. *Sci Rep*. 2017;7(1). doi:10.1038/s41598-017-00662-2

76. **Weinberg JB, Matthews TJ, Cullen BR, Malim MH.** Productive human immunodeficiency virus type 1 (HIV-1) infection of nonproliferating human monocytes. *J Exp Med*. 1991;174(6):1477-1482. doi:10.1084/jem.174.6.1477
77. **Naldini L, Trono D, Verma IM.** Lentiviral vectors, two decades later. *Science*. 2016;353(6304):1101-1102. doi:10.1126/science.aah6192
78. **Naldini L, Blomer U, Gallay P, et al.** In Vivo Gene Delivery and Stable Transduction of Nondividing Cells by a Lentiviral Vector. *Science (80-)*. 1996;272(5259):263-267. doi:10.1126/science.272.5259.263
79. **Kobayashi M, Iida A, Ueda Y, Hasegawa M.** Pseudotyped lentivirus vectors derived from simian immunodeficiency virus SIVagm with envelope glycoproteins from paramyxovirus. *J Virol*. 2003;77(4):2607-2614. doi:10.1128/JVI.77.4.2607-2614.2003
80. **McKay T, Patel M, Pickles RJ, Johnson LG, Olsen JC.** Influenza M2 envelope protein augments avian influenza hemagglutinin pseudotyping of lentiviral vectors. *Gene Ther*. 2006;13(8):715-724. doi:10.1038/sj.gt.3302715
81. **Sinn PL, Hickey MA, Staber PD, et al.** Lentivirus Vectors Pseudotyped with Filoviral Envelope Glycoproteins Transduce Airway Epithelia from the Apical Surface Independently of Folate Receptor Alpha. *J Virol*. 2003;77(10):5902-5910. doi:10.1128/JVI.77.10.5902-5910.2003
82. **Modlich U, Bohne J, Schmidt M, et al.** Cell-culture assays reveal the importance of retroviral vector design for insertional genotoxicity. *Blood*. 2006;108(8):2545-2553. doi:10.1182/blood-2005-08-024976
83. **Cooney AL, Abou Alaiwa MH, Shah VS, et al.** Lentiviral-mediated phenotypic correction of cystic fibrosis pigs. *JCI Insight*. 2016;1(14). doi:10.1172/jci.insight.88730
84. **Srivastava A, Lusby EW, Berns KI.** Nucleotide sequence and organization of the adeno-associated virus 2 genome. *J Virol*. 1983;45(2):555-564. http://www.ncbi.nlm.nih.gov/pubmed/6300419%5Cnhttp://www.pubmedcentral.nih.gov/articlerender.fcgi?artid=PMC256449.
85. **Kotin RM, Siniscalco M, Samulski RJ, et al.** Site-specific integration by adeno-associated virus. *Proc Natl Acad Sci U S A*. 1990;87(6):2211-2215. doi:10.1073/pnas.93.21.11288
86. **Flotte TR, Carter BJ.** Adeno-associated virus vectors for gene therapy. *Gene Ther*. 1995;2(6):357-362. doi:10.1128/CMR.00008-08
87. **The American Society of Gene & Cell Therapy.** ASGCT Celebrates FDA Approval of Voretigene Neparvovec (Luxturna) as Treatment for Inherited Retinal Disease.
88. **Rowe WP, Huebner RJ, Gilmore LK, Parrott RH, Ward TG.** Isolation of a Cytopathogenic Agent from Human Adenoids Undergoing Spontaneous Degeneration in Tissue Culture. *Exp Biol Med*. 1953;84(3):570-573. doi:10.3181/00379727-84-20714
89. **St George JA.** Gene therapy progress and prospects: Adenoviral vectors. *Gene Ther*. 2003;10(14):1135-1141. doi:10.1038/sj.gt.3302071
90. **Okada T, Nomoto T, Yoshioka T, et al.** Large-scale production of recombinant viruses by use of a large culture vessel with active gassing. *Hum Gene Ther*. 2005;16(10):1212-1218. doi:10.1089/hum.2005.16.1212
91. **Ghebremedhin B.** Human adenovirus: Viral pathogen with increasing importance. *Eur J Microbiol Immunol*. 2014;4(1):26-33. doi:10.1556/EuJMI.4.2014.1.2
92. **Bergelson JM, Cunningham JA, Droguett G, et al.** Isolation of a common receptor

for coxsackie B viruses and adenoviruses 2 and 5. *Science (80-)*. 1997;275(5304):1320-1323. doi:10.1126/science.275.5304.1320

93. **Roelvink PW, Lizonova A, Lee JG, et al.** The coxsackievirus-adenovirus receptor protein can function as a cellular attachment protein for adenovirus serotypes from subgroups A, C, D, E, and F. *J Virol*. 1998;72(10):7909-7915. http://www.pubmedcentral.nih.gov/articlerender.fcgi?artid=110119&tool=pmcentrez&rendertype=abstract.
94. **Leopold PL, Ferris B, Grinberg I, Worgall S, Hackett NR, Crystal RG.** Fluorescent virions: dynamic tracking of the pathway of adenoviral gene transfer vectors in living cells. *Hum Gene Ther*. 1998;9(3):367-378. doi:10.1089/hum.1998.9.3-367
95. **Frisch SM, Mymryk JS.** Adenovirus-5 E1A: Paradox and paradigm. *Nat Rev Mol Cell Biol*. 2002;3(6):441-452. doi:10.1038/nrm827
96. **Lowe SW, Earl Ruley H.** Stabilization of the p53 tumor suppressor is induced by adeno virus 5 E1A and accompanies apoptosis. *Genes Dev*. 1993;7(4):535-545. doi:10.1101/gad.7.4.535
97. **White E, Cipriani R.** Role of adenovirus E1B proteins in transformation: altered organization of intermediate filaments in transformed cells that express the 19-kilodalton protein. *Mol Cell Biol*. 1990;10(1):120-130. doi:10.1128/MCB.10.1.120.
98. **Bett a J, Prevec L, Graham FL.** Packaging capacity and stability of human adenovirus type 5 vectors. *J Virol*. 1993;67(10):5911-5921.
99. **Danthinne X, Imperiale MJ.** Production of first generation adenovirus vectors: a review. *Gene Ther*. 2000;7(20):1707-1714. doi:10.1038/sj.gt.3301301
100. **Engelhardt JF, Litzky L, Wilson JM.** Prolonged expression in cotton rat lung with recombinant adenoviruses defective in E2a. *Hum Gene Ther*. 1994;5(10):1217. doi:10.1089/hum.1994.5.10-1217
101. **Chirmule N, Hughes J V, Gao GP, Raper SE, Wilson JM.** Role of E4 in eliciting CD4 T-cell and B-cell responses to adenovirus vectors delivered to murine and nonhuman primate lungs [In Process Citation]. *J Virol*. 1998;72(7):6138-6145.
102. **Zhang Y, Chirmule N, Gao GP, et al.** Acute cytokine response to systemic adenoviral vectors in mice is mediated by dendritic cells and macrophages. *Mol Ther*. 2001;3(5 Pt 1):697-707. doi:10.1006/mthe.2001.0329
103. **Raper SE, Yudkoff M, Chirmule N, et al.** A pilot study of in vivo liver-directed gene transfer with an adenoviral vector in partial ornithine transcarbamylase deficiency. *Hum Gene Ther*. 2002;13(1):163-175. doi:10.1089/10430340152712719
104. **Lozier JN, Csako G, Mondoro TH, et al.** Toxicity of a first-generation adenoviral vector in rhesus macaques. *Hum Gene Ther*. 2002;13(1):113-124. doi:10.1089/10430340152712665
105. **Palmer DJ, Ng P.** Helper-Dependent Adenoviral Vectors for Gene Therapy. *Hum Gene Ther*. 2005;16(January):1-16. doi:10.1089/hum.2005.16.1
106. **Toietta G, Koehler DR, Finegold MJ, Lee B, Hu J, Beaudet AL.** Reduced inflammation and improved airway expression using helper-dependent adenoviral vectors with a K18 promoter. *Mol Ther*. 2003;7(5 I):649-658. doi:10.1016/S1525-0016(03)00059-5
107. **Cao H, Machuca TN, Yeung JC, et al.** Efficient gene delivery to pig airway epithelia and submucosal glands using helper-dependent adenoviral vectors. *Mol Ther - Nucleic*

Acids. 2013;2(OCT). doi:10.1038/mtna.2013.55
108. **Palmer D, Ng P.** Improved system for helper-dependent adenoviral vector production. *Mol Ther*. 2003;8(5):846-852. doi:10.1016/j.ymthe.2003.08.014
109. **Parks RJ, Chen L, Anton M, Sankar U, Rudnicki MA, Graham FL.** A helper-dependent adenovirus vector system: removal of helper virus by Cre-mediated excision of the viral packaging signal. *Proc Natl Acad Sci U S A*. 1996;93(24):13565-13570. doi:10.1073/
pnas.93.24.13565
110. **Palmer DJ, Ng P.** Methods for the production of helper-dependent adenoviral vectors. *Methods Mol Biol*. 2008;433:33-53. doi:10.1007/978-1-59745-237-3_3
111. **Kotin RM, Menninger JC, Ward DC, Berns KI.** Mapping and direct visualization of a region-specific viral DNA integration site on chromosome 19q13-qter. *Genomics*. 1991;10(3):831-834. doi:10.1016/0888-7543(91)90470-Y
112. **Walz C, Schlehofer JR.** Modification of some biological properties of HeLa cells containing adeno-associated virus DNA integrated into chromosome 17. *J Virol*. 1992;66(5):2990-3002.
http://www.ncbi.nlm.nih.gov/entrez/query.fcgi?cmd=Retrieve&db=PubMed&dopt=Citation&list_uids=1313913.
113. **Winocour E, Puzis L, Etkin S, et al.** Modulation of the cellular phenotype by integrated adeno-associated virus. *Virology*. 1992;190(1):316-329. doi:10.1016/0042-6822(92)91218-J
114. **DeKelver RC, Choi VM, Moehle EA, et al.** Functional genomics, proteomics, and regulatory DNA analysis in isogenic settings using zinc finger nuclease-driven transgenesis into a safe harbor locus in the human genome. *Genome Res*. 2010;20(8):1133-1142. doi:10.1101/gr.106773.110
115. **Smith JR, Maguire S, Davis LA, et al.** Robust, Persistent Transgene Expression in Human Embryonic Stem Cells Is Achieved with AAVS1-Targeted Integration. *Stem Cells*. 2008;26(2):496-504. doi:10.1634/stemcells.2007-0039
116. **Hockemeyer D, Wang H, Kiani S, et al.** Genetic engineering of human pluripotent cells using TALE nucleases. *Nat Biotechnol*. 2011;29(8):731-734. doi:10.1038/nbt.1927
117. **Alfano JR, Collmer A.** TYPE III SECRETION SYSTEM EFFECTOR PROTEINS: Double Agents in Bacterial Disease and Plant Defense. *Annu Rev Phytopathol*. 2004;42(1):385-414. doi:10.1146/annurev.phyto.42.040103.110731
118. **Grant SR, Fisher EJ, Chang JH, Mole BM, Dangl JL.** Subterfuge and Manipulation: Type III Effector Proteins of Phytopathogenic Bacteria. *Annu Rev Microbiol*. 2006;60(1):425-449. doi:10.1146/annurev.micro.60.080805.142251
119. **Boch J, Bonas U.** *Xanthomonas* AvrBs3 Family-Type III Effectors: Discovery and Function. *Annu Rev Phytopathol*. 2010;48(1):419-436. doi:10.1146/annurev-phyto-080508-081936
120. **Boch J, Scholze H, Schornack S, et al.** Breaking the code of DNA binding specificity of TAL-type III effectors. *Science (80-)*. 2009;326(5959):1509-1512. doi:10.1126/science.1178811
121. **Moscou MJ, Bogdanove AJ.** A simple cipher governs DNA recognition by TAL effectors. *Science (80-)*. 2009;326(5959):1501. doi:10.1126/science.1178817
122. **Miller JC, Tan S, Qiao G, et al.** A TALE nuclease architecture for efficient genome

editing. *Nat Biotechnol*. 2011;29(2):143-150. doi:10.1038/nbt.1755
123. **Lamb BM, Mercer AC, Barbas CF.** Directed evolution of the TALE N-terminal domain for recognition of all 5′ bases. *Nucleic Acids Res*. 2013;41(21):9779-9785. doi:10.1093/nar/gkt754
124. **Christian M, Cermak T, Doyle EL, et al.** Targeting DNA double-strand breaks with TAL effector nucleases. *Genetics*. 2010;186(2):756-761. doi:10.1534/genetics.110.120717
125. **Reyon D, Khayter C, Regan MR, Keith Joung J, Sander JD.** Engineering designer transcription activator-like effector nucleases (TALENs) by REAL or REAL-Fast assembly. *Curr Protoc Mol Biol*. 2012;(SUPPL.100). doi:10.1002/0471142727.mb1215s100
126. **Weber E, Gruetzner R, Werner S, Engler C, Marillonnet S.** Assembly of designer tal effectors by golden gate cloning. *PLoS One*. 2011;6(5). doi:10.1371/journal.pone.0019722
127. **Reyon D, Tsai SQ, Khgayter C, Foden JA, Sander JD, Joung JK.** FLASH assembly of TALENs for high-throughput genome editing. *Nat Biotechnol*. 2012;30(5):460-465. doi:10.1038/nbt.2170
128. **SHEN Y, XIAO A, HUANG P, WANG W-Y, ZHU Z-Y, ZHANG B.** TALE nuclease engineering and targeted genome modification. *Hered*. 2013;35(4):395-409. doi:10.3724/SP.J.1005.2013.00395
129. **Kim Y, Kweon J, Kim JS.** TALENs and ZFNs are associated with different mutation signatures. *Nat Methods*. 2013;10(3):185. doi:10.1038/nmeth.2364
130. **Tesson L, Usal C, Meq´noret S, et al.** Knockout rats generated by embryo microinjection of TALENs. *Nat Biotechnol*. 2011;29(8):695-696. doi:10.1038/nbt.1940
131. **Carlson DF, Tan W, Lillico SG, et al.** Efficient TALEN-mediated gene knockout in livestock. *Proc Natl Acad Sci*. 2012;109(43):17382-17387. doi:10.1073/pnas.1211446109
132. **Lieber MR.** The Mechanism of Double-Strand DNA Break Repair by the Nonhomologous DNA End-Joining Pathway. *Annu Rev Biochem*. 2010;79(1):181-211. doi:10.1146/annurev.biochem.052308.093131
133. **Zlotorynski E.** DNA repair: The cell cycle flavours of repair. *Nat Rev Genet*. 2016;17(2):65. doi:10.1038/nrg.2015.35
134. **Branzei D, Foiani M.** Regulation of DNA repair throughout the cell cycle. *Nat Rev Mol Cell Biol*. 2008;9(4):297-308. doi:10.1038/nrm2351
135. **Agarwal S, Kanaar R, Essers J.** The Cell Biology of Homologous Recombination. In: *Molecular Genetics of Recombination*. Vol 17. ; 2007:335-362. http://dx.doi.org/10.1007/4735_2006_0214.
136. **Shrivastav M, De Haro LP, Nickoloff J a, Haro LP De.** Regulation of DNA double-strand break repair pathway choice. *Cell Res*. 2008;18(1):134-147. doi:10.1038/cr.2007.111
137. **Buis J, Stoneham T, Spehalski E, Ferguson DO.** Mre11 regulates CtIP-dependent double-strand break repair by interaction with CDK2. *Nat Struct Mol Biol*. 2012;19(2):246-253. doi:10.1038/nsmb.2212
138. **Elliott B, Jasin M.** Repair of double-strand breaks by homologous recombination in mismatch repair-defective mammalian cells. *Mol Cell Biol*. 2001;21(8):2671-2682.

doi:10.1128/MCB.21.8.2671-2682.2001
139. **Zeitlin PL, Lu L, Rhim J, et al.** A cystic fibrosis bronchial epithelial cell line: immortalization by adeno-12-SV40 infection. *Am J Respir Cell Mol Biol*. 1991;4(4):313-319. doi:10.1165/ajrcmb/4.4.313
140. **Gruenert DC, Willems M, Cassiman JJ, Frizzell RA.** Established cell lines used in cystic fibrosis research. *J Cyst Fibros*. 2004;3(SUPPL. 2):191-196. doi:10.1016/j.jcf.2004.05.040
141. **Chow YH, Tsui LC, Hu J.** Regulated expression of the human CFTR gene in epithelial cells. Mol Ther. 2001;3(5 Pt 1):723-733. doi:10.1006/mthe.2001.0314
142. **Horwitz JP, Chua J, Cubby RJ, et al.** Substrates for Cytochemical Demonstration of Enzyme Activity. I. Some Substituted 3-Indolyl-β-D-glycopyranosides. *J Med Chem*. 1964;7(4):574-575. doi:10.1021/jm00334a044
143. **Cao H, Ouyang H, Grasemann H, et al.** Transducing airway basal cells with a helper-dependent adenoviral vector for lung gene therapy. *Hum Gene Ther*. 2018:hum.2017.201. doi:10.1089/hum.2017.201
144. **Koehler DR, Chow YH, Plumb J, et al.** A human epithelium-specific vector optimized in rat pneumocytes for lung gene therapy. *Pediatr Res*. 2000;48(2):184-190. doi:10.1203/00006450-200008000-00011
145. **Sandig V, Youil R, Bett AJ, et al.** Optimization of the helper-dependent adenovirus system for production and potency in vivo. Proc Natl Acad Sci U S A. 2000;97(3):1002-1007. doi:10.1073/pnas.97.3.1002
146. **Graham FL, Prevec L.** Manipulation of adenovirus vectors. InGene transfer and expression protocols 1991 (pp. 109-128). Humana press.
147. **Wang X, Wang Y, Huang H, et al.** Precise gene modification mediated by TALEN and single-stranded oligodeoxynucleotides in human cells. PLoS One. 2014;9(4). doi:10.1371/journal.pone.0093575
148. **Zischewski J, Fischer R, Bortesi L.** Detection of on-target and off-target mutations generated by CRISPR/Cas9 and other sequence-specific nucleases. Biotechnology advances. 2017 Jan 1;35(1):95-104.
149. **Maruyama T, Dougan SK, Truttmann M, Bilate AM, Ingram JR, Ploegh HL.** Inhibition of non-homologous end joining increases the efficiency of CRISPR/Cas9-mediated precise [TM: inserted] genome editing. Nature biotechnology. 2015 May;33(5):538.
150. **McLenachan S, Sarsero JP, Ioannou PA.** Flow-cytometric analysis of mouse embryonic stem cell lipofection using small and large DNA constructs. Genomics. 2007 Jun 30;89(6):708-20.
151. **Zhang YZ, Naleway JJ, Larison KD, Huang ZJ, Haugland RP.** Detecting lacZ gene expression in living cells with new lipophilic, fluorogenic beta-galactosidase substrates. The FASEB Journal. 1991 Dec 1;5(15):3108-13.
152. **Singh P, Schimenti JC, Bolcun-Filas E.** A mouse geneticist's practical guide to CRISPR applications. Genetics. 2015 Jan 1;199(1):1-5.
153. **Koehler, D. R., Chow, Y. H., Plumb, J., Wen, Y., Rafii, B., Belcastro, R., ... & Hu, J.** (2000). A human epithelium-specific vector optimized in rat pneumocytes for lung gene therapy. *Pediatric research*, *48*(2), 184-190.

154. **Ahmadi S, Bozoky Z, Paola M, Xia S, Li C, Wong AP, Wellhauser L, Molinski SV, Ip W, Ouyang H, Avolio J.** Phenotypic profiling of CFTR modulators in patient-derived respiratory epithelia. NPJ genomic medicine. 2017 Apr 14;2(1):12.
155. **Cheng SH, Gregory RJ, Marshall J, Paul S, Souza DW, White GA, O'Riordan CR, Smith AE.** Defective intracellular transport and processing of CFTR is the molecular basis of most cystic fibrosis. Cell. 1990 Nov 16;63(4):827-34.
156. **Amaral MD.** CFTR and chaperones. Journal of Molecular Neuroscience. 2004 Feb 1;23(1-2):41-8.
157. **Luciani A, Villella VR, Esposito S, Brunetti-Pierri N, Medina D, Settembre C, Gavina M, Pulze L, Giardino I, Pettoello-Mantovani M, D'apolito M.** Defective CFTR induces aggresome formation and lung inflammation in cystic fibrosis through ROS-mediated autophagy inhibition. Nature cell biology. 2010 Sep;12(9):863.
158. **Du K, Karp PH, Ackerley C, Zabner J, Keshavjee S, Cutz E, Yeger H.** Aggregates of mutant CFTR fragments in airway epithelial cells of CF lungs: new pathologic observations. Journal of Cystic Fibrosis. 2015 Mar 1;14(2):182-93.
159. **Sartori AA, Lukas C, Coates J, Mistrik M, Fu S, Bartek J, Baer R, Lukas J, Jackson SP.** Human CtIP promotes DNA end resection. Nature. 2007 Nov;450(7169):509.
160. **Mimitou EP, Symington LS.** Sae2, Exo1 and Sgs1 collaborate in DNA double-strand break processing. Nature. 2008 Oct;455(7214):770.
161. **Liu X, Luo M, Zhang L, Ding W, Yan Z, Engelhardt JF.** Bioelectric properties of chloride channels in human, pig, ferret, and mouse airway epithelia. American journal of respiratory cell and molecular biology. 2007 Mar;36(3):313-23.